



Department of Hydrology and Hydraulic Engineering
Faculty of Applied Sciences
Vrije Universiteit Brussel

**Hydrogeological Study and Artificial Recharge
Modeling of the Gaza Coastal Aquifer
Using GIS and MODFLOW**

by

Adnan M. Aish

November 2004

Dissertation submitted in fulfillment of the requirements
for the award of the degree of Doctor of
Philosophy in Applied Sciences

Promotor: Prof. Dr. ir. F. De Smedt

This PhD thesis is dedicated to my wife and children

WITH ALL MY LOVE

LIST OF PUBLICATIONS

1. Aish, A., and De Smedt, F., 2003. Hydrogeological study of a proposed artificial recharge of groundwater, Gaza Strip- Palestine. Proceedings of the second international conference on wadi hydrology, 1-4 July, Amman- Jordan, WH 42.
2. Aish, A., and De Smedt, F., 2004. Artificial recharge modeling in the Gaza coastal aquifer, Palestine. To be submitted to the second environmental symposium of the German-Arabic society for environmental studies: water resources and environmental protection in the Middle East and North Africa, October, 4 and 5, Amman-Jordan.
3. Aish, A., and De Smedt, F., 2004. Modeling of a groundwater mound resulting from artificial recharge in the Gaza Strip, Palestine. Submitted to the second Israel-Palestinian international conference on water for life in the Middle East, October, 10–14, Antalya, Turkey.

ACKNOWLEDGEMENT

I would like to extend my deepest and humble gratitude to my promoter professor Hilaire De Smedt for providing me the opportunity to work under his research group. Professor De Smedt I am always impressed by your academic ability and unique personality. Thank you very much.

I am very much indebted to Prof. Dr. Ir. Willy Bauwens and Prof. Dr. Riad El Khudary for giving me the opportunity to join the Inter-University program at the Free University- Brussels.

I would like to express my sincere gratitude to the UNESCO – Cairo office and the Flemish Government for funding the Water Research Centre at Al-Azhar University – Gaza, Palestine through a UNESCO Fund-in Trust Project.

I would like to thank Eng. Adel Abu Kemal and Eng. Ehab Abu Swereh from AA Consulting Engineers and Eng. Emad El Shareef from the Arab Centre for Engineering Studies for their assistance in the field. Also, thanks to Eng. Ahmad Yaqubi, Eng. Sady Ali and Eng. Samy Hamdan from the Palestinian Water Authority for their kind cooperation.

I am really grateful to my jury members: Prof. A. Van der Beken (Vrije Universiteit Brussel), Prof. W. Bauwens (Vrije Universiteit Brussel), Prof. K. Walraevens (Ghent Universiteit), Prof. D. Raes (Katholieke Universiteit Leuven), Prof. R. Herman (Ministry of the Flemish community) and Prof. J. Vereecken (Vrije Universiteit Brussel) for their acceptance to be members of jury of my PhD thesis. Their critical review and evaluation of my work resulted in the success of this PhD thesis.

Acknowledgement

During my study at Vrije Universiteit Brussel (VUB), I had the opportunity to work and interact with many enthusiastic and hard working people of the department of Hydrology and Hydraulic Engineering. I would like to thank the members of the department: Okke Batelaan, Yves Meyus, Jo Severeyns, Edward van den Storme, Hilde De Coninck, Boud Verbeiren, El Houcyne El Idrisy, Jan Cools, Abdolreza Bahremand, Solomon Tuccu, Jan Coruly, Justius Rwetabula, Charles Magori, Anja Cosemans and Le Quoc Hung. These people, in one way or the other, had helped to make my stay at the VUB so enjoyable.

I would like to thank my Palestinian friends, Abdelghany Moshtaha, Moustafa Jarar, Mohamed Ghazal, Feras melhem, Diab Kadah, Mazen El Shaer, Maher El Behaisy and his wife Samah, Jihad El Najjar and Kamal El Safady.

I would express my gratitude to my parents, brothers and sisters, as they always remained very close, loving and supporting me from Palestine.

I would like to thank my beautiful wife Amal for her love, care and support throughout my study. Amal, you are really the pillar of my life.

Last not but least to my lovely daughter Diana and to my wonderful sons Ramez, Mohamed and Ahmed. You always bring inspiration, meaning and purpose to my life, I love you all.

ABSTRACT

Hydrogeological Study and Artificial Recharge Modeling of the Gaza Coastal Aquifer Using GIS and MODFLOW

by

Adnan M. Aish

Doctor of Philosophy Degree in Applied Sciences
(Water Resources Engineering)
Department of Hydrology and Hydraulic Engineering
Faculty of Applied Sciences
Vrije Universiteit Brussel

This research work investigates the first phase of a feasibility study on the impact of artificial recharge from a planned wastewater treatment plant on the groundwater quantity and quality of the coastal aquifer in the Gaza Strip, Palestine. During September 2001 to August 2002, an extensive program of hydrogeological investigation and laboratory analysis of soil samples were undertaken to achieve the most reliable characterization of the subsoil and eventually to assist in the design and implementation of a pilot artificial recharge system for treated wastewater to groundwater.

The main concerns of the hydrogeological study are to determine the hydrological parameters, lithological description, and geological setting. The study area extends over 336,000 m², of which 212,000 m² is used for a

Abstract

treatment plant and artificial recharge basin. Three sets of boreholes have been drilled. The first set consists of 19 shallow boreholes that penetrate the silty clay layer and the underlying sandstone (kurkar). The second set consists of five boreholes that penetrate the unsaturated zone to at least 5 m below the groundwater level. The last set consists of three deep boreholes and one pumping well. The deep boreholes were drilled at 100 m to 120 m depth going through the kurkar and clay formations. The pumping well was drilled at 156 m reaching the Saqiye formation. Packer tests were carried out to determine the hydraulic conductivity of the unsaturated zone. Also, 5 infiltration tests were conducted to assess the infiltration capacity at the location of the proposed artificial recharge. In addition, a pumping test was also carried out to determine the hydraulic properties of the aquifer.

In the local model of the artificial recharge simulation, an analytical and numerical solution of the transient groundwater flow is used to predict the time-dependency of the groundwater response in case of the planned artificial infiltration pond of the wastewater treatment plant. The maximum rise of the groundwater mound after 100 days would be 14 m in the center of the infiltration pond and about 12 m at the edges.

Regional groundwater flow simulations are made using the three-dimensional numerical model MODFLOW. The groundwater mounding has been simulated with a constant recharge of 60000 m³/d, and an infiltration rate of 0.75 m/d, while all other hydrogeological conditions are assumed as present conditions. The simulation shows that the groundwater mound beneath the center of the recharge basin can be expected to rise to about 15 m above the

Abstract

present water table, and after about 2 years will be a slight increment in the groundwater mound. The native groundwater downstream of the recharge area will gradually be influenced by the water originating from the infiltrated water and the cone of depression will diminish substantially due to the infiltration.

In the solute transport model MT3D we assumed the infiltration water is at a hypothetical conservative concentration of 100 mg/l that no absorption or adsorption solute is present, and that the initial concentration in the aquifer is 0 mg/l. In the analysis of the results, the 100 mg/l of solute will be considered as the reference concentration (100% injected water) and the simulated concentration in the aquifer will be expressed relative to this value. The results indicate that 90% of the infiltrated water will be mixed with the aquifer water after 1 year beneath the recharge area with decreasing percentages in the surrounding area.

SYMBOLS AND ABBREVIATIONS

Symbol	Description	Units
Al ³⁺	Aluminium	mg/l
As ³⁺	Arsenic	mg/l
B ⁻	Boron	mg/l
BOD	Biochemical Oxygen Demand	mgO ₂ /l
Ca ²⁺	Calcium	mg/l
Cd ²⁺	Cadmium	mg/l
Cl ⁻	Chloride	mg/l
CN ⁻	Cyanide	mg/l
Co ³⁺	Cobalt	mg/l
COD	Chemical Oxygen Demand	mgO ₂ /l
Cr ²⁺	Chromium	mg/l
Cu ⁺	Copper	mg/l
DO	Dissolved Oxygen	mg/l
E.C	Electrical Conductivity	μs/cm
F ⁻	Fluoride	mg/l
FC	Faecal Coliforms (Colony Forming Unit) CFU/100ml	
Fe ²⁺	Iron	mg/l
Hg ⁺	Mercury	mg/l
K ⁺	Potassium	mg/l
Mg ²⁺	Magnesium	mg/l
Mn ²⁺	Manganese	mg/l
Na ⁺	Sodium	mg/l
NH ₄ ⁺ -N	Ammonia as Nitrogen	mg/l
Ni ²⁺	Nickel	mg/l
N-KjD	Kjeldahl Nitrogen	mg/l
NO ₃ ⁻ -N	Nitrate as Nitrogen	mg/l
Pb ²⁺	Lead	mg/l

Symbols and Abbreviations

pH	Acidity	
PO_4^{3-} -P	Phosphate	mg/l
Se^{2+}	Selenium	mg/l
SO_4^{2-}	Sulfate	mg/l
TDS	Total Dissolved Solids	mg/l
TS	Total Solids	mg/l
TSS	Total Suspended Solids	mg/l
TVSS	Total Volatile Suspended Solid	mg/l
Zn^{2+}	Zinc	mg/l

ABBREVIATIONS

GIS	Geographic Information System
HMOC	Hybrid Method of Characteristics
MMOC	Modified Method of Characteristics
MOC	Method of Characteristic
msl	Mean sea level
NNE	North North East
PNA	Palestinian National Authority
PWA	Palestinian Water Authority
SSW	South South West
WHO	World Health Organization
WWTP	Waste Water Treatment Plant

TABLE OF CONTENTS

LIST OF PUBLICATIONS.....	IV
ACKNOWLEDGEMENT	VI
ABSTRACT	VIII
SYMBOLS AND ABBREVIATIONS.....	XII
TABLE OF CONTENTS.....	XIV
LIST OF FIGURES	XVIII
LIST OF TABLES	XXI
Chapter 1: General introduction.....	1
1.1 General.....	1
1.2 Scope and objectives	3
1.3 The structure of dissertation	3
Chapter 2: General literature review	5
2.1 History of artificial recharge	5
2.2 Methods for artificial recharge	5
2.2.1 Infiltration basins	5
2.2.2 Well infiltration.....	6
2.3 Soil clogging.....	6
2.4 Treatment of wastewater for aquifer recharge.....	8
2.5 Groundwater modeling.....	10
2.5.1 General groundwater flow equations.....	10
2.5.2 Numerical methods to solve equations.....	16
2.5.2.1 Finite difference methods	17
2.5.2.2 Finite elements methods.....	18
2.5.3 Solute transport.....	21

Table of Contents

2.5.4	Numerical solutions of solute transport equations.....	23
2.6	Computational tools.....	25
2.6.1	Visual MODFLOW.....	25
2.6.2	MODPATH	26
2.6.3	MT3D	26
2.7	Geographic Information Systems (GIS) tools	27
2.7.1	Arc-View.....	27
2.7.2	WetSpas.....	27
Chapter 3: Description of the study area		29
3.1	Geography and demography.....	29
3.2	Climate	30
3.2.1	Temperature.....	30
3.2.2	Reference crop evapotranspirations (ET _o)	31
3.2.3	Rainfall	31
3.3	Topography	33
3.4	Soil	34
3.5	Geology.....	35
3.6	Hydrogeology	36
3.7	Water quality	38
3.7.1	Chloride.....	38
3.7.2	Nitrate.....	39
3.8	Wastewater treatment	41
Chapter 4: Hydrogeological study.....		43
4.1	Location and site description.....	43
4.2	Site investigation	44

Table of Contents

4.3	Soil permeability	48
4.3.1	Field permeability (packer test)	48
4.3.2	Permeability from grain size	51
4.3.3	Infiltration tests	54
4.4	Pumping test	57
4.5	Water quality	61
4.6	Summary	67
Chapter 5:	Groundwater mound modeling (Local model)	69
5.1	Analytical solution.....	69
5.2	Numerical modeling.....	73
5.2.1	The conceptual model and grid design.....	73
5.2.2	Model construction	74
5.2.3	Model input parameters.....	75
5.2.4	Results	76
5.3	Comparison of numerical and analytical results	78
5.4	Summary.....	79
Chapter 6:	Regional groundwater modeling	81
6.1	Conceptual model and grid design	81
6.2	Model input.....	83
6.2.1	Hydraulic parameters	83
6.2.2	Pumping wells	84
6.2.3	Settlements abstraction.....	86
6.2.4	Recharge.....	87
6.2.5	Return flows	88
6.3	Model calibration	89

Table of Contents

6.4	Artificial recharge simulation.....	94
6.4.1	Groundwater mound.....	94
6.4.2	Predicted groundwater table	97
6.4.3	Particles pathlines	100
6.4.4	Solute transport model	103
6.5	Summary.....	106
Chapter 7: Conclusions and Recommendations.....		107
7.1	Conclusion about the hydrogeological study	107
7.2	Conclusion about the groundwater modeling	109
7.3	Conclusion about the artificial recharge simulation	110
7.4	Conclusion about water migration and solute transport.....	111
7.5	Recommendations	113
References		115
Appendix: 1.....		125
Appendix: 2.....		189

LIST OF FIGURES

Figure 2.1 Finite difference Grid	18
Figure 2.2 Discretisation of the flow domain in finite element	19
Figure 2.3 Different types of finite elements	20
Figure 3.1 Location map of the Gaza Strip	29
Figure 3.2 Mean monthly maximum, minimum and average temperature (C°) for the Gaza Strip (period 1970 – 2000)	30
Figure 3.3 Mean monthly reference crop evapotranspiration for the Gaza Strip	31
Figure 3.4 Temporal distributions of annual rainfall in the Gaza strip	32
Figure 3.5 Spatial distribution of average annual rainfall in the Gaza Strip (period 1974-2000)	32
Figure 3.6 Topography of the Gaza Strip (m)	33
Figure 3.7 Soil map of the Gaza Strip (PWA, 2003)	34
Figure 4.1 View of the study area	43
Figure 4.2 Geographic location of the study area with indication of the drilled boreholes and infiltration test ponds	44
Figure 4.3 Geological cross-section A-A'	47
Figure 4.4 Geological cross-section B-B'	47
Figure 4.5 Inflatable Packer test used in the field	48
Figure 4.6 Hydraulic conductivity vs. depth using Hazen formula.....	53
Figure 4.7 Observed infiltration rate in the infiltration test ponds, fitted with theoretical Philip equation	55
Figure 4.8 Comparison of hydraulic conductivity vs. depth in sandy material	56

List of Figures

Figure 4.9 Results of the pumping test analysis by means of a Theis-curve fit	58
Figure 4.10 Comparison of estimated hydraulic conductivity vs. depth	60
Figure 4.11 Location of the municipal wells in the north of the Gaza Strip	63
Figure 4.12 Chloride and nitrate trend near the study area	65
Figure 4.13 Trilinear diagram of major –ion composition of groundwater	66
Figure 5.1 Diagrammatic representation of the rise of the water table beneath a rectangular recharging area.....	70
Figure 5.2 MOUNDHT interface: A sample front section view	71
Figure 5.3 Height of the groundwater mound under the center of the basin ..	72
Figure 5.4 Conceptual model and grid design	73
Figure 5.5 Model layers: 1- Sand with fine gravel, 2- Clay, 3- Sandstone, 4- Clay, 5-Sandstone, 6- Clay and 7- Sandstone.....	74
Figure 5.6 Height of the groundwater mound beneath the recharge basin calculated with the numerical model.....	76
Figure 5.7 Groundwater mound after 100 days beneath recharge basin with five observation wells	77
Figure 5.8 Comparison of numerical and analytical results showing the rise of the groundwater mound in the center of the infiltration basin	78
Figure 6.1 Plan of the model area showing the grid size and boundary conditions	82
Figure 6.2 Model topography and 3-D view of stratigraphy in Gaza Strip.....	83
Figure 6.3 Location of Municipal and agricultural wells.....	85
Figure 6.4 Settlements locations in the Gaza Strip.....	86

List of Figures

Figure 6.5 Annual groundwater recharge, calculated by the WetSpass model	87
Figure 6.6 Simulated groundwater heads with distributed observation well...	90
Figure 6.7 Long-term records of water levels (m.s.l.) near the study area....	91
Figure 6.8 Calibration graph of observed vs. calculated water levels in observation Wells	92
Figure 6.9 Height of the groundwater mound beneath the recharge basin for the first 100 days, simulated with the regional model	94
Figure 6.10 Groundwater mound after 100 days beneath the recharge area	95
Figure 6.11 Groundwater mound beneath the recharge basin	96
Figure 6.12a Simulated water levels in the north of the Gaza Strip	97
Figure 6.12b Simulated groundwater levels with infiltration after 1 year.....	98
Figure 6.12c Simulated groundwater levels with infiltration after 2 years.....	98
Figure 6.12d Simulated groundwater levels with infiltration after 5 years.....	99
Figure 6.12e Simulated groundwater levels with infiltration after 10 years....	99
Figure 6.13a Pathlines for virtual particles infiltrated after 1 year.	100
Figure 6.13b Pathlines for virtual particles infiltrated after 2 years... ..	101
Figure 6.13c Pathlines for virtual particles infiltrated after 5 years.....	101
Figure 6.13d Pathlines for virtual particles infiltrated after 10 years.....	102
Figure 6.14a Simulation of mass transport after 1 year	104
Figure 6.14b Simulation of mass transport after 2 years.....	104
Figure 6.14c Simulation of mass transport after 5 years.....	105
Figure 6.14d Simulation of mass transport after 10 years.....	105
Figure 7.1 Comparison of numerical and analytical results	111

LIST OF TABLES

Table 2.1 Palestinian treated wastewater reuses guidelines	9
Table 3.1 Treatment plant in the Gaza Strip	41
Table 3.2 The quality of influent and effluent of wastewater in the Gaza Strip	42
Table 4.1 Summary of hydraulic conductivity of the packer test	50
Table 4.2 Interpreted hydraulic conductivity using Hazen Formula	52
Table 4.3 Comparison of methods used for the pumping test	59
Table 4.4 Summary of hydraulic conductivity test results	61
Table 4.5 Chemical analysis of groundwater from observation wells	63
Table 4.6 Chemical analysis for municipal wells in the north of the Gaza Strip (Autumn 2002).....	64
Table 5.1 Hydraulic parameters value for model inputs.....	75
Table 6.1 Hydraulic parameters value for model inputs.....	84
Table 6.2 Summary of steady-state calibration statistics.....	91
Table 6.3 Summary of water balance in the Gaza Strip for year 2000	93

Chapter 1: General introduction

1.1 General

Water is the most abundant substance on the earth, the principal constituent of all living things, and a major force constantly shaping the surface of the earth. It is also a key factor in conditioning the earth for human existence and in influencing the civilization process.

The hydro-sciences deal with the earth's water resources with regard to their distribution, circulation, their physical and chemical properties, and their interaction with the environment, including interaction with all living things, especially human beings.

In the last decades the interest and the extent of groundwater investigations have increased rapidly with the growing environmental concern. The groundwater investigations have developed from quantifying the groundwater resources for groundwater exploitation to complex problems involving three-dimensional flow and transport. The present groundwater problems include determination, monitoring, protection, and prediction of the groundwater quality. The most common method to assess these complex problems and to predict how a future situation will behave with and without possible actions taken is to apply numerical models.

Many numerical models have been developed for a large variety of purposes. However, as the numerical models get more comprehensive and complex the requirements for detailed and reliable input parameters increase. Many types

of hydrogeological parameters estimation techniques exist and it's important to choose the proper method to achieve the most suitable estimates.

Water is generally scarce in the Palestine region. Sustainable water management calls not only for careful use of freshwater but also for reuse of treated wastewater. Indications of the need for changing the current management are seen in the lowering of the water table and the increasing chloride concentrations in the groundwater. Reclaiming wastewater involves management of groundwater recharge by introducing treated wastewater into the aquifer and taking advantage of either the raised groundwater levels or the actual water volume or a combination of the two.

The increasing demand for water has increased awareness towards the use of artificial recharge to augment groundwater supplies. Stated simply, artificial recharge is a process by which excess surface water is directed into the ground - either by spreading on the surface, by using recharge wells or by alternating natural conditions to increase infiltration - to replenish an aquifer. It refers to the movement of water through man-made systems from the surface of the earth to underground water bearing strata where it may be stored for future use. Artificial recharge is a way to store water underground in times of water surplus to meet demand in times of shortage (N. N., 1994).

1.2 Scope and objectives

The artificial recharge project in the Gaza Strip is aimed to break the trend of decreasing groundwater table and to control sea water intrusion in coastal aquifer, by using reclaimed wastewater. The objectives of this research work are:

- Investigate and study hydrogeological properties, lithological description and geological setting of the artificial recharge area.
- Construct a groundwater model, to predict water levels extent of the recharge mound, spreading radius, and transport time.
- Determine if the proposed discharge of treated wastewater to the site would cause excessive mounding of water table.
- Investigate and assess the impact of artificial recharge of treated wastewater on groundwater migration and to determine the potential quantity and quality of water that can be recharged.

1.3 The structure of dissertation

The dissertation is organized into different chapters that range from chapter 1 to 7 and two appendices. Chapter 1: is a general introduction with an overview of the groundwater investigations, discussion about awareness the use of artificial recharge to augment groundwater supplies and the objectives of the research. Chapter 2: begins with a brief review of the history and methods of artificial recharge. It also discusses the main soil clogging problems in infiltration systems for the artificial recharge of groundwater. Its highlights the Palestinian Standards for treated wastewater reuse. Its also

Chapter 1 : Introduction

discusses the groundwater modeling, computational tools and groundwater flow equations. It highlights about GIS and its use in hydrologic modeling environment, and discusses methods of integration GIS and WetSpass with distributed hydrologic modeling. Chapter 3: this chapter starts with a brief description of the Gaza Strip, and discussions of the soil and hydrogeology of the Gaza coastal aquifer. Also in this chapter, a brief description of the groundwater quality and wastewater treatment plants in the Gaza Strip.

Chapter 4: discusses the general site investigation and highlights the geological setting of the study area. It also describes measurement and experimental techniques used as field permeability (packer test), permeability from grain size and infiltration tests. Chapter 4 discusses pumping test and the Theis method. Chapter 5: discusses the analytical solution of groundwater mound and numerical modeling of local model of the recharge area.

Chapter 6: provides a modeling approach for the Gaza coastal aquifer, to derive the artificial recharge simulation. It also discusses the predicted groundwater table, particles tracking and solute transport in the recharge area. Chapter 7: gives conclusions and recommendations about the research work described in this dissertation and outlines of future work in similar research direction. Appendix 1: provides a grain size distribution test results and grain size distribution graphs. It also provides the lithologic description of drilled boreholes in study area. In addition, provides infiltration and pumping test data. Appendix 2: provides some maps of the Gaza strip used in WetSpass model.

Chapter 2: General literature review

2.1 History of artificial recharge

Artificial recharge applications have been documented from the early 19th century, when European countries first attempted to ease the stress on their groundwater supplies. According to European Environment Agency (Lallana and Krinner 2001), shows a growing increase in artificial recharge is noted in several countries as Belgium, Denmark, Finland, Greece, the Netherlands, Poland, Spain and Switzerland. Other countries in which artificial recharge schemes are operating include Australia, Austria, Hungary, Iran, Israel, Jamaica, Morocco and South Africa (Jos, H. P., 1996).

The motivation for artificial recharge is highly dependent of the country. While some countries practice recharge to match pre-development levels, others go beyond these levels to create temporary storage for dry seasons. Coastal regions are more concerned about saline water intrusion, and industrialized countries might see artificial recharge as an alternative means for treated wastewater disposal (N. N., 1994).

2.2 Methods for artificial recharge

2.2.1 Infiltration basins

Infiltration basins require a substantial amount of land area with a suitable geology, allowing the water to infiltrate into the aquifer and percolate to the groundwater table. It is simple to maintain and regular restoration of infiltration capacity and removal of clogging layers is relatively easy though time consuming. This method also allows for natural, quality improving processes

to take place in the infiltration ponds and subsoil. Construction is normally comparatively simple and low cost. Impermeable topsoil may, however, rise the costs (Herman B., 1996). The infiltration from a recharge basin produces a groundwater mound above the original water table. The groundwater mound grows over time and once the infiltration stops, it decays gradually.

2.2.2 Well infiltration

Infiltration wells or injection wells are used where permeable soils and/or sufficient land area for surface infiltration are not available. Well infiltration calls for very high quality of the infiltration water if clogging of the well screen and the aquifer in the vicinity of the well is to be avoided. The construction is more complicated and costly and restoration of the hydraulic conductivity around the wells may be unfeasible if not impossible. The best strategy for dealing with clogging of recharge wells is to prevent it by proper treatment of the water before injection. This means removal of suspended solids, assimilable organic carbon, nutrients like nitrogen and phosphorous, and microorganisms (Herman, 2002).

2.3 Soil clogging

The main problem in infiltration systems for artificial recharge of groundwater is clogging on the infiltrating surface and resulting reduction in infiltration rates. Clogging is caused by physical, biological and chemical processes (Baveye et al., 1998). Physical processes are accumulation of inorganic and organic suspended solids in the recharge water, such as clay and silt

particles, algae cells, microorganism cells and fragments, and sludge flocs in sewage effluent. Another physical process is downward movement of fine particles in the soil that were in the applied water or in the soil itself, and accumulation of these fine particles at some depth where the soil is denser or finer, and where they form a thin subsurface clogging layer. The depth of this layer ranges from a few mm to a few cm or more. In the soils literature, this fine-particle movement and accumulation deeper down are called “wash out – wash in” (Sumner and Stewart, 1992).

Biological clogging processes include:

- Accumulation of algae and bacterial flocs in the water on the infiltrating surface; and
- Growth of microorganisms on and in the soil to form biofilms and biomass (including polysaccharides and other metabolic end products) that block pores and/or reduce pore sizes.

Chemical clogging processes include precipitation of calcium carbonate, gypsum, phosphate ($\text{PO}_4^{3-}\text{-P}$), and other minerals, solids and deposits in the soil. Bacteria also produce gases (nitrogen, methane) that block pores and accumulate below clogging layers to create vapor barriers to infiltration. Gas is also formed in soils below recharge basins or in trenches or wells when the recharge water contains entrained or dissolved air and/or is cooler than the soil or aquifer itself. The water then warms up in the soil or aquifer; air goes out of solution and forms entrapped air, which reduces the hydraulic conductivity (Dillon and Pavelic, 1996).

2.4 Treatment of wastewater for aquifer recharge

Typical treatment schemes in developed countries include at least primary and secondary steps. The primary level usually acts based on physical properties, and it serves to remove fast decantable and floating material. The secondary step is generally a biological process used to remove most of the remaining dissolved and suspended organic material. Due to the negative effects observed when returning secondary effluents to the environment, there is a third step or tertiary treatment which refers to the refining of the quality of the secondary treatment, and may have different meanings in each country or region depending on their specific problems.

Generally, the third step is used to remove nitrogen and phosphorus; however, the development of compact processes to eliminate these contaminants in previous stages, is increasingly raising doubts about the idea of treatment schemes by steps.

Palestinian Authority established its own standards for wastewater reuse which was based on other countries standards (Zubiller, 2002). These standards take into consideration the quality of treated effluent and treatment methods. Table 2.1 shows Palestinian Standards for treated wastewater reuse.

Table 2.1 Palestinian treated wastewater reuses guidelines (Zubiller, 2002)

Quality parameters (mg/l)	Aquifer recharge	Sea 500 m inside	Parks, Playgrounds	Forests	Seeds as corn	Productive trees (citrus, olive)
BOD	40	60	40	60	60	45
COD	150	200	200	200	200	150
DO	> 1	> 1	> 0.5	> 0.5	> 0.5	> 0.5
TDS	1500	-	1200	1500	1500	1500
TSS	50	60	30	50	50	40
NO ₃ -N	15	25	50	50	50	50
NH ₄ -N	10	5	50	-	-	-
PO ₄ -P	15	5	30	30	30	30
Cl	600	-	350	500	500	400
SO ₄	1000	1000	500	500	500	500
Na	230	-	200	200	200	200
Mg	150	-	60	60	60	60
Ca	400	400	400	400	400	400
AL	1	5	5	5	5	5
As	0.05	0.05	0.1	0.1	0.1	0.1
Cu	0.2	0.2	0.2	0.2	0.2	0.2
F	1.5	-	1	1	1	1
Fe	2	2	5	5	5	5
Mn	0.2	0.2	0.2	0.2	0.2	0.2
Ni	0.2	0.2	0.2	0.2	0.2	0.2
Pb	0.1	0.1	0.1	1	1	1
Se	0.02	0.02	0.02	0.02	0.02	0.02
Cd	0.01	0.01	0.01	0.01	0.01	0.01
Zn	5	5	2	2	2	2
CN	0.1	0.1	0.05	0.05	0.05	0.05
Cr	0.05	0.5	0.1	0.1	0.1	0.1
Hg	0.001	0.001	0.001	0.001	0.001	0.001
Co	0.05	1	0.05	0.05	0.05	0.05
B	1	2	0.7	0.7	0.7	0.7
pH	6-9	6-9	6-9	6-9	6-9	6-9
FC	1000	50000	200	1000	1000	1000

(-): un determined

2.5 Groundwater modeling

A groundwater model is a representation of reality and, if properly constructed, it can be a valuable predictive tool used for management of groundwater resources (Wang and Anderson, 1982). A mathematical model simulates groundwater flow indirectly by means of governing equation though to represent the physical processes that occur in the system, together with equations that describe heads or flows along the boundaries of the model. For time-dependent problems, an equation describing the initial distribution of heads in the system is also needed (Anderson and Woessner, 1992).

2.5.1 General groundwater flow equations

Differential equations that govern the flow of groundwater flow can essentially represent the groundwater flow system derived from the basic principles of groundwater flow hydraulics. The main flow equation for saturated groundwater flow is derived by combining a water balance equation with Darcy's law, which leads to a general form of the 3-D groundwater flow governing equation:

$$\frac{\partial}{\partial x} \left(K_x \frac{\partial h}{\partial x} \right) + \frac{\partial}{\partial y} \left(K_y \frac{\partial h}{\partial y} \right) + \frac{\partial}{\partial z} \left(K_z \frac{\partial h}{\partial z} \right) + R(x,y,z) = S_s \frac{\partial h}{\partial t} \quad (2.1)$$

Where K_x , K_y and K_z , are the hydraulic conductivity components in the x,y and z direction (LT^{-1}), h is the hydraulic head (L), R is the local source or sink of water per unit volume (T^{-1}), S_s is the specific storage coefficient (L^{-1}) and t is the time (T).

Darcy's law

In differential form, Darcy's law is expressed as:

$$q = -K \cdot \text{grad} (h) \quad (2.2)$$

where q is the groundwater flux (LT^{-1}), K is the conductivity tensor (LT^{-1}) and $\text{grad} (h)$ is the gradient operator.

This equation clearly shows that the cause of groundwater movement is the difference in the hydraulic potential. The potential is a function of all three-space coordinates, that is $h = h(x,y,z)$, the rate of change of head with position giving the gradient, which multiplied by the conductivity yields the groundwater flux (Wang and Anderson, 1982).

The hydraulic conductivity is represented by a second order tensor that takes into account anisotropic conditions. Usually, anisotropy is only considered in the vertical and horizontal direction, hence

$$q_x = -K_x \frac{\partial h}{\partial x} \quad (2.3a)$$

$$q_y = -K_y \frac{\partial h}{\partial y} \quad (2.3b)$$

$$q_z = -K_z \frac{\partial h}{\partial z} \quad (2.3c)$$

Where q_x , q_y , q_z are the three components of the flux, and K_x , K_y , K_z the hydraulic conductivity values in the horizontal (x,y) and vertical (z) direction.

In case of isotropic conditions, $K_x = K_y = K_z$ each component of q is the same

scalar multiple K of the corresponding component of $-\text{grad}(h)$, such that the vectors q and $-\text{grad}(h)$ both point in the same direction.

Continuity equation for steady state flow: Law of conservation of mass

Darcy's law, equation (2.2) summarizes much of the physics of groundwater flow by relating the flux vector to the gradient of the potential. Continuity or conservation is a second important law. For steady state condition, continuity requires that the amount of water flowing in to a representative elemental volume is equal to the amount flowing out, if the elemental volume contains no source or sink.

The existence of steady state condition implies that head and the flow are independent of time. The sign convention is that inflows are positive and outflows negative (Wang and Anderson, 1982).

The net change in the discharge rate in the x direction is $-\frac{\partial q_x}{\partial x} \Delta v$, where

$\Delta v = \Delta x \Delta y \Delta z$ is the elemental volume. Change in the discharge rate in the y

direction is $-\frac{\partial q_y}{\partial y} \Delta v$ and the net change in the discharge in the z direction

is $-\frac{\partial q_z}{\partial z} \Delta v$. The sum, $\frac{\partial q_x}{\partial x} \Delta v - \frac{\partial q_y}{\partial y} \Delta v - \frac{\partial q_z}{\partial z} \Delta v$, must be equal to zero.

Dividing by Δv gives the continuity equation for steady state conditions,

$$\frac{\partial q_x}{\partial x} + \frac{\partial q_y}{\partial y} + \frac{\partial q_z}{\partial z} = 0 \tag{2.4}$$

In case of steady state conditions with sources or sinks, the net inflow in an

elemental volume flows the source or sink should equal zero, or

$$-\frac{\partial q_x}{\partial x} - \frac{\partial q_y}{\partial y} - \frac{\partial q_z}{\partial z} + R = 0 \quad (2.5)$$

where R is the source (positive) or sink (negative) amount of water per volume of soil (Δv).

Transient conditions the general flow equation is formulated by applying the law of conservation of mass over an elemental volume of an aquifer situated in the flow field in function of time. Continuity requires that the net inflow into the elemental control volume must be equal to the rate at which water is accumulating within the volume under investigation, which is outflow minus inflow equals change in storage.

The change in storage is represented by the specific storage, or specific storage coefficient, S_s as explained in equation (2.1) which is defined as the volume of water released from storage per volume of soil for a unit decline in hydraulic head, that is:

$$S_s = \frac{\Delta W}{\Delta h \Delta v} \quad (2.6)$$

where ΔW is the volume of water released from storage. The rate of change in storage is then given by:

$$\frac{\Delta W}{\Delta t} = S_s \frac{\Delta h}{\Delta t} \Delta v \quad (2.7)$$

Chapter 2 : Literature review

Combining all terms and dividing by ΔW yields the general form of the mass balance equation as:

$$-\frac{\partial q_x}{\partial x} - \frac{\partial q_y}{\partial y} - \frac{\partial q_z}{\partial z} + R = S_s \frac{\partial h}{\partial t} \quad (2.8)$$

where this equation is combined with Darcy's law, the general flow equation (2.1) is obtained for steady state flow, the term $\frac{\partial h}{\partial t}$ in equation (2.1) is zero

and the equation thus reduces to

$$\frac{\partial}{\partial x} \left(K_x \frac{\partial h}{\partial x} \right) + \frac{\partial}{\partial y} \left(K_y \frac{\partial h}{\partial y} \right) + \frac{\partial}{\partial z} \left(K_z \frac{\partial h}{\partial z} \right) + R = 0 \quad (2.9)$$

In most cases for field applications, it is convenient to work in two dimensions since thickness of strata is often small in comparison to the lateral extent. For a confined aquifer with thickness D , where $K = K_x = K_y$, the two dimensional form of equation (2.1) becomes:

$$\frac{\partial}{\partial x} \left(T \frac{\partial h}{\partial x} \right) + \frac{\partial}{\partial y} \left(T \frac{\partial h}{\partial y} \right) + R = S_s \frac{\partial h}{\partial t} \quad (2.10)$$

where T is the transmissivity given by $T = KD$ (L^2T^{-1}), with $K = K_x = K_y$, S is the aquifer storage coefficient, which is dimensionless, given by $S = S_s D$, and R is the overall source or sink rate per surface area of aquifer. For steady state conditions equation (2.10) becomes:

$$\frac{\partial}{\partial x} \left(T \frac{\partial h}{\partial x} \right) + \frac{\partial}{\partial y} \left(T \frac{\partial h}{\partial y} \right) + R = 0 \quad (2.11)$$

In the case of phreatic aquifer, a horizontal flow approximation is a little more complicated, because the upper boundary of the aquifer is a water table, which can fluctuate in time. One consequence is that the transmissivity becomes variable in time, as the saturated thickness of the aquifer fluctuates. Integrating the saturated flow equation over the vertical yields,

$$\frac{\partial}{\partial x} \left(K(b-a) \frac{\partial h}{\partial x} \right) + \frac{\partial}{\partial y} \left(K(b-a) \frac{\partial h}{\partial y} \right) + q_a + q_b = S_s (b-a) \frac{\partial h}{\partial t} \quad (2.12)$$

where $D = b-a$ is the thickness of the aquifer.

Another complication is the fact when part of the porous medium change from saturated to unsaturated, or vice versa, The flux coming from the unsaturated zone, q_b , consists of recharge, R , which is the natural flow of water through the unsaturated zone feeding the groundwater at the water table, but should also include effects due to changes in water storage in the unsaturated zone.

However, an approximation can be obtained, by assuming that pseudo steady state water content profiles exist in the unsaturated zone above the water table, such that a change in water table elevation, Δh , results in a change of amount of water stored equal to the difference between the original and final water content profiles. This amount is equal to $\alpha \Delta h$, where α is the specific yield. The specific yield is defined as the amount of water released per unit water table surface and per unit decline of the water table position. The upper

boundary, $z = b$, represents the position of the water table, and because of relation, also should coincide with the hydraulic potential at the water table, and hence be approximately equal to the average potential, $b \cong h$ (De Smedt, 2003). The general horizontal flow equation for a phreatic aquifer,

$$\frac{\partial}{\partial x} \left(K(h-a) \frac{\partial h}{\partial x} \right) + \frac{\partial}{\partial y} \left(K(h-a) \frac{\partial h}{\partial y} \right) + q_a + R = [S_s (h-a) + \alpha] \frac{\partial h}{\partial t} \quad (2.13)$$

This is a non-linear partial differential equation. Usually, changes in storage due to compaction or expansion of porous medium can be ignored with respect to changes in storage due to variations of the water table position. One last approximation assumes that the water table elevation is approximately known, such that an approximate transmissivity can be defined, $T = K(b-a)$ and equation 2.13 can be written as

$$\frac{\partial}{\partial x} \left(T \frac{\partial h}{\partial x} \right) + \frac{\partial}{\partial y} \left(T \frac{\partial h}{\partial y} \right) + q_a + R = \alpha \frac{\partial h}{\partial t} \quad (2.14)$$

2.5.2 Numerical methods to solve equations

Ground water flow equations are usually not easy to solve analytically. This is because either the flow is described by a partial differential equation or usually the medium properties are heterogeneous. In such cases, numerical solution techniques can be used to obtain approximations.

Two major classes of numerical methods have been accepted for solving the groundwater flow equation. These are finite difference methods and finite

element methods. Each of these includes a variety of subclasses and implementation alternatives.

2.5.2.1 Finite difference methods

The basic idea is to replace partial derivatives in the flow equation by finite differences, which are ratios of the change of the variable over a small but finite distance:

$$\frac{\partial h}{\partial x} = \lim_{\Delta x \rightarrow 0} \frac{\Delta h}{\Delta x} \approx \frac{\Delta h}{\Delta x} \quad (2.15)$$

An area of interest is subdivided by a grid into a number of smaller sub-areas (cells) that are associated with nodal points. Nodes can be placed in different manners as shown in Figure 2.1. The difference between them mainly lies in the way in which the flux boundaries are handled. In the block centered approach the flux boundaries are located at the edge of the block. In the mesh-centered grid the boundaries coincide with the nodes. For time-dependent problems, the time is divided into increments, which need not be all equal. The solution obtained is only approximate, the resulting error, that is to say the difference between the time (analytical) solution and the exact solution of the finite difference equation, is termed the truncation error. A computer is needed to solve the finite difference equations, but this introduces an error between the true value and the calculated value, this error is termed the round of error (De Smedt, 1999)

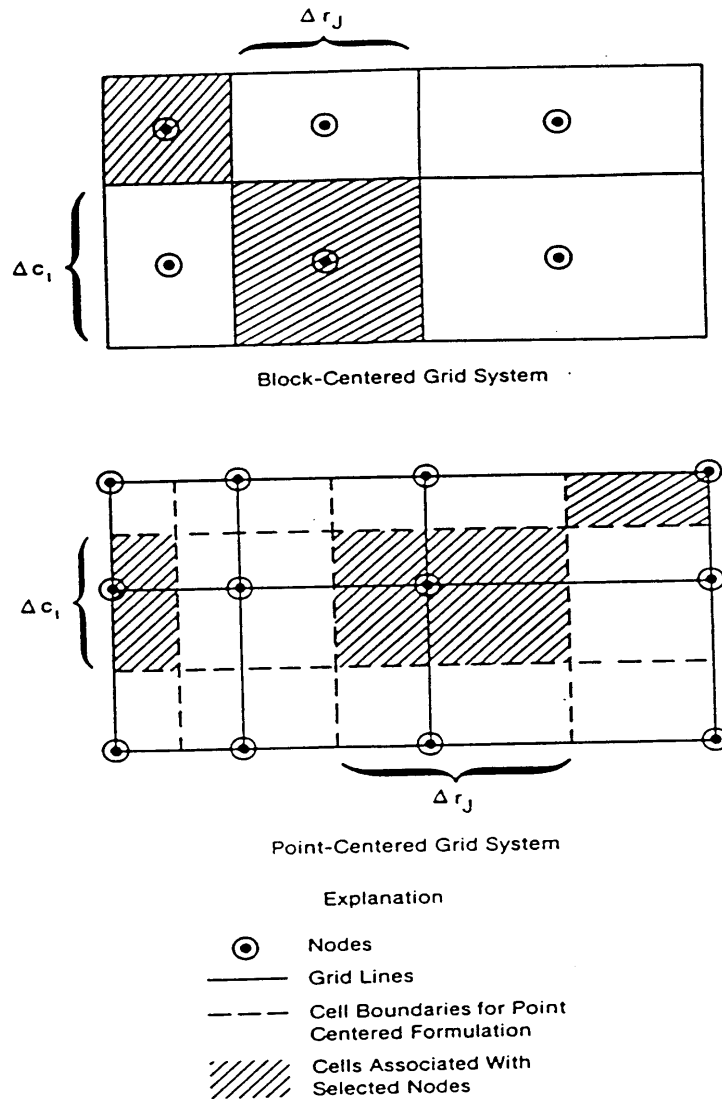


Figure 2.1 Finite difference Grid

2.5.2.2 Finite elements methods

The main idea of the finite element method is to have a larger freedom in the position of the nodes, such that for instance nodes can be placed in interesting locations, the density of the nodes can be chosen according to the expected variations of the variables, and the geometry of the flow domain can

better be approximated. Consider a flow equation, which is a partial differential equation of the form

$$F(h) = 0 \quad (2.16)$$

The flow domain is shown schematically in Figure 2.2. Nodes are positioned arbitrary, such that pattern and spacing in between the node is irregular. The nodes are numbered in an arbitrary order, $n = 1..N$, and the potential in the nodes are denoted as

$$h_n = h(x_n, y_n) \quad (2.17)$$

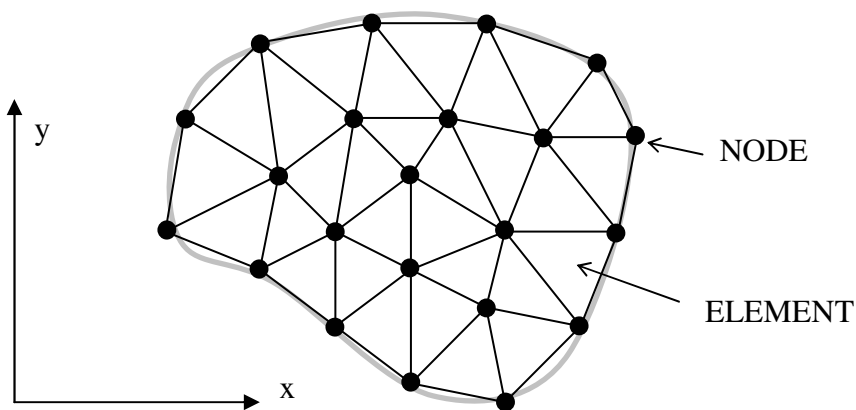


Figure 2.2 Discretisation of the flow domain in finite element

The numerical technique consists of finding approximate values for the nodal potentials and the question is how to obtain N algebraic equations that will enable to calculate the N unknown nodal potentials.

The division of the domain in triangles is not unique, because other arrangements are possible. But also other types of sub-zones and interpolation schemes are possible, as for instance quadrilaterals or triangles with parabolic sides, etc (Figure 2.3). These sub-zones are called finite elements, the main purpose of which is to enable that potentials can be interpolated from nodal values. Hence, an approximate solution, h^* , can be formulated as function of the nodal potentials (De Smedt, 2003).

$$h^* = h^*(h_n, x, y) \tag{2.18}$$

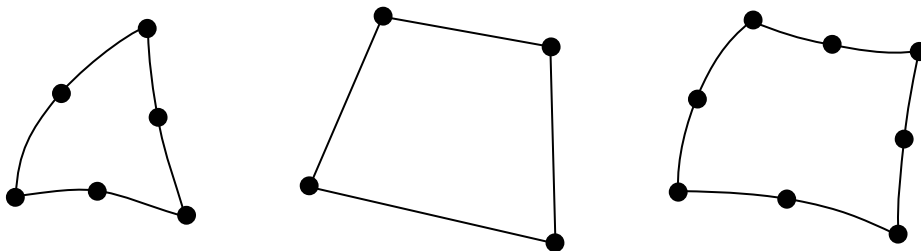


Figure 2.3 Different types of finite elements

At first sight, the finite element technique looks a lot more complicated than the finite difference technique, and this is partly true, although it is also a matter of practice and experience, but a main advantage is the larger flexibility and also accuracy.

2.5.3 Solute transport

The primary transport mechanism by which a pollutant can be transported through a ground water system is advection, which is the movement of a dissolved chemical along with the ground water flow. Hence, knowledge about the direction and magnitude of groundwater flow yields a first insight into the transport of pollutants. The advective flux, ϕ_a , is the mass of solute passing through an elementary cross-sectional area per time [$ML^{-2}T^{-1}$], due to ground water flow, and is given by

$$\phi_a = qC \quad (2.19)$$

In addition to transport by advection, dissolved particles are also subjected to hydrodynamic dispersion, a process accounting for the seemingly random spreading of solutes. Dispersion causes particles to deviate from the macroscopic advective flow paths that do not take into account the actual geometry of the pore space. Hence, some particles will move faster and some slower due to the difference in size of the pores, while also deviations in direction of the flow will because the particles have to move around the solid material. The resulting dispersion is rather random and as such very similar to diffusive spreading, but generally it has a much wider impact on the transport of dissolved chemicals compared to diffusion. Because dispersion resembles diffusion transport, the dispersive flux, ϕ_d [$ML^{-2}T^{-1}$], can be described by a relationship similar to Fick's law of diffusion.

$$\phi_d = -\theta D \nabla C \quad (2.20)$$

where D is a dispersion tensor [L^2T^{-1}] and ∇C the concentration gradient; the water content θ represents the fact that dispersion can only occur in the water filled portion of the pore space.

Combining advection and dispersion yields the total solute flux ϕ [$ML^{-2}T^{-1}$]

$$\phi = \phi_a + \phi_d = qC - \theta D \nabla C \quad (2.21)$$

In addition to transport by advection and dispersion, other processes can affect the transport of solutes, as adsorption of chemicals on the solid material of the porous medium.

The general transport equation can be obtained by combining the effects of all processes (equation 2.22). The total amount of a chemical that can be present in a ground layer per volume of soil is given by the sum of the amount dissolved in the groundwater and the amount adsorbed on the solid material. Taking into account the amounts of water and solid material this is equal to $\theta C + \rho S$, where ρ is the dry bulk density of the solid material [M/L^3]. The rate of change in time of the total amount of a chemical is balanced by the divergence of the advective and dispersive fluxes and by the reaction rates, i.e. (De Smedt, 2003).

$$\frac{\partial(\theta C + \rho S)}{\partial t} = -\nabla \phi - \lambda \theta C = \nabla (\theta D \nabla C) - \nabla (qC) - \lambda \theta C \quad (2.22)$$

where S is the amount of mass absorbed of a certain chemical mass per dry mass of soil (M/M) and λ is a first order reaction rate coefficient (T^{-1}).

2.5.4 Numerical solutions of solute transport equations

The numerical solutions for solute transport are different and rather difficult. This difficulty is essentially due to the advective component of solute transport. Most of the numerical solutions to solute transport equations can be classified as Eulerian or Lagrangian (Zheng and Bennette, 1995).

The method of characteristic (MOC)

The method of characteristic consists of computing the advective term of the transport equation, using moving particles that represent the solute concentrations. First, a set of particles is assigned. The particle has the concentration of the cell where it is located. Then, if only the advective effect is assumed, the concentrations will travel through the flow paths since the advective term is proportional to the velocity vector. Hence, the concentrations will be estimated by a forward particle tracking method. Then having the advective term, these concentrations are injected into the dispersion, sink/sources and chemical reaction terms and solved by Eulerian method, with finite-difference or finite-elements.

Modified method of characteristics (MMOC)

The modified method of characteristics was originally developed to approximate the advection term, but the particles are assigned to fixed coordinates that are the grid nodes and the tracking is no more forward, but rather backward. So, in the MMOC, for each particle, that is the node position, we calculate the preceding position (corresponding to time step $n-1$) from the

present time step n . Assigning immobile coordinates for the particles at each time step saves a lot of time processing and computer storage.

Hence, the modified method of characteristic reduces dramatically the time consuming in the solute transport equation solution. However, the advantage of saving huge computer memory is balanced by numerical problems in zones where sharp fronts of solute concentration are present.

Hybrid method of characteristics (HMOC)

The two previous methods have shown their limitations when applied to solute transport equations. As a matter of fact, to take advantage of the MOC and MMOC, a concept of combining these two methods was developed, the hybrid method of characteristic, referred to as HMOC (Zheng, 1993). The HMOC consists of using the method of characteristic when sharp fronts of solute exist, while away from those zones the modified method of characteristic is used. An automatic choice of the method is based on the solute concentration distribution during the time period, and after each time step.

2.6 Computational tools

2.6.1 Visual MODFLOW

Three-dimensional numerical model MODFLOW (Harbaugh and McDonald, 1996) is applied through the use of the interface a commercial pre- and post-processor software program, the model was developed by USGS. Visual MODFLOW version 3.0 was used to conduct the modeling. MODFLOW numerically evaluates the partial differential equations for groundwater flow (McDonald and Harbaugh, 1988).

The interface of visual MODFLOW is divided into three modules, the Input Module, the Run Module, and the Output Module. The input Module provides users with the ability to create a graphical three-dimensional representation of the study area. The modeler can assign values directly to the study area and the software creates the appropriate files. The Run Module allows the user to alter the parameters and options that are run specific, such as the solver package, recharge and rewetting applications and the tolerances for convergence. The Output Module provides the user with the ability to display all of the modeling and calibration results. Although Visual MODFLOW graphically represents the study area, the inputs, and the outputs, the files are translated and processed by the version of MODFLOW 2000 (Harbaugh, Banta, Hill, and McDonald, 2000).

2.6.2 MODPATH

MODPATH is an extension of MODFLOW to calculate flow paths and travel times of water particles. The model was also developed by USGS. Simulation results obtained with MODFLOW are used as input to MODPATH. The streamlines and travel times of water particles can be calculated starting from the groundwater flow velocities using Darcy's law.

$$v_x = \frac{K}{n_e} \frac{\partial h}{\partial x}; v_y = \frac{K}{n_e} \frac{\partial h}{\partial y}; v_z = \frac{K}{n_e} \frac{\partial h}{\partial z} \quad (2.24)$$

with n_e the effective porosity, which enables to take into account only the mobile fraction of the groundwater that is taking part in the flow (De Smedt, 2003).

2.6.3 MT3D

MT3D is a model for the simulation of pollutant transport. MT3D stands for "Mass Transport in 3 Dimensions". The model was developed by the US Environmental Protection Agency (EPA) as an extension of MODFLOW. Using simulation results of MODFLOW, MT3D will predict the fate of chemicals dissolved in the groundwater in function of advection, dispersion, absorption and decay. Hence, the model uses output files from MODFLOW as input for obtaining the groundwater flows. Boundary conditions for transport can be added together with dispersive and absorptive properties of the ground layers, as well as chemical reaction characteristics.

There are several extensions and improvements of MT3D available, as for instance:

- RT3D: a pollutant transport model for specific pollutants as hydrocarbons that transform into other chemicals or are subjected to more complicated decay processes as in MT3D.

MT3DMS is an extension of MT3D for the solution of simultaneous transport of different interacting chemicals. The code also allows for kinetic absorption processes, instead of instantaneous equilibrium as described by absorption isotherms (De Smedt, 2003).

2.7 Geographic Information Systems (GIS) tools

2.7.1 Arc-View

The use of (GIS) provides a powerful and efficient means of data preparation and visualization of simulation results (Clarke, 1999). Arc-View was used for basic spatial data management tasks (data storage, manipulation, preparation, extraction, etc.) and spatial data processing.

2.7.2 WetSpass

WetSpass stands for Water and Energy Transfer between Soil, Plants and Atmosphere under quasi-Steady State (Batelaan and De Smedt, 2001). It is a physically based model for the estimation of long-term average spatial patterns of groundwater recharge, surface runoff and evapotranspiration employing physical and empirical relationships. WetSpass is specially suited

for studying long-term effects of land-use changes on the water regime in a watershed. The water balance for vegetated surfaces is given by:

$$P=I+S_v +ET_v +R_v \quad (2.25)$$

where P is the average seasonal precipitation (LT-1), I is the interception by vegetation (LT-1), S_v is runoff over land surface beneath vegetation (LT-1), ET_v is the actual evapotranspiration (LT-1) and R_v is groundwater recharge (LT-1).

WetSpass is completely integrated in GIS Arc-View as a raster model, coded in Avenue. Inputs for this model include grids of land-use, groundwater depth, precipitation, potential evapotranspiration, wind-speed, temperature, soil, and slope where by parameters such as land-use and soil types are connected to the model as attribute tables of their respective grids.

The spatially distributed recharge output of WetSpass model can improve the prediction of simulated groundwater level and the locations of discharge and recharge areas for a Steady state groundwater models. Therefore WetSpass-MODFLOW interface perform simulations one after the other exchanging inputs of groundwater and recharge values respectively resulting in a stable solution for the groundwater level and discharge areas.

Chapter 3: Description of the study area

3.1 Geography and demography

The Gaza Strip is located on the south-eastern coast of the Mediterranean Sea, between longitudes $34^{\circ} 2''$ and $34^{\circ} 25''$ east, and latitudes $31^{\circ} 16''$ and $31^{\circ} 45''$ north. Its area is about 365 km^2 and its length is approximately 45 km along the coast line. The location of the Gaza Strip is shown in Figure 3.1.



Figure 3.1 Location map of the Gaza Strip

The population characteristics are strongly influenced by political developments, which have played a significant role in its growth and distribution of the Gaza Strip. The total population is around 1,300,000 (P. C. B. S., 2002).

3.2 Climate

The Gaza Strip has a characteristically semi-arid climate and is located in the transitional zone between a temperate Mediterranean climate in the west and north, and an arid desert climate of the Sinai Peninsula in the east and south. In this study, the climate parameters are average monthly and annually.

3.2.1 Temperature

Figure 3.2 presents the maximum, minimum and mean monthly air temperatures as observed in the meteorological station of Gaza city for the period lasting from 1970 until 2000. Temperature gradually changes throughout the year, reaches its maximum in August (summer) and its minimum in January (winter), average of the monthly maximum temperature range from about 17.6 C° for January to 29.4 C° for August. The average of the monthly minimum temperature for January is about 9.6 C° and 22.7 for August.

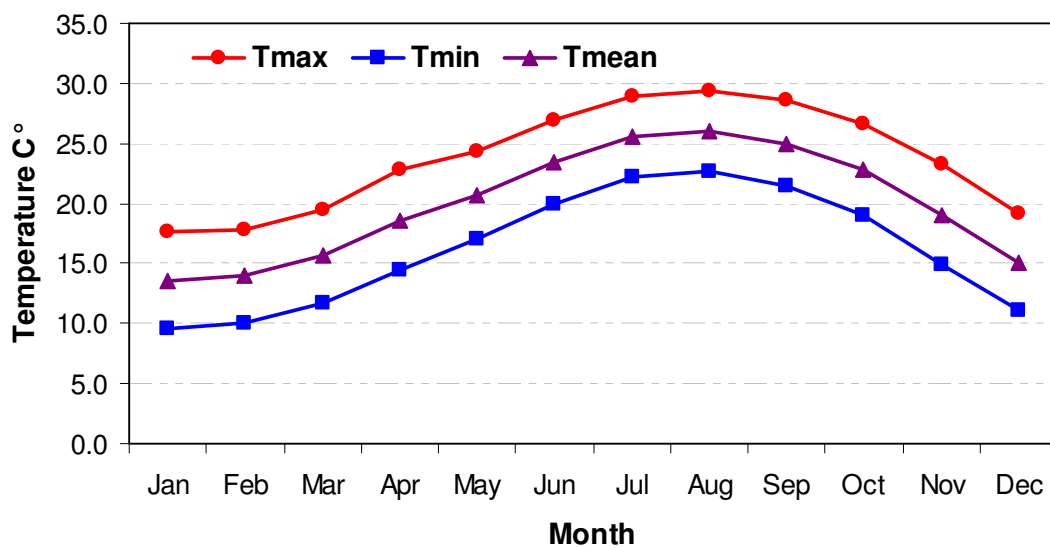


Figure 3.2 Mean monthly maximum, minimum and average temperature (C°) for the Gaza Strip (period 1970 – 2000)

3.2.2 Reference crop evapotranspirations (ET_o)

The monthly values for the reference crop evapotranspiration (ET_o), as determined with the FAO Penman-Monteith method (Allen et al., 1998) are plotted in Figure 3.3. The reference evapotranspiration is a climatic index integrating the effect of air temperature, humidity, wind speed and solar radiation. It expresses the evaporating power of the atmosphere.

ET_o is small in winter about 2 to 2.5 mm/d, and reaches its maximum in summer at about 5 mm/d.

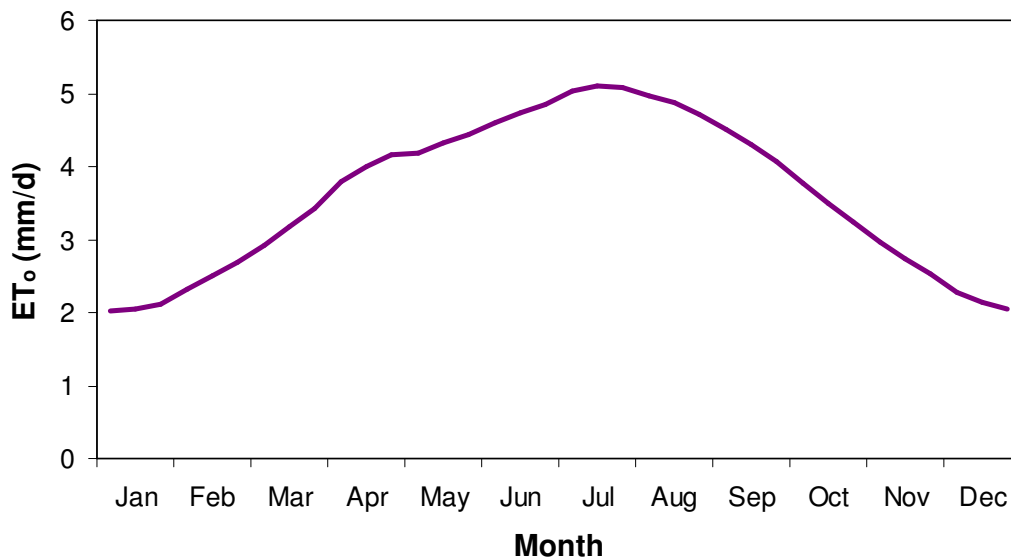


Figure 3.3 Mean monthly reference crop evapotranspiration for the Gaza Strip

3.2.3 Rainfall

The rainfall in the Gaza Strip gradually decreases from the north to the south. There are 8 measuring stations with daily data for period 1974 to 2000. The variation of the annual rainfall for the meteorological station of Gaza City is presented in Figure 3.4. The spatial annual rainfall distribution is shown in Figure 3.5. The values range from 410 mm/year in the north to 230 mm/year in the south.

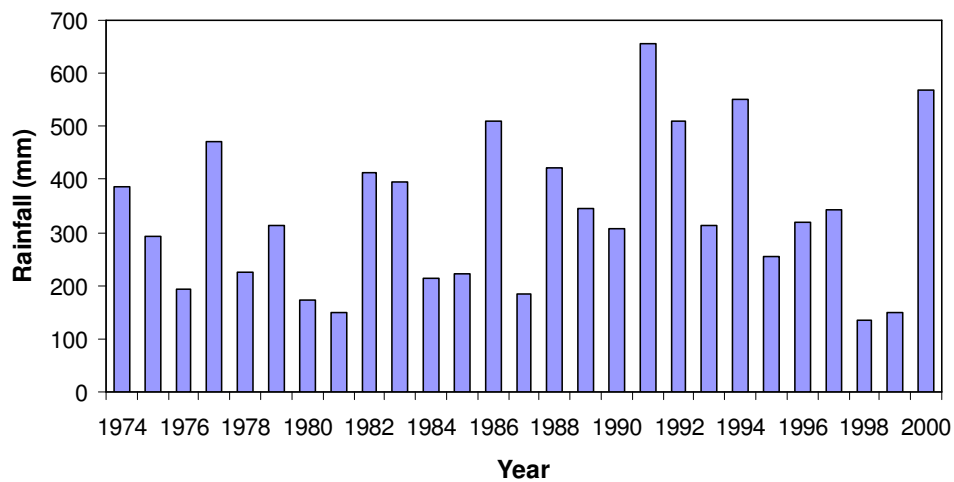


Figure 3.4 Temporal distributions of annual rainfall in the Gaza strip

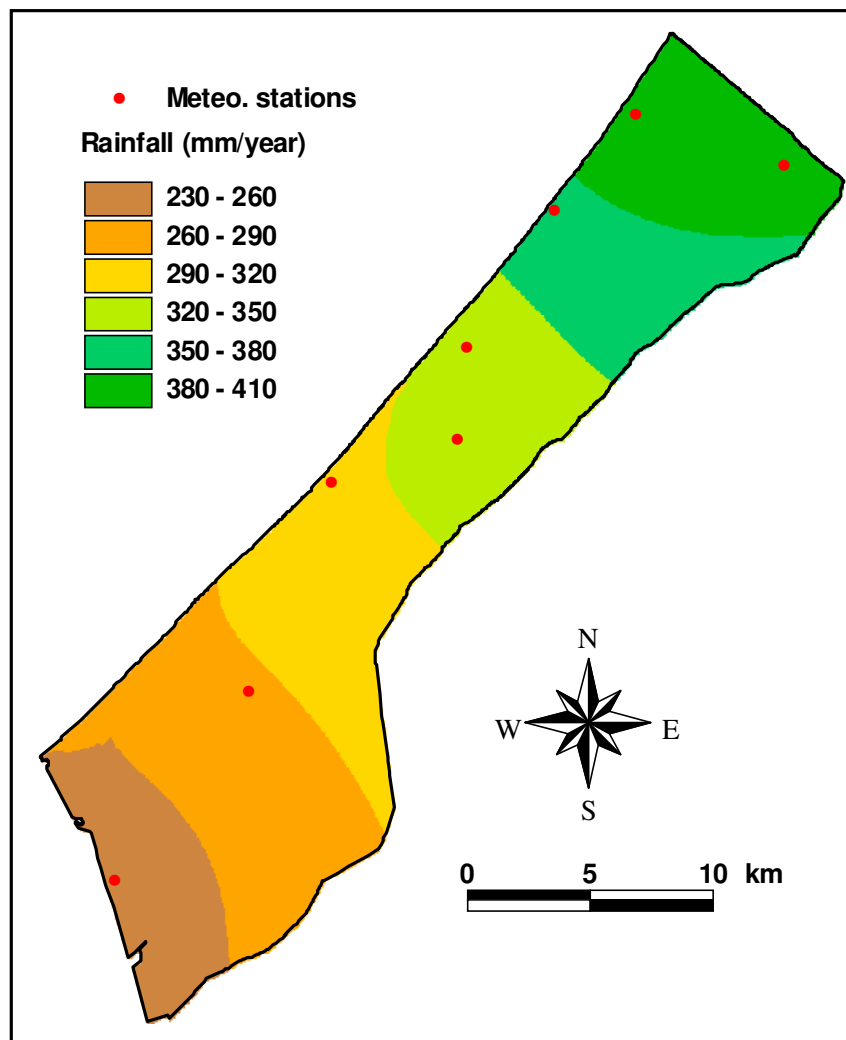


Figure 3.5 Spatial distribution of average annual rainfall in the Gaza Strip (period 1974-2000)

3.3 Topography

The Gaza topography is characterized by elongated ridges and depressions, dry streambeds and shifting sand dunes. The ridges and depressions generally extend in a NNE- SSW direction, parallel to the coastline. They are narrow and consist primarily of sandstone (Kurkar). In the south, these features tend to be covered by sand dunes. Land surface elevations range from mean sea level to about 110 m above mean sea level as shown in Figure 3.6. The ridges and depressions show considerable vertical relief, in some places up to 60 m. Surface elevations of individual ridges range between 20 m and 90 m above mean sea level.

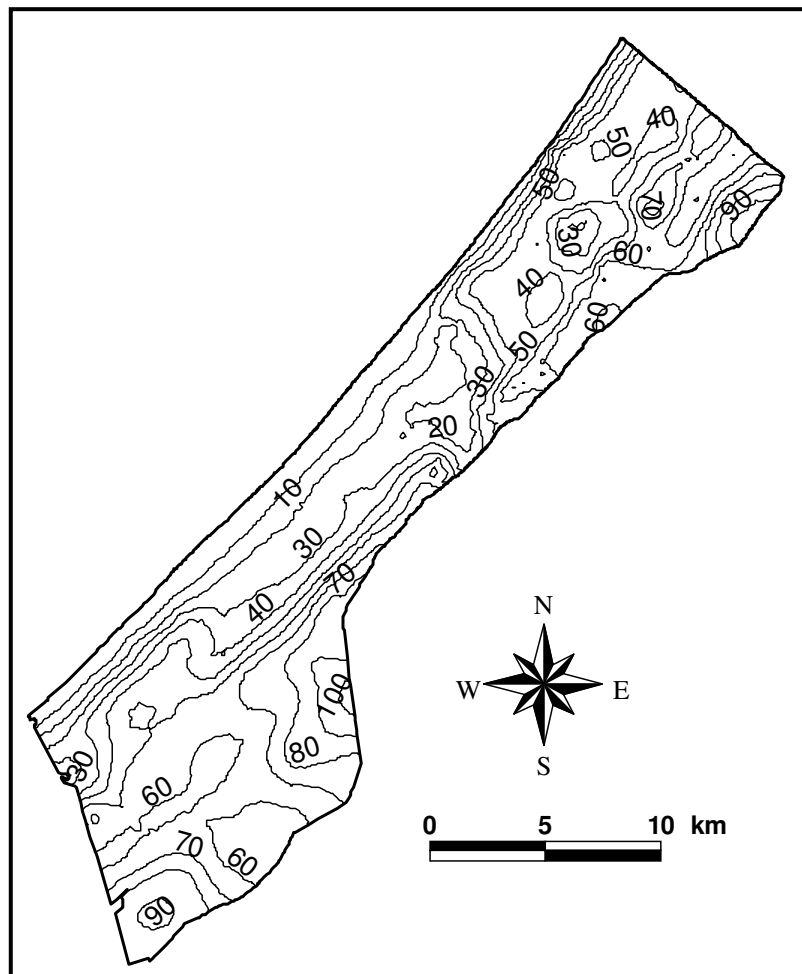


Figure 3.6 Topography of the Gaza Strip (m)

3.4 Soil

The soil in the Gaza Strip is composed mainly of three types, sands, clay and loess. The sandy soil is found along the coastline extending from south to outside the northern border of the Strip, at the form of sand dunes. The thickness of sand fluctuates from two meters to about 50 meters due to the hilly shape of the dunes. Clay soil is found in the north eastern part of the Gaza Strip. Loess soil is found around Wadis, where the approximate thickness reaches about 25 to 30 m. (Jury and Gardner, 1991). The soil map of the Gaza Strip is shown in Figure 3.7.

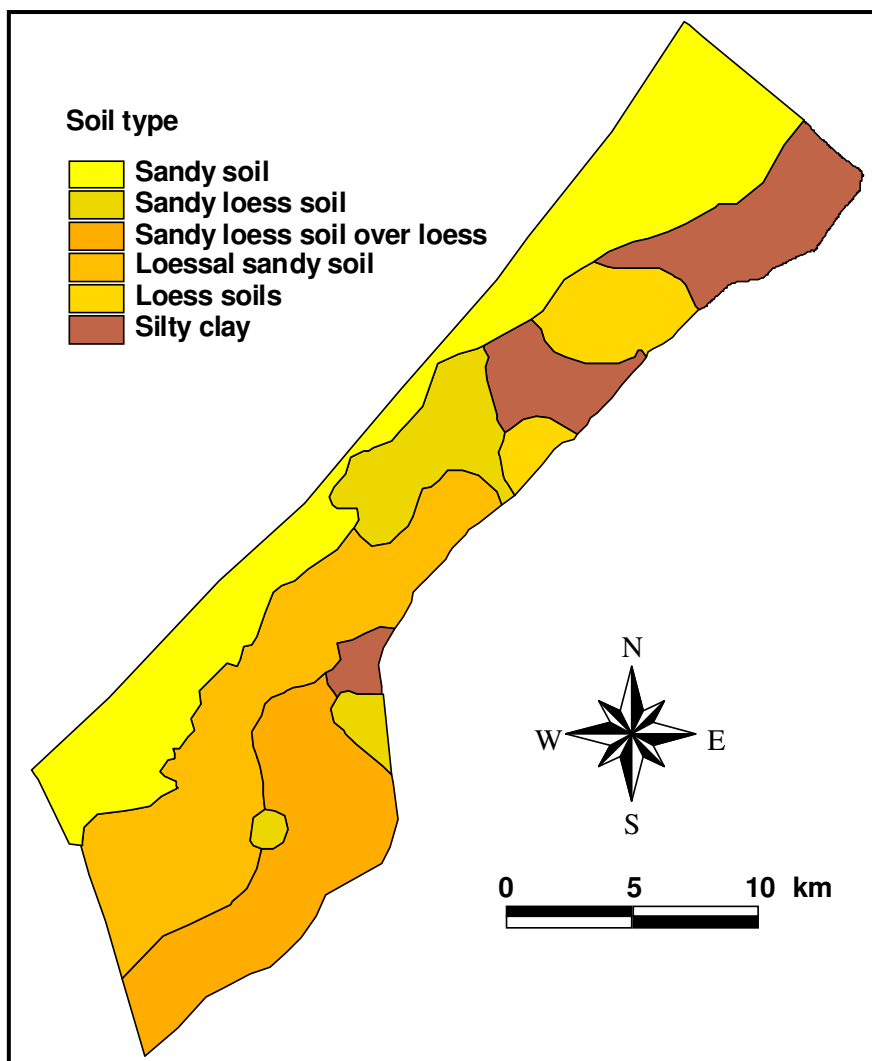


Figure 3.7 Soil map of the Gaza Strip (PWA, 2003)

3.5 Geology

The coastal aquifer of the Gaza strip consists of the Pleistocene age Kurkar group (Gvirtzman, 1969) and recent (Holocene age) sand dunes. The Kurkar group consists of marine and Aeolian calcareous sandstone (Kurkar), reddish silty sandstone (Hamra), silts, clays, unconsolidated sands and conglomerates. Regionally, the Kurkar group is distributed in a belt parallel to the coastline, from Haifa in the north to the Sinai in the south. Near the Gaza Strip, the belt extends about 15-20 km inland, where it unconformably overlies Eocene age chalks and limestones (the Eocene), or the Miocene-Pliocene age Saqiye group, a 400-1000 m thick aquitard beneath the Gaza Strip, consisting of a sequence of marls, marine shale's and claystones. Figure 3.8 presents a generalized geological cross-section of the coastal aquifer.

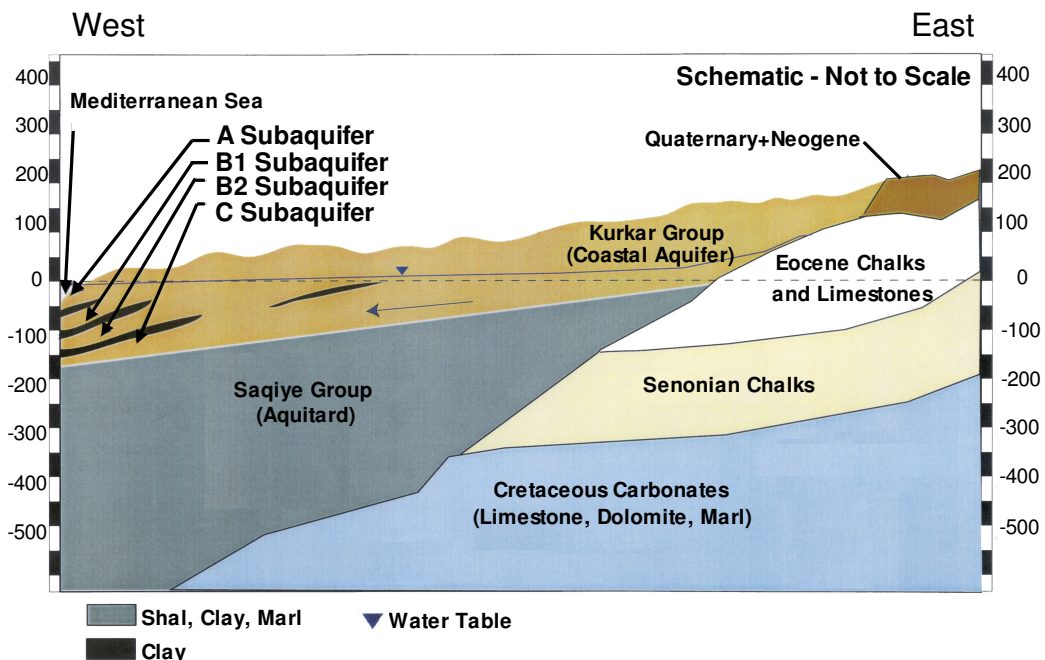


Figure 3.8 Generalized geological cross-section of the coastal plain (Metcalf and Eddy, 2000)

The Kurkar group consists of complex sequence of coastal, near-shore and marine sediments. Issar (1981) and Gvirtzman (1984) defined six sedimentary cycles of transgressions and regressions that have been mapped in the Israel coastal plain by correlating electric borehole geophysical logs. Marine calcareous sandstone forms the base of each transgress sequence and marine clays from the end of regressions.

3.6 Hydrogeology

The Gaza Strip Pleistocene granular aquifer is an extension of the Mediterranean seashore coastal aquifer. It extends from Askalan (Ashqelon) in the North to Rafah in the South, and from the seashore to 10 km inland. The aquifer is composed of different layers of dune sandstone, silt clays and loams appearing as lenses, which begin at the coast and feather out to about 5 km from the sea, separating the aquifer into major upper and deep sub aquifers as shown in Figure 3.8. The aquifer is built upon the marine marly clay (Saqiye group) from the Neocene (Fink, 1970), having a hydraulic conductivity of about 10^{-10} m/s (Goldenberg, 1992). In the east-south part of the Gaza Strip, the coastal aquifer is relatively thin and there are no discernible sub aquifers (Melloul and Collin, 1994).

The Gaza aquifer is a major component of the water resources in the area. It is naturally recharged by precipitation and additional recharge occurs by irrigation return flow. The consumption has increased substantially over the past years; the total groundwater use in year 2000 is about 145 Mm³/year, the

Chapter 3 : Study area

agricultural use about 90 Mm³/year, domestic and industrial consumption about 51 Mm³/year (Metcalf and Eddy, 2000). The groundwater level ranges between 5 m below mean sea level (msl) to about 6 m above mean sea level as shown in Figure 3.9. The groundwater level corresponds to depth below the soil surface between 0 and 95 m as shown in Appendix 2.2.

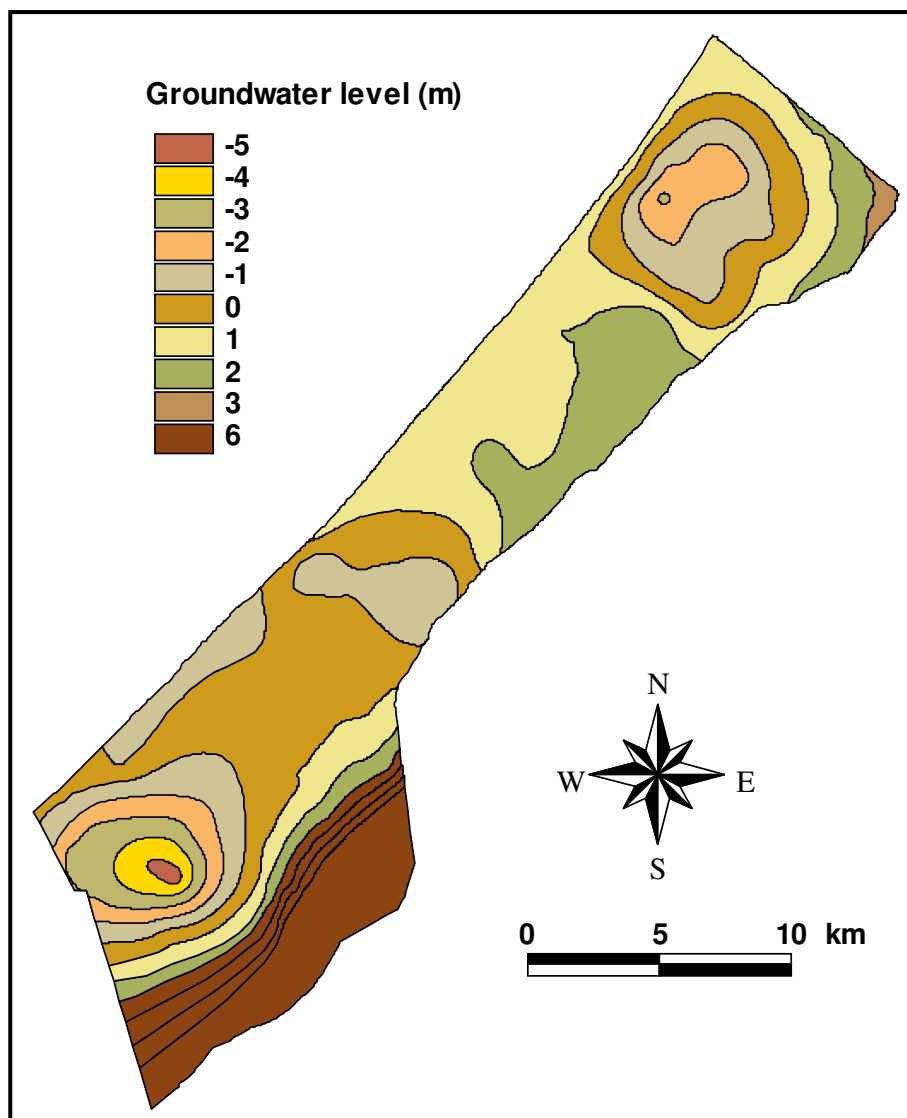


Figure 3.9 Contour map of groundwater level for year 2000 (PWA, 2003)

3.7 Water quality

Ongoing deterioration of the water supply of Gaza poses a major challenge for water planners and sustainable management of the coastal aquifer. The aquifer is presently being overexploited, with total pumping exceeding total recharge. In addition, anthropogenic sources of pollution threaten the water supplies in major urban centers. Many water quality parameters presently exceed World Health Organization (WHO) drinking water standards. The major documented water quality problems are elevated chloride (salinity) and nitrate concentrations in the aquifer.

3.7.1 Chloride

Salinity in the Gaza coastal aquifer is most often described by the concentration of chloride in groundwater. Sea water intrusion and intensive exploitation of groundwater have resulted in increased salinity in the most areas in Gaza Strip. According to Palestinian Water Authority (PWA), a generalized contour map of year 2000 is shown in Figure 3.10. Chloride concentrations are the highest along the Gaza border in the middle and south areas with concentrations exceeding 1000 mg/l. The best water quality is found in the sand dune areas in the north, mainly in the range of 50 – 250 mg/l.

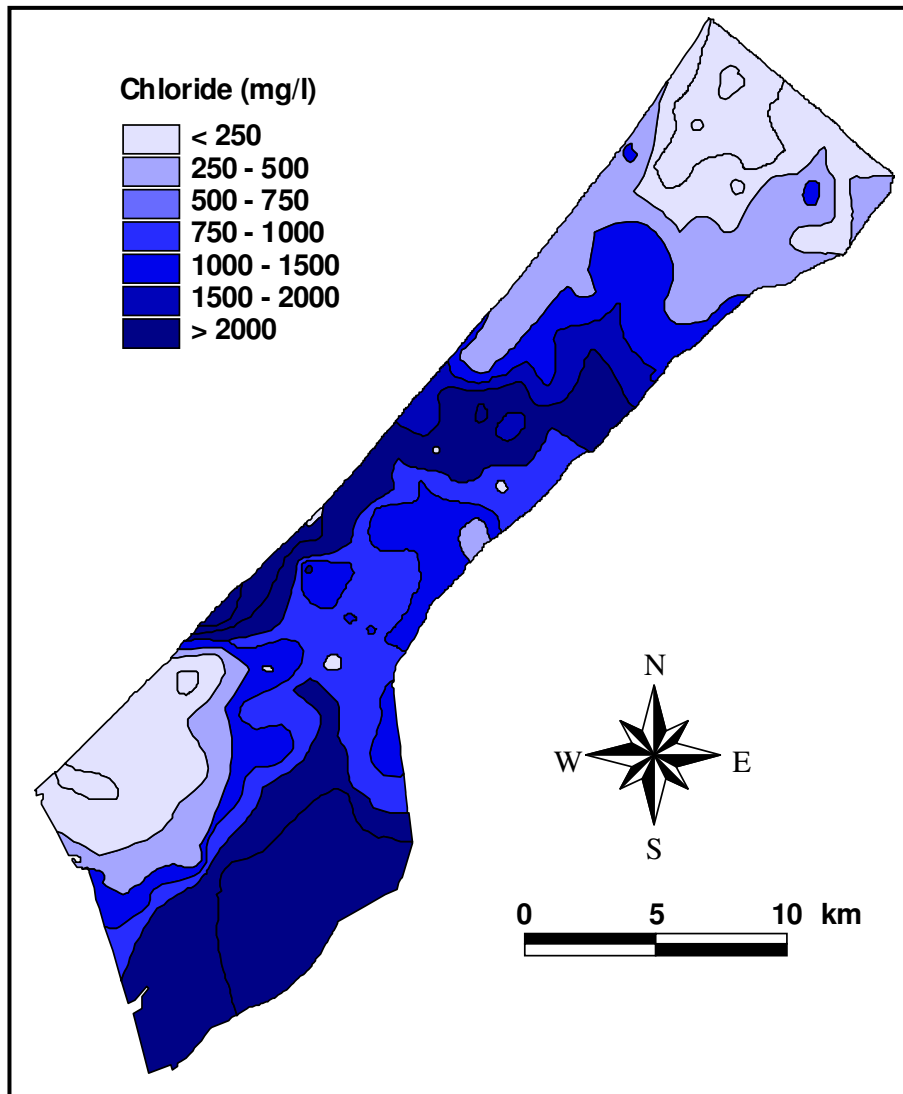


Figure 3.10 Chloride concentrations map of the Gaza Strip for year 2000 (PWA, 2003)

3.7.2 Nitrate

Nitrate is the most important pollutant of the groundwater all over the Gaza Strip. According to the Palestinian Water Authority, the nitrate concentrations of year 2000 in shallow groundwater are shown in Figure 3.11. Few wells in

Chapter 3 : Study area

Gaza remain unaffected by high nitrate concentrations and only about 10 % of the municipal water supply remains below the WHO drinking water standard of 50 mg/l. The main sources of the nitrates are believed to be fertilizers and domestic sewage effluent.

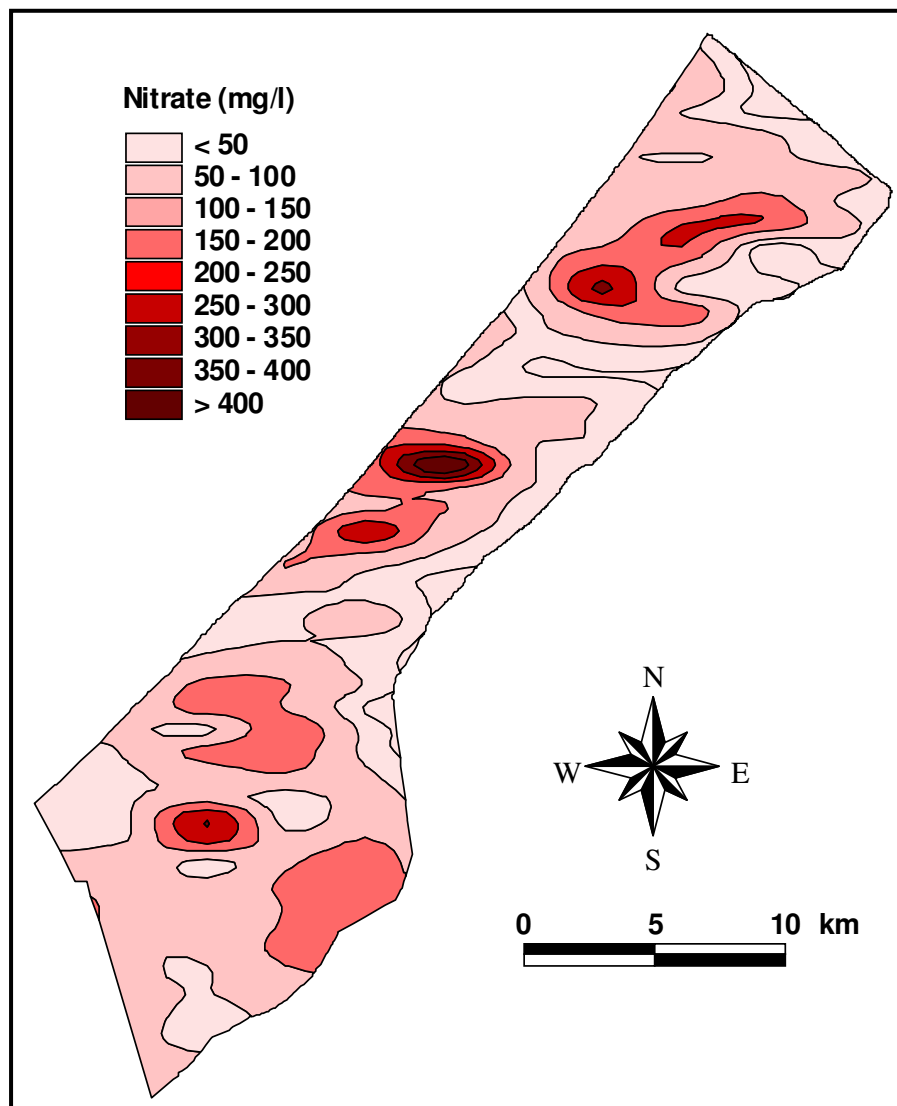


Figure 3.11 Nitrate concentration map of the Gaza Strip for year 2000 (PWA, 2003)

3.8 Wastewater treatment

Wastewater treatment has been considered in the Gaza Strip since 1970. Stabilization ponds were the technology proposed at that time. Greater attention has been paid to improve this sector following the coming of the Palestinian National Authority (PNA) in 1993. The PNA intends to draw a Palestinian policy regarding wastewater treatment and reuse. This policy needs to determine the proper treatment technology using local experience technology.

There are three wastewater treatment plants (WWTP) operating in the Gaza Strip: Beit-Lahia WWTP in the north, Gaza WWTP in the Gaza City and Rafah WWTP in the south. The type of treatment, quantity and final disposal of each plant is summarized in Table 3.1. The wastewater quality parameters of the wastewater treatment plants in the Gaza Strip are shown in Table 3.2.

Table 3.1 Treatment plant in the Gaza Strip (Zubiller, 2002)

Location	Treatment method	Quantity (m ³ /d)	Final disposal
Beit-Lahia	Stabilization ponds and aerated lagoons	8,000-10,000	Surrounding sand dunes
Gaza	Anaerobic ponds followed with bio-towers	40,000-45,000	75% to the sea and 25 % infiltrated to the ground aquifer
Rafah	One aerated lagoon	3,000-4,000	To the sea

Table 3.2 The quality of influent and effluent of wastewater in the Gaza Strip (Zubiller, 2002)

Parameter	Jabalia			Gaza			Rafah		
	No. of tests	Influent	Effluent	No. of tests	Influent	Effluent	No. of tests	Influent	Effluent
pH	2	7.8	7.2	50	7.4-7.8	7.6-7.8	2	7.4	7.5
Temperature C ⁰	2	16.1	15.0	50	14-20.7	16 - 19	2	23.5	22.2
TS mg/l	2	1888	1480	28	1472-3960	1024-1536	2	2140	1610
TDS mg/l	2	1471	1445	28	1094-2267	905-1503	2	1518	1484
TSS mg/l	2	417	35	40	244-1693	31-79	2	622	126
TVSS mg/l	2	370	30	40	212-1397	24-57	2	550	110
NH ₃ -N mg/l	2	61.6	54.6	4	51-70	41-47.6	2	88	63.6
N-KjD mg/l	2	102.7	75.6	2	74	57	2	128.8	88.2
Cl mg/l	2	-	310-340	2	-	340-400	2	-	-
BOD mgO ₂ /l	2	420	40	10	360-1600	35-41	2	760	240
COD mgO ₂ /l	2	1078	120	15	608-3100	114-162	2	1298	556
F. Coliform CFU/100cm	2	4.4E8	8.3E5	10	2.5E8-5E9	3.4E6-5E7	2	2E9	7.5E7

(-): un determined

Chapter 4: Hydrogeological study

4.1 Location and site description

The study area is located in the northern Governorate, north-east of Gaza city, east of Jabalia town, next to the border with Israel. A view of the area is shown in Figure 4. 1.



Figure 4.1 View of the study area

The study area extends over 336,000 m², of which 212,000 m² is used for a treatment plant and artificial recharge basin. A general site plan showing the locations of the drilled boreholes is shown in Figure 4. 2. The site is located on a slope with the eastern part at 70 m and the western part at 50 m above sea level. Groundwater levels as measured in boreholes within the site and in private wells in the vicinity are approximately 1 m meter above sea level.

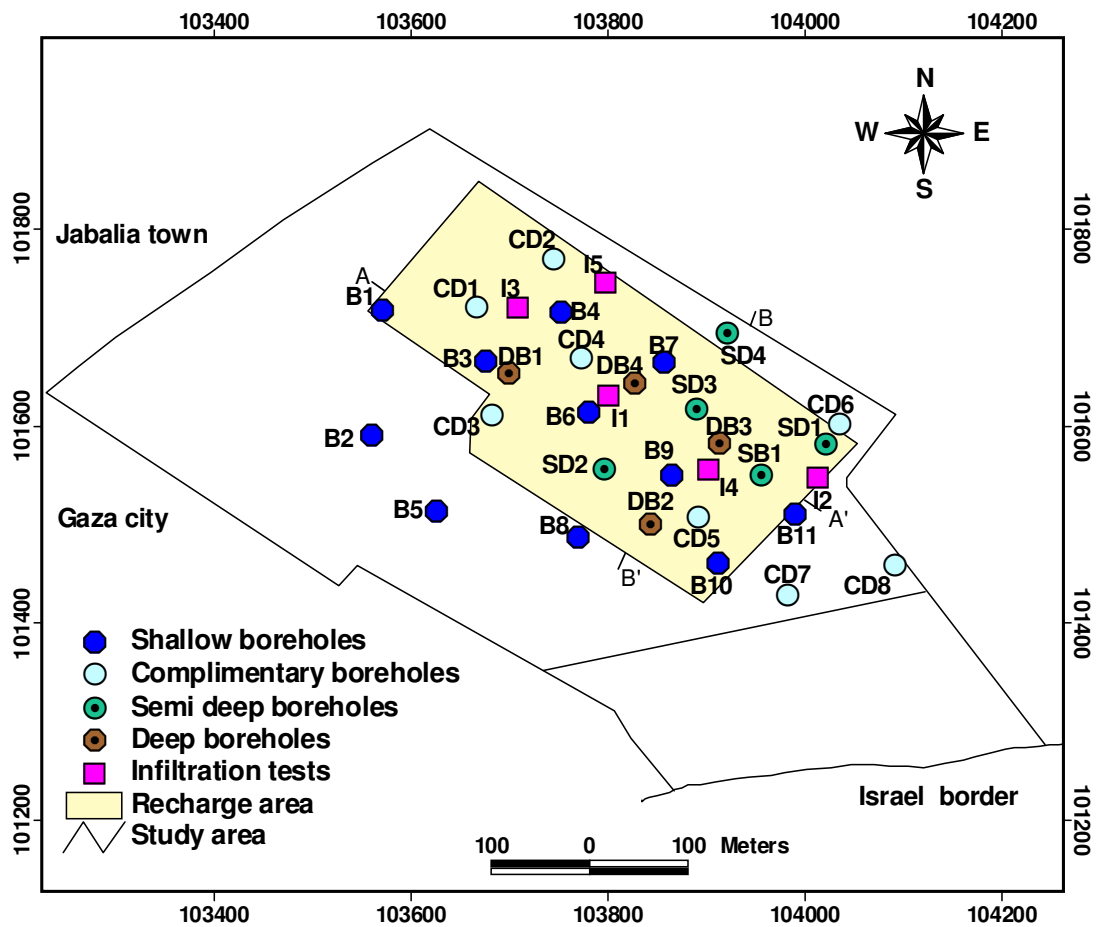


Figure 4.2 Geographic location of the study area with indication of the drilled boreholes and infiltration test ponds

4.2 Site investigation

During September 2001 to August 2002, an extensive program of hydrogeological investigation was undertaken to achieve the most reliable characterization of the subsoil and eventually to assist in the design and implementation of a pilot artificial recharge system for treated wastewater to groundwater. The hydrogeological study was carried out within the framework of the Northern Gaza storm water and sewerage project where I was working as a site engineer supervising the field work of boreholes drilling, packer

tests, infiltration tests and pumping test. The project was financed by the Swedish Government supporting the Palestinian Water Authority.

The drilling methods used were rotary auger and cable percussion drillings. For the shallow boreholes and the semi-deep boreholes, the drilling methods were rotary air flush and rotary water circulation drilling. In the deep boreholes auger and cable tool percussion methods were used.

During the drillings, disturbed samples (bulk samples) were collected for each 1-2 m drilling and/or at the change of formation. The samples were checked ocular at the site with regards of the soil texture and color. The laboratory analysis of soil samples were carried out in the Arab Centre for Engineering Studies. The soil samples were placed in plastic bags before placing in wooden box. The grain size distributions are shown in appendix 1.2 and 1.3. The grain size classification systems were determined according to Unified Soil Classification System (USCS), the grain size interval is > 2 mm for gravel, sand from 2 mm to 0.075 mm and silt and clay < 0.075 mm.

Shallow boreholes B1-B11 were drilled penetrating the clay layer into the underlying sand material. After completion of these boreholes, it was found that there was a need for more information regarding the thickness of the clay in some areas. Hence, 8 complementary boreholes CD1-8 were drilled also penetrating the clay into the underlying sand material. Semi deep boreholes SD1-4 and SB1 were drilled to 66-73 m depth, penetrating the unsaturated zone to at least 5 m below the groundwater table. Also, deep boreholes DB were drilled; DB1-3 to 100-120 m depth ending in the kurkar or clayey

formation and DB4 to a depth of 156 m penetrating the kurkar formation fully and reaching the Saqiye group as shown in appendix 1.1 and appendix 1.4. Deep borehole (DB4) was used as a pumping well during the pumping test.

The drillings revealed the followings local geological build-up. The topsoil consists of a continuous silty clay layer, with a thickness of 3 to 14 m. The clay can be described as a brownish, slightly moist to moist, very stiff to hard, and slightly sandy and silty.

In the semi-deep and deep boreholes, coarser material underlays the clay layer; consisting of sand and kurkar (sand with fine gravels of sandstone). Within the kurkar and sand formations, the degree of packing varies as well as texture. Normally, the sand varies between fines to coarse, while the gravel usually is fine to medium. Also brownish clayey or silty layers of variable thickness and at different depths are found.

In all of these boreholes, except for DB2, one or more layers of clayey to silty material are found between 20 to 40 m above the sea level. Clayey formations are also found below 40 m under the sea level. The lithological description based on the field observation, grain size analysis and USDA soil textural triangle. The geological setting and the thickness of the top clay layer were interpolated from the boreholes logs as shown in the geological cross-sections NW-SE (A-A') and NE-SW (B-B') in Figure 4. 3 and Figure 4.4. The locations of the geological cross-sections are shown in Figure 4.2.

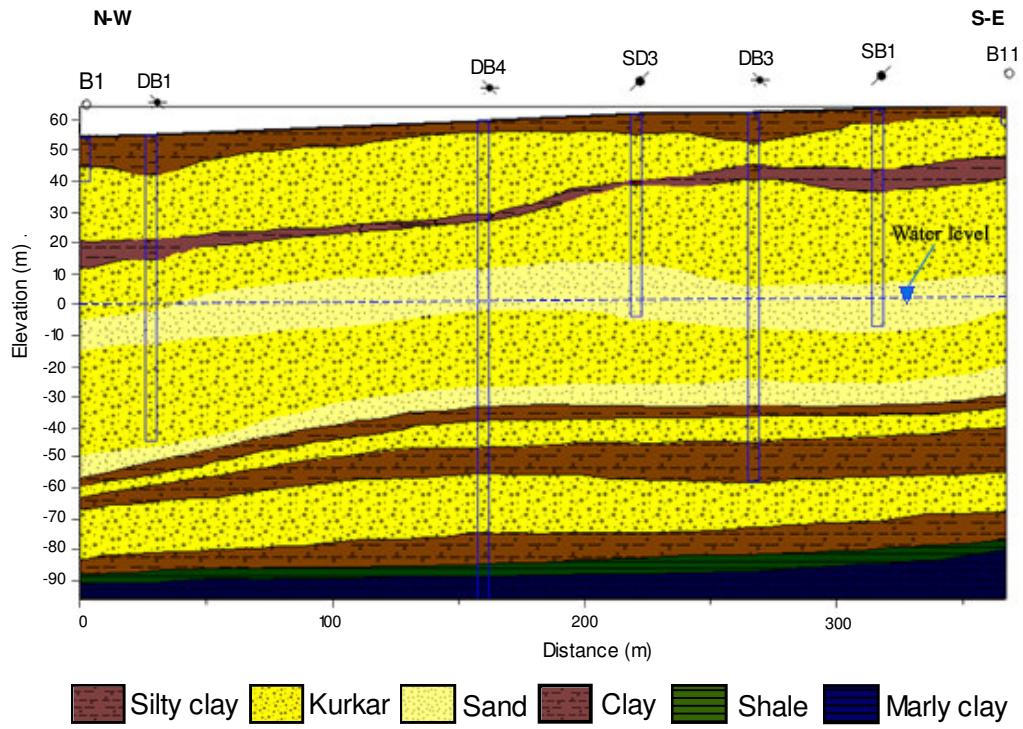


Figure 4.3 Geological cross-section A-A'

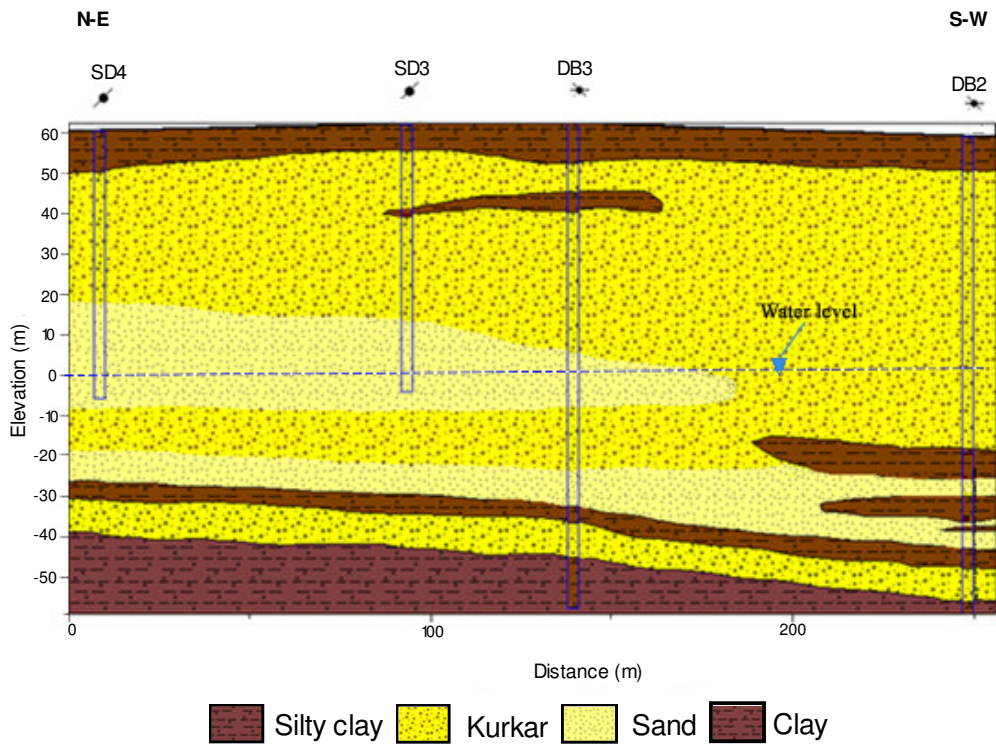


Figure 4.4 Geological cross-section B-B'

4.3 Soil permeability

4.3.1 Field permeability (packer test)

Packer or Lugeon test gives a measure of the acceptance by in situ rock of water under pressure. The test was originally introduced by Lugeon (1933) to provide an acceptable standard for the permeability of dam foundations. The packer test was used during boreholes drilling to determine the hydraulic conductivity, K , at different depths in eight boreholes (B1, B2, B3, B5, B7, B10, SD1 and SD4). Figure 4.5 shows the packer test was used in the field.



Figure 4.5 Inflatable Packer test used in the field

The packer test method comprises measurement of water that can escape from an uncased section of the borehole in a given time under a given pressure. Flow is confined between two packers in the double packer test, or between one packer and the bottom of the borehole in the single packer test. A probe was lowered to the testing depth and inflated, using pressurized

nitrogen gas, to seal off the test section. Pressure was applied to the section in five stages; each pressure cycle was maintained constant for 5 min. The applied pressure and the corresponding volume of water discharged were recorded. Before the test started, the probe was calibrated for conditions expected to prevail during the test to determine the probable head loss.

The K-values are computed in accordance with the formula given in the earth manual of the US Bureau of Reclamation (1974).

$$K = \frac{Q}{2\pi L H_T} \ln \left(\frac{L}{r} \right) \quad (4.1)$$

where

K is the hydraulic conductivity (m/d);

Q is the constant rate of flow into the hole (m³/d);

H_T is the total head causing flow into the soil or rock (m);

$$H_T = P + H - H_f$$

P is the pressure gauge reading converted to head (m)

H is the height of pressure gauge above the test section (m);

H_f is the head loss in the pipes (m);

ln is the natural logarithm;

L is the test length (m), and

r is the radius of the hole (m)

The summary of results of the packer test is given in Table 4.1 and Appendix 1.5. The Hydraulic conductivity for the clay varies between 0.03 m/d and 0.86 m/d, with an average of 0.37 m/d and the hydraulic conductivity for the coarser materials (sand with fine gravel) range from 1.4 m/d to 39 m/d, with an average of 11.6 m/d.

Table 4.1 Summary of hydraulic conductivity of the packer test

Borehole no.	Depth (m)	Lithology	K (m/d)
B1	13.0 – 13.5	Sand with fine gravel	39.0
B2	11.0 – 12.0	Clay	0.27
B3	6.2 – 7.2	Clay	0.04
	11.8 – 12.3	Sand with fine gravel	6.6
B5	8.5 – 9.5	Clay	0.86
	14.5 – 15.0	Sand with fine gravel	9.5
B7	7.5 – 8.0	Sand with fine gravel	21.0
B10	10.5 – 11.0	Sand with fine gravel	1.4
SD1	13.5 – 14.0	Sand with fine gravel	1.6
SD4	7.5 – 8.5	Clay	0.03
	13.0 – 13.5	Sand with fine gravel	1.8

4.3.2 Permeability from grain size

Several formulae have been published relating the permeability of soils, especially sands, to their size characteristics and other classification data. Hazen (1930) related the permeability to the effective grain size of a soil using following equation

$$K = C(D_{10})^2 \quad (4.2)$$

Where:

K = hydraulic conductivity (m/d),

D_{10} = effective grain size (mm) for which 10% (by weight) of the particles is smaller, and

C = constant (0.004 to 0.012)

The effective grain size of a soil, D_{10} , is an important value for characterizing the size of the pores, which is the dominant factor regulating flow of water through a pores medium. The higher the D_{10} value the coarser the soil and the better its drainage characteristics. Interpreted permeability values of sand material using Hazen Formula with the lowest value of $C = 0.004$ range from 2.2 m/d to 22 m/d with an average value of 6 m/d; maximum value are obtained for $C = 0.012$ and range from 6 m/d to 65 m/d, with an average value of 18 m/d, as shown in Table 4. 2.

Table 4.2 Interpreted hydraulic conductivity using Hazen Formula

Borehole no.	Sample depth (m)	D ₁₀ (mm)	K _{min} (m/d)	K _{max} (m/d)
B1	12 - 13	0.18	11.2	33.6
	14 - 15	0.22	16.7	50.2
B2	15 - 16	0.08	2.2	6.6
B3	13 - 14	0.12	5.0	14.9
B5	15 -15.5	0.15	7.8	23.3
B6	7 - 7.5	0.10	3.5	10.4
B7	8 - 8.5	0.11	4.2	12.6
B11	4 - 4.5	0.10	3.5	10.4
SD1	8 - 9	0.08	2.2	6.6
	10 - 10.5	0.10	3.1	9.4
	11 - 12	0.12	5.0	14.9
	14 - 14.5	0.11	4.2	12.6
	16.5 - 17	0.09	2.8	8.4
	20 - 20.5	0.11	4.2	12.6
	26 - 27	0.15	7.8	23.3
	30 - 31	0.16	8.9	26.5
	37 - 38	0.10	3.5	10.4
	44 - 45	0.11	4.2	12.6
	49 - 50	0.09	2.8	8.4
SD2	56 - 57	0.11	4.2	12.6
	63 - 64	0.11	4.2	12.6
	12 - 12.5	0.09	2.8	8.4
	14 - 15	0.12	5.0	14.9
	17 - 18	0.10	3.5	10.4
	19 - 20	0.12	5.0	14.9
	29 - 30	0.21	15.2	45.7
	34 - 35	0.14	6.8	20.3
SD3	55 - 56	0.13	5.8	17.5
	60 - 61	0.13	5.8	17.5
	62 - 63	0.13	5.8	17.5
	17 - 18	0.13	5.8	17.5
	20 - 21	0.18	11.2	33.6
	25 - 26	0.12	5.0	14.9
	27 - 28	0.12	5.0	14.9
	33 - 34	0.14	6.8	20.3
SD4	39 - 40	0.25	21.6	64.8
	47 - 48	0.17	10	30.0
	54 - 55	0.11	4.2	12.6
	59 - 60	0.11	4.2	12.6
	62 - 63	0.11	4.2	12.6
	20 -20.5	0.11	4.2	12.6
	31 - 32	0.13	5.8	17.5
	34 - 35	0.11	4.2	12.6
SD4	39 - 40	0.11	4.2	12.6
	46 - 46	0.16	8.9	26.6
	52 - 53	0.14	6.8	20.3
	56 - 57	0.11	4.2	12.6
	59 - 60	0.12	5.0	14.9

The relationship between hydraulic conductivity and depth within the upper 65 m of soil tested, are shown in Figure 4.6 which is a plot of hydraulic conductivity vs. depth. The diagram shows that generally, the hydraulic conductivity is larger than about 5 m/d, but however some samples were too fine to be analyzed with the Hazen formula. This shows that the ground layers consist of sand and sandstone intermixed with finer sediments.

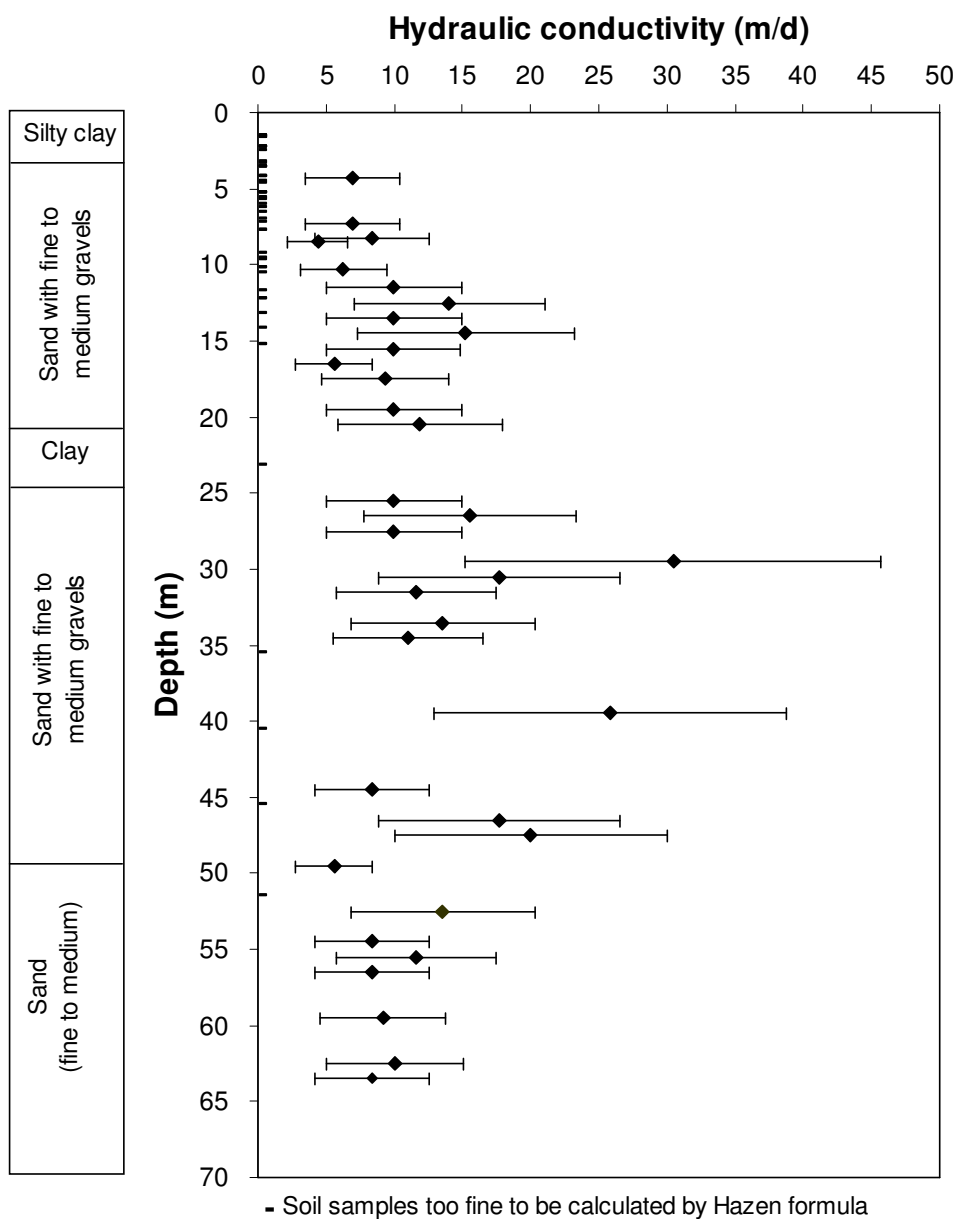


Figure 4.6 Hydraulic conductivity vs. depth using Hazen formula

4.3.3 Infiltration tests

Infiltration is the process of downward water entry into the soil. The rate of infiltration is usually sensitive to near-surface conditions as well as the antecedent water content of the soil. Hence, infiltration rates are subject to significant change with soil use and management, and time (Schwartz and Zhang, 2002). The infiltration model developed by Philip (1969) was used to describe infiltration in the study area. Philip's infiltration law simulates infiltration of water into a homogeneous sandy soil profile. Soil water content at the inflow – end is held constant and at saturation.

$$q \cong \frac{S}{2\sqrt{t}} + K \quad (4.3)$$

where q is infiltration rate (m/d), S is sorption depending on the pore configuration of the soil and the initial water content ($m/d^{1/2}$). Values of S can be determined by plotting q versus $\frac{1}{\sqrt{t}}$ which should give a straight line relationship that enables to estimate S and K .

Five infiltration tests were conducted (I1-5) as shown in appendix 1.6. Experiments 1 and 2 were conducted in a square basin 1.5 by 1.5 m, placed 0.25 m deep into the underlying sandy material after excavating to the required depth. Water was allowed in the basin until a water height of 1.0 m (± 1 cm). Afterwards, the drop in water elevation due to infiltration in the sand was recorded versus time. Experiments 3 and 4 were conducted in a drilled, cased borehole with a diameter of 0.75 m. The bottom of the boreholes was located at 0.5 m and 1.5 m below the top clay layer. Water was injected 1 m

high and the subsequent decrease of the water level was monitored continuously using an electrical water level indicator according to the British Standard (1981). Experiment 5 was conducted in a 5 m by 5 m wide and 5.5 m deep excavated pit and a circular basin 3.6 m in diameter made of metal sheets inserted about 0.20 m into the underlying sandy material, in accordance with the Washington Department of Ecology (2001).

The observed infiltration rates versus time are plotted in Figure 4.7. All infiltration rates decrease with decline in head, i.e. water level in the ponds.

The infiltration rate of the sand with fine gravel materials obtained from infiltration test varies between 9.9 m/d and 15.1 m/d, with an average of 12.0 m/d. The hydraulic conductivity obtained from Philip equation varies between 5.6 m/d and 10.9 m/d with an average 7.8 m/d.

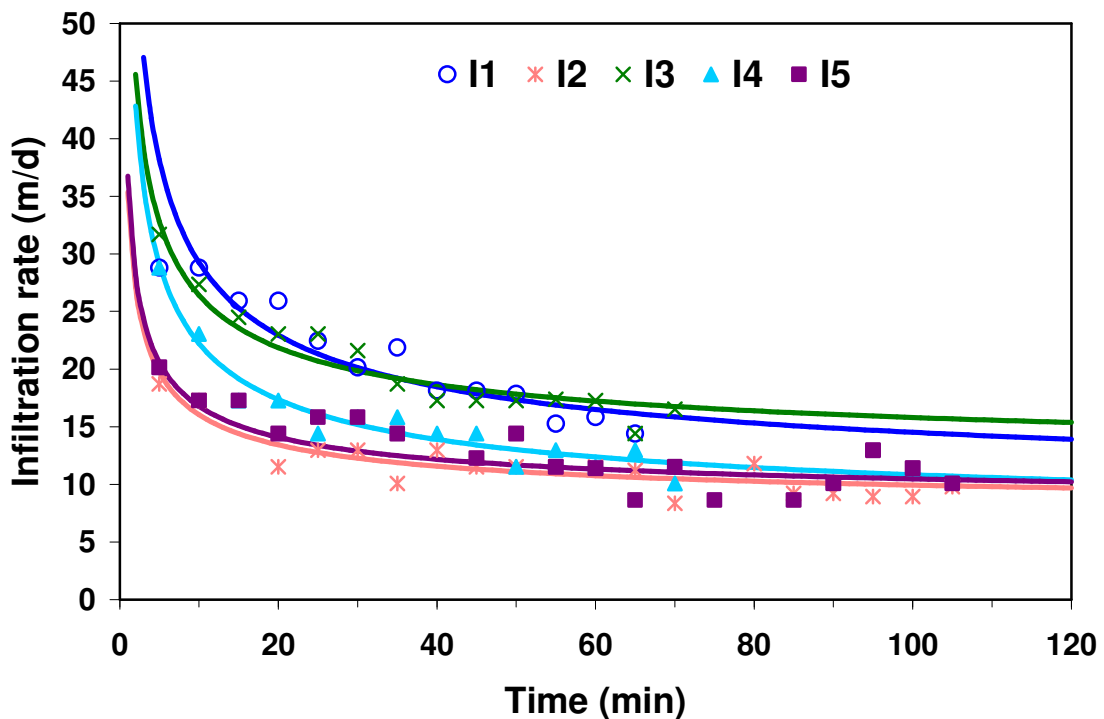


Figure 4.7 Observed infiltration rate in the infiltration test ponds, fitted with theoretical Philip equation

The comparison of the hydraulic conductivity of the sand with fine to medium gravel material below the top clay layer to depth of 16 m from packer test, Hazen formula and infiltration test are shown in Figure 4.8. The results indicate that the hydraulic conductivity is in good agreement between the analysis of Hazen formula and infiltration test. However, the packer test results show more variation in the hydraulic conductivity with depth.

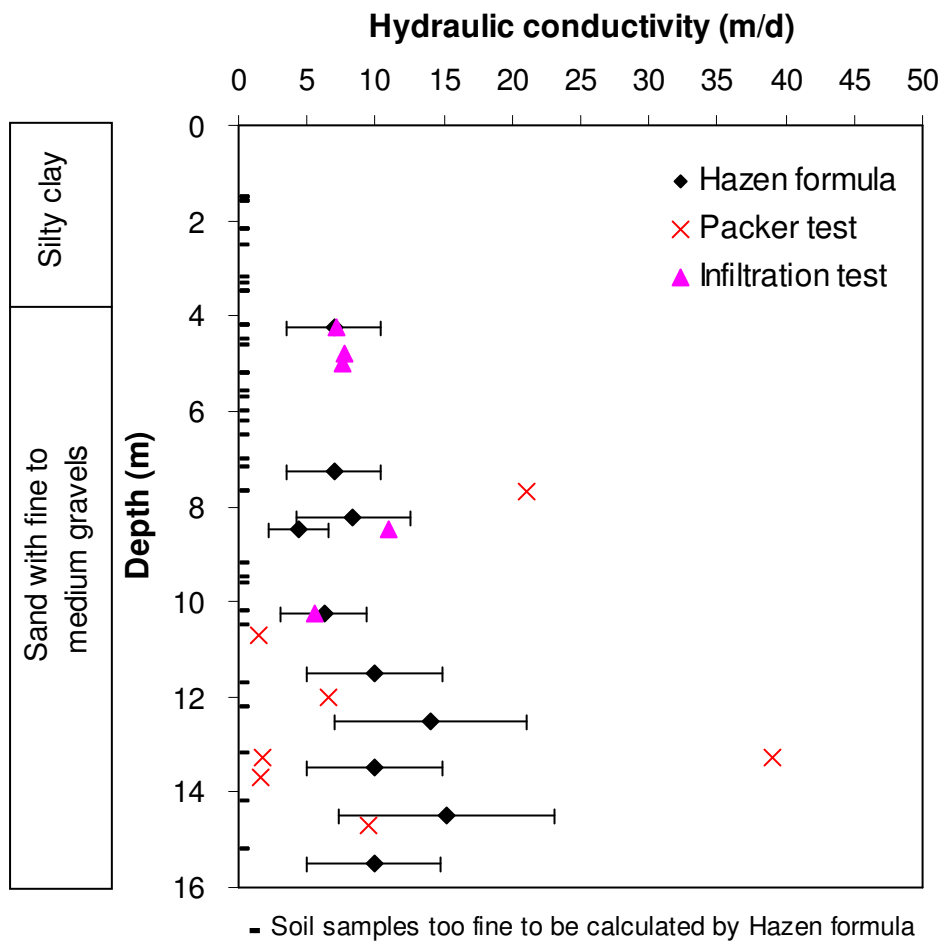


Figure 4.8 Comparison of hydraulic conductivity vs. depth in sandy material

4.4 Pumping test

The most commonly used field technique to determine the hydraulic conductivity in groundwater layers is the pumping test. Theis (1935) derived the following equations for determination of the aquifer transmissivity, and storativity, under transient conditions:

$$s = \left(\frac{Q}{4\pi T} \right) W(u) \quad (4.3)$$

Where:

s = the drawdown (m)

Q = constant well discharge (m³/d)

T = transmissivity (m²/d)

W(u) = Theis well function.

and

$$u = \frac{r^2 S}{4Tt} \quad (4.4)$$

where:

r = the distance between pumping and observation wells (m)

S = storage coefficient (-) and

t = time (d)

Chapter 4 : Hydrogeological study

This relationship plotted on a log-log plot with $W(u)$ along the Y axis and $1/u$ along the X axis is commonly called the Theis curve. To analyze the pumping test, field measurements are plotted on the same log-log graphic paper as t or t/r^2 along the X axis and s along the Y axis. The data analysis is done by matching the plotted observed data to the Theis curve.

A pumping test was conducted in well DB4 to determine the hydraulic conductivity, transmissivity and storage coefficient.

Analyses of the test results were performed using Aquifer Test software of Waterloo Hydrogeologic, for the observations made in wells DB1, DB2, SD2 and SD4. The results are shown in appendix 1.7 and Figure 4.9, depicting that all results show that the hydraulic conductivity is approximately equals. It can be seen from a Theis curve that all measurements more or less agree and yield following results: a transmissivity of $2400 \text{ m}^2/\text{d}$, an average hydraulic conductivity of 32 m/d , and a specific yield of 0.24 .

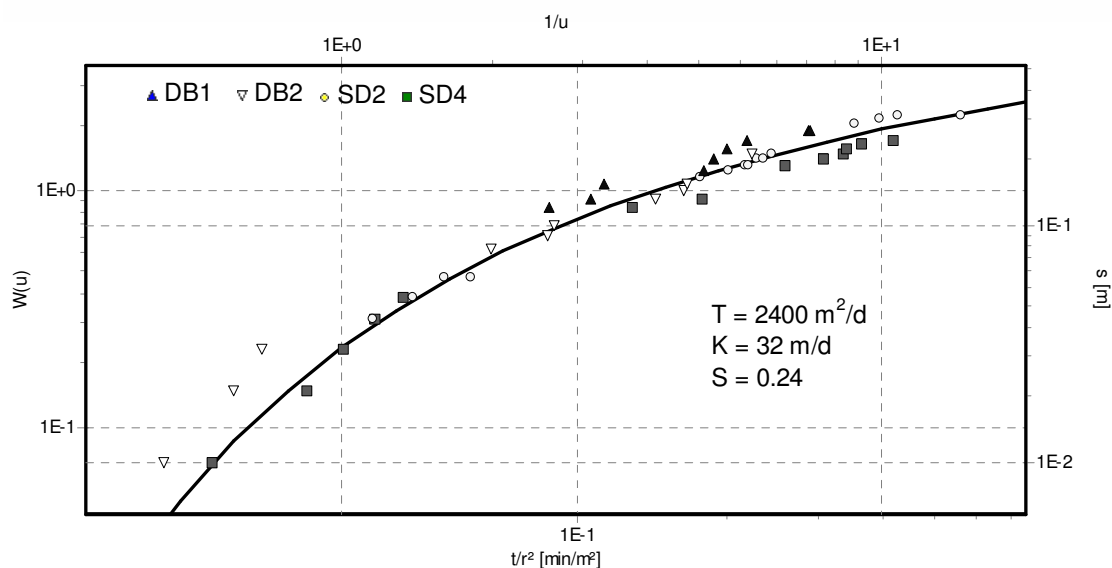


Figure 4.9 Results of the pumping test analysis by means of a Theis-curve fit

Chapter 4 : Hydrogeological study

The details and graphs of different analysis methods of pumping test shown in appendix 1.7 and Table 4.3 shows the summary results of different methods used of analysis of the pumping test.

Table 4.3 Comparison of methods used for the pumping test

Well	Analysis method	Transmissivity (m²/d)	Hydraulic conductivity (m/d)	Storativity
OB DB1	Theis	2150	28.0	0.22
	Theis Recovery	2200	28.0	
OB DB2	Theis	2800	38.0	0.22
	Theis Recovery	2700	36.0	
OB SD2	Theis	2200	29.0	0.23
	Theis Recovery	2150	28.0	
OB SD4	Theis	2450	33.0	0.27
	Theis Recovery	2500	34.0	
All OB. wells	Theis	2400	32.0	0.24
All OB. wells	Cooper-Jacob Distance-Drawdown	2420	32.0	0.23

The results of different methods in Table 4.3 show that small variation in the methods. The transmissivity is ranged between 2150 m²/d to 2800 m²/d and the hydraulic conductivity is ranged between 28 m/d to 38 m/d. The highest value of transmissivity and hydraulic conductivity were found in the observation borehole DB2. The storativity is varies from 0.22 to 0.27 with the highest value were found in the observation borehole SD4.

The comparison of the hydraulic conductivity of the sand with fine gravel material (Kurkar) from Packer test, Hazen formula, infiltration test and pumping test, are plotted in Figure 4.10 to show the variation of hydraulic conductivity with depth. The variation of hydraulic conductivity at the same depth in deferent boreholes shows the nonhomogenety of the soil. The results from pumping test in the aquifer show generally larger values,

which can be explained by the scale of the experiment and the large volume of tested soil, which promotes high conductivity areas to dominate flow processes.

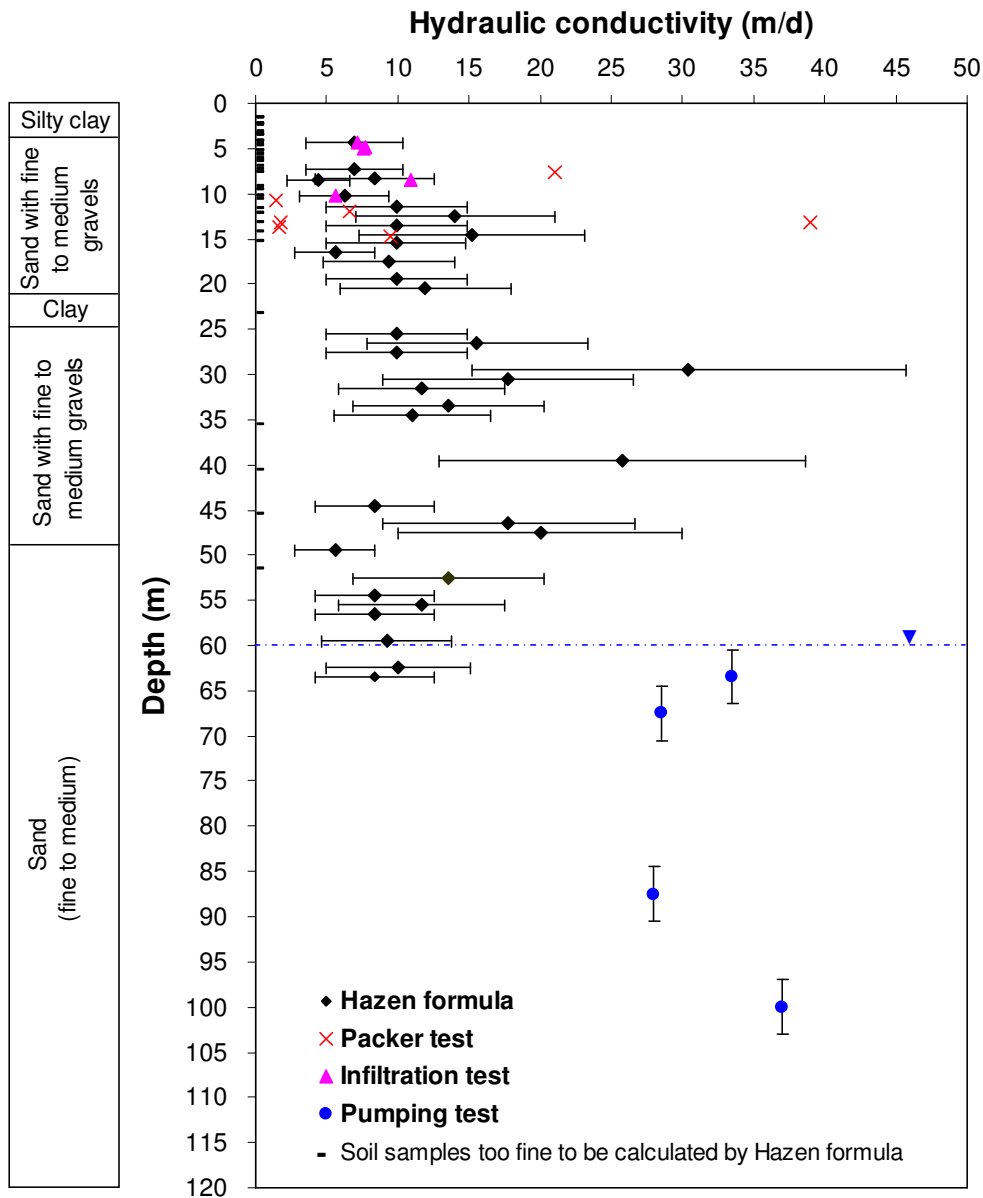


Figure 4.10 Comparison of estimated hydraulic conductivity vs. depth

A statistical analysis of all the hydraulic conductivity was carried out to have a quantitative comparison. The results of this analysis are given in Table 4.4, and show that the range of hydraulic conductivity values from 1.4 m/d to 64.8

m/d. Such a range indicates soil drainage from poor to good. This implies that the results of the various field tests are relatively close to each other in the unsaturated zone with slightly greater value of 32.0 m/d in the aquifer, such variation in hydraulic conductivity is considered reasonable. Therefore, the various field tests may be said to compare favorably.

Table 4.4 Summary of hydraulic conductivity test results

No.	Test method	Hydraulic conductivity (m/d)			Stdev	Test no.
		Range	Median	Average		
1	Packer test	1.4 - 39.0	6.6	11.6	13.96	7
2	Hazen formula					
	K_{min}	2.2 - 21.6	5.0	6.0	3.83	48
	K_{max}	6.6 - 64.8	14.9	18.0	11.49	48
3	Infiltration test	5.6 - 10.9	7.6	7.8	1.94	5
4	Pumping test	28 - 38	32.0	31.8	3.55	10

4.5 Water quality

Water Samples were collected from 5 boreholes on the site on March, 2002 and analyzed at Al-Azhar University Laboratories in Gaza according to standard methods for examination of water and wastewater (Lenore, 1999). Electrical conductivity, water temperature, and pH were measured directly in the field. The pH is controlled by the amount of dissolved carbon dioxide (CO_2), carbonates (CO_3^{2-}) and bicarbonate (HCO_3^-) (Domenico and Schwartz, 1990). The pH ranges from 7.1 to 7.4. The TDS can be estimated by multiplying the electrical conductivity measurement by a predetermined factor. This factor, which is determined gravimetrically, ranges between 0.55 and 0.9. In the present case a value of 0.62 was used. The content of total dissolved solids in ground water samples ranged from 1130 mg/l to 1270

mg/l. Alkalinity is a measure of the bicarbonate, carbonate, and hydroxide ions. The bicarbonate- ion was determined volumetrically by titration against dilute sulphuric acid using the methyl orange indicator, where the yellow color changes to orange at the reaction's end point. The alkalinity concentration in the water samples ranges from 287 mg/l to 326 mg/l. The calcium-ion (Ca^{2+}) concentration in groundwater samples was determined complexometrically by addition of the hydroxylamine to adjust the pH value at 10. The Murexide indicator was then used where its color changes from red to violet at the end point. The calcium-ion concentration (Ca^{2+}) ranged from 11 mg/l to 36 mg/l. The chloride ion (Cl^-) is the most widely distributed in the natural water. The chloride ion concentration in groundwater samples was determined by silver nitrate titration method. Chloride ions are titrated with silver nitrate in the sample solution in the presence of potassium chromate. Silver chloride precipitate is first formed, and when this reaction is completed, red silver chromate is formed at the end point. Chloride ion concentration ranged from 268 mg/l to 329 mg/l. The dissolved nitrogen in form of nitrate (NO_3^-) is the most common contaminant identified in groundwater in the Gaza Strip. Nitrates were determined by the Cadmium reduction method, followed by spectrophotometric measurement at 540 nm wavelength. Nitrate nitrogen has proved to be a health hazard when it occurs in drinking water at concentrations in excess of 10 mg/l according to World Health Organization (WHO) standard. Nitrate concentration ranged from 15 mg/l to 20 mg/l. The summary of water quality results are shown in Table 4.5.

Table 4.5 Chemical analysis of groundwater from observation wells

Well No.	Temp. C°	pH	TDS (mg/l)	Alkalinity (mg/l) as CaCO ₃	Nitrate (mg/l) as (NO ₃)	Calcium (mg/l)	Chloride (mg/l)
SD2	25.0	7.1	1180	326	15	12	268
SD4	24.5	7.1	1230	324	16	36	300
DB1	25.5	7.4	1250	296	20	11	329
DB2	25.0	7.3	1130	287	17	32	315
DB4	23.0	7.2	1270	305	18	29	325

Also, groundwater samples are analyzed regularly by the Palestinian Water Authority. The chemical analyses shown in Table 4.6 were done in the autumn of 2002 for the municipal wells in the northern Gaza Strip. Locations of the municipal wells in the northern of the Gaza Strip are show in Figure 4.11. The trend of nitrate and chloride concentration in the surrounding towns of the study area as Jabalia, Beit-Hanun and beitlahia from year 1990 to year 2002, in spring and autumn are shown in Figure 4.12.

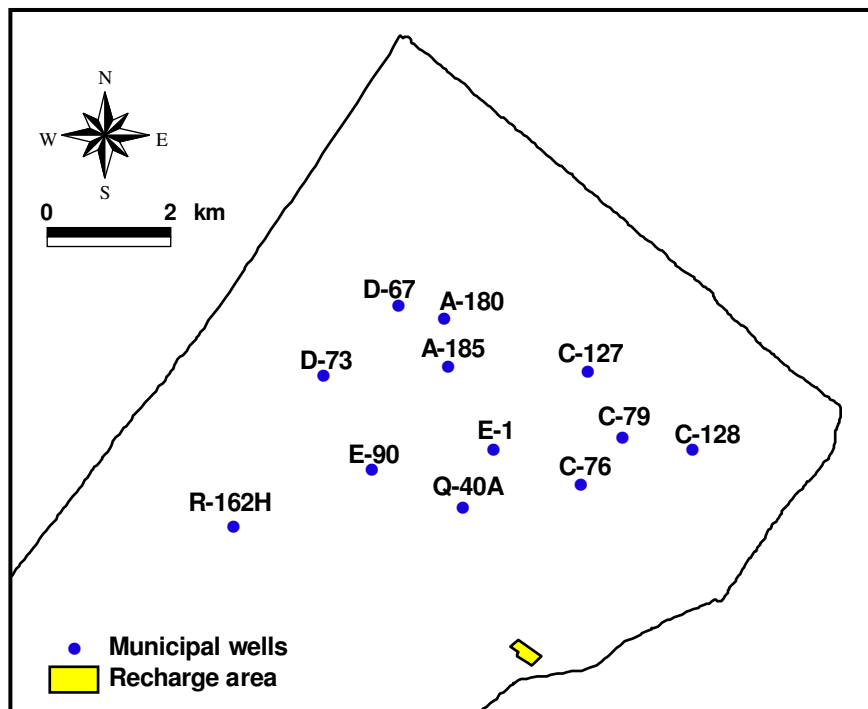


Figure 4.11 Location of the municipal wells in the north of the Gaza Strip

Table 4.6 Chemical analysis for municipal wells in the north of the Gaza Strip (Autumn 2002)

Well No.	E.C μs/cm	TDS mg/l	pH	Hardness mg/l	F mg/l	Ca mg/l	Mg mg/l	Na mg/l	K mg/l	Cl mg/l	NO ₃ mg/l	Alkalinity mg/l	SO ₄ mg/l
A-180	954	593	7.98	369	0.4	94	32	50	2.6	99	75	312	28
A-185	1058	655	7.98	389	0.55	95	36	52	6.2	106	125	299	45
C-127	870	540	8	239	0.75	52	26	80	2.1	92	48	251	76
C-128	1533	952	8.01	322	0.81	59.2	42.4	184	2.4	248	64	312	55
C-76	2200	1364	7.81	589	0.86	106	77	250	3	476	46	327	50
C-79	2453	1521	7.7	560	0.65	106	71	265	3.1	476	105	398	80
D-67	591	368	8.3	183	1.5	46	16	30	1.5	35	36	213	15
D-73	747	464	8.17	272	0.55	71	22	42	4.6	64	52	271	25
E-1	835	548	7.27	309.1	0.61	74.8	29.6	60	2.4	120.4	81.2	251.2	33
Q-40A	1170	725	7.39	317.1	0.45	63.41	38.5	120	4.93	177.1	62.81	333.2	40
E-90	1675	1038	7.04	544	1.1	110	65	106	3.5	191	223	322.9	43
R-162H	2799	1738	7.42	482	1.3	91.4	61	415	8	490	224.5	405.7	195

(PWA, data bank, 2003)

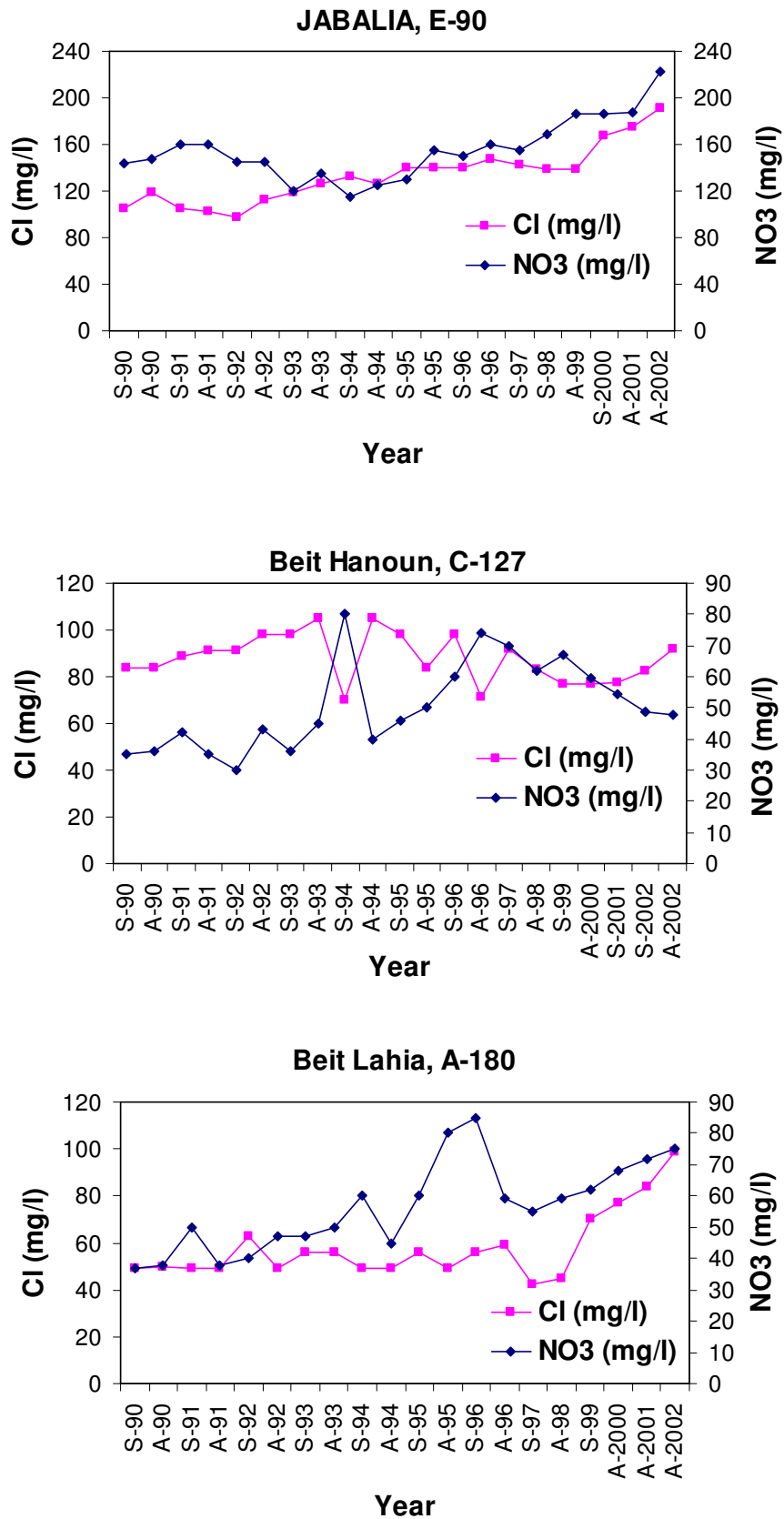


Figure 4.12 Chloride and nitrate trend near the study area

Chapter 4 : Hydrogeological study

Hydrochemical facies can be classified on the basis of the dominant ions by means of the trilinear diagram as shown in Figure 4.13. Analyses are plotted on the basis of the percent of each major cation or anion. The groundwater extracted from the municipal wells in the northern of the Gaza Strip are generally considered as having no dominant type of cations, but anions clearly dominated by chloride. No specific cation-anion pair exceeds 50 percent of the total dissolved constituent load. Such waters could result from multiple mineral dissolution or mixing of different chemically distinct groundwater bodies, while wells C-128 and R-162H are considered as brackish or saline; combined concentrations of alkali metals, sulphate and chloride are greater than 50 percent of the TDS.

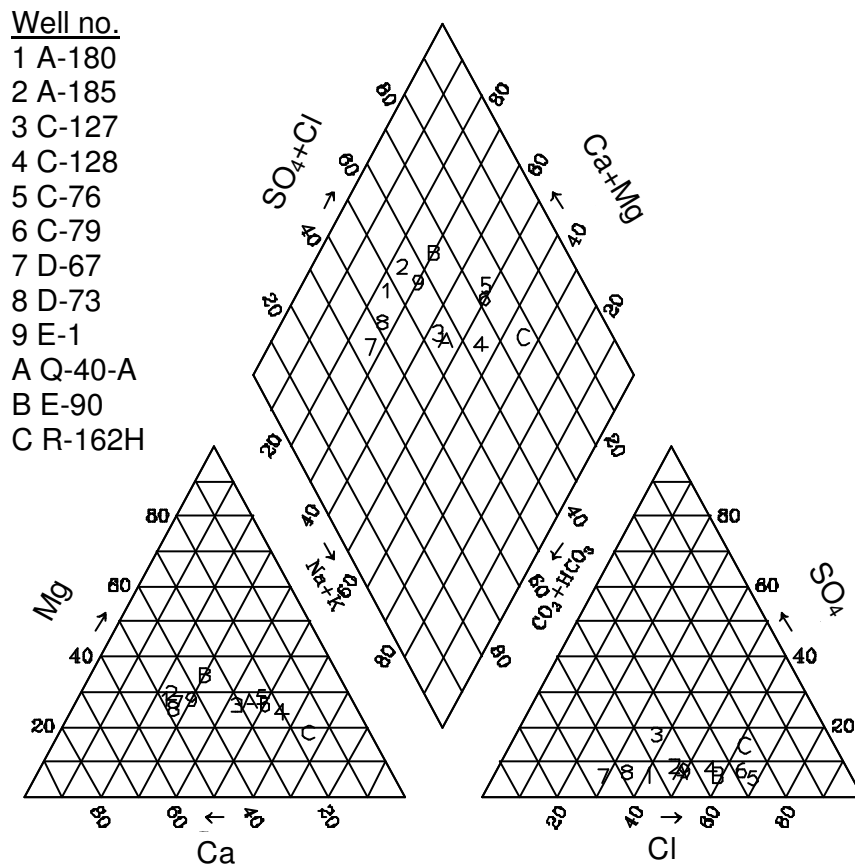


Figure 4.13 Trilinear diagram of major –ion composition of groundwater

4.6 Summary

The field investigation gives clear information about the study area. The topsoil consists of a 3 to 14 m thick clay layer. The excavation of clay is needed. The soil underlying the clay layer is sandy material (kurkar). Interbedded clay layers separate the aquifer into major upper and deeper sub-aquifers. The average hydraulic conductivity of the upper sandy material obtained from packer test and Hazen formulae are 11.6 m/d and 12 m/d. The infiltration test shows that the infiltration capacity of the sand with gravel ranges from 9.9 m/d to 15.1 m/d. The hydraulic conductivity obtained from infiltration tests varies between 5.6 m/d and 10.9 m/d.

The hydraulic properties of the aquifer system were determined by a pumping test, yielding a transmissivity of 2400 m²/d and a specific yield of 0.24. The groundwater level is found at about 50-60 m depth, which approximately is 1m above sea level. This means that the unsaturated zone is extensive. The hydrogeological investigations of the study area indicate the suitability for artificial recharge of treated wastewater by mean of infiltration basins.

Chapter 5: Groundwater mound modeling

(Local model)

The purpose of the local model is to determine if a proposed discharge of treated wastewater in the northern of the Gaza Strip to an unconfined aquifer would be feasible and not cause excessive mounding of the water table. The recharge area is about 80000 m², and the expected maximum amount of treated wastewater in year 2020 is about 60,000 m³/d, such that the infiltration rate will be 0.75 m/d. Analytical and numerical models for calculating the groundwater mounding are applied.

5.1 Analytical solution

Infiltration from a recharge basin produces a groundwater mound above the original water table as shown schematically in Figure 5.1. The dimensions of the mound are governed by the basin size and shape, recharge rate and aquifer characteristics. Theoretical and experimental studies on the subject of artificial recharge of groundwater through surface spreading have been reported by Glover (1961), Marmion (1962), Marino (1967, 1974), Hantush (1967), Bianchi and Muckel (1970), Rao and Sarma (1983), and Latinopoulos (1986). Most of these solutions are based on the assumption of a constant rate of recharge applied continuously or periodically. Common to all these solutions are the assumptions that percolation moves vertically downward until it joins the main groundwater body and that the flow of groundwater takes place in a homogeneous, isotropic, unconfined aquifer having hydraulic properties that remain constant with both time and space. The shape of a

Chapter 5 : Groundwater mound modeling

mound beneath a rectangular recharge area, expressed by $h-h_0$ (Figure 5.1), is the mound height in function of time and space, depending upon the artificial recharge flux, the storage coefficient and transmissivity of the aquifer.

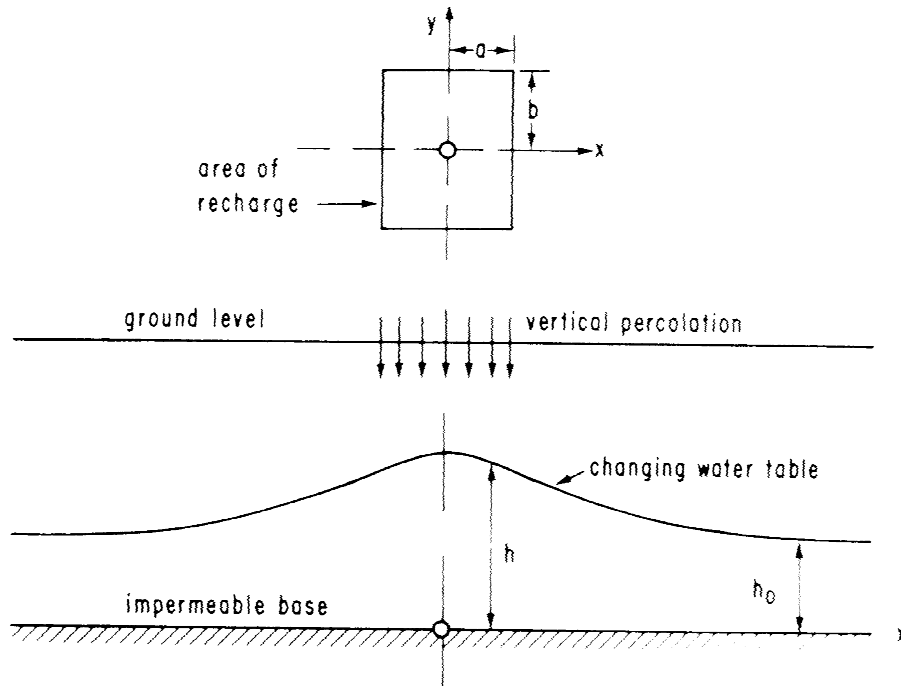


Figure 5.1 Diagrammatic representation of the rise of the water table beneath a rectangular recharging area

In the local model an analytical solution is used to compare with a numerical solution of the transient groundwater flow to predict the time-dependency of the groundwater response in case of the planned artificial infiltration pond of the wastewater treatment plant in the northern of the Gaza Strip, Palestine.

The analytical solution provided by Hantush (1967) to predict mounding beneath a rectangular infiltration basin was applied using a public-domain software program called MOUNDHT (Finnemore, 1995) as shown in Figure 5.2.

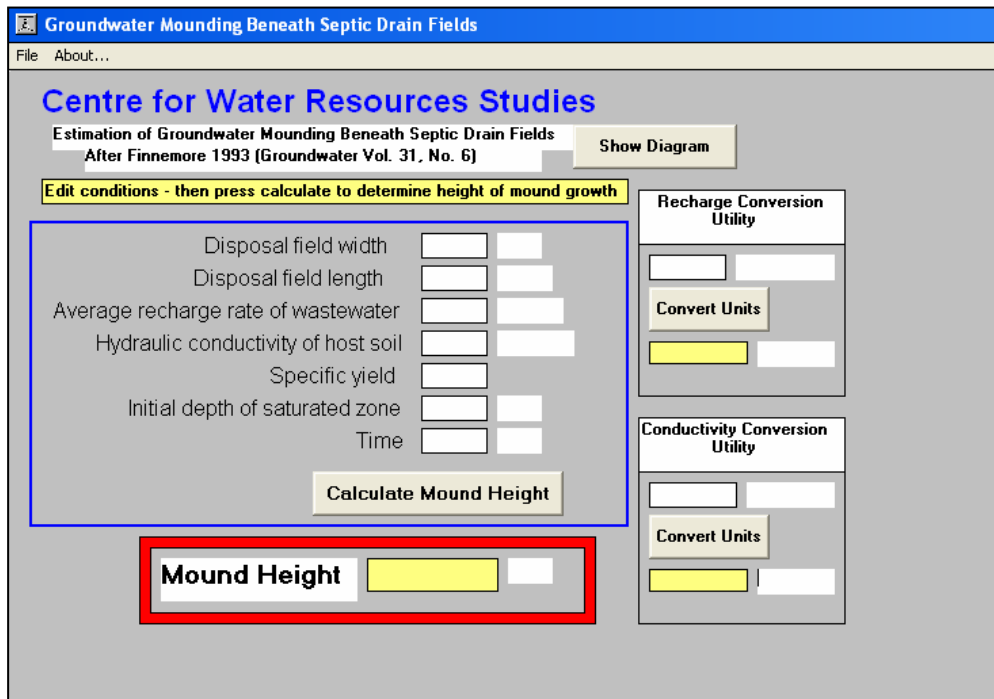


Figure 5.2 MOUNDHT interface: A sample front section view

The Hantush method assumes an infinite, initially near-horizontal saturated zone in an isotropic, homogeneous aquifer, bounded at its base by an impermeable layer (Hantush, 1967; Finnemore, 1993). The method assumes that a constant vertical recharge is applied to a rectangular infiltration area of fixed dimension, and that the water table mound remains below the base of the infiltration area at all times. The maximum groundwater mound is given by equation 5.1.

$$h = \frac{It}{S_y} S^*(\alpha, \beta) \quad (5.1)$$

where h is maximum mound height, I is the constant rate of percolation, t is the time since percolation began, S_y is the specific yield of the aquifer and $S^*(\alpha, \beta)$ is the tabulated values of a function, S^* . The arguments α, β are

given by $\alpha = \frac{L}{4} \sqrt{\frac{S_y}{Kht}}$ and $\beta = \frac{W}{L} \alpha$ where L is the basin length, W is its width and K is horizontal hydraulic conductivity of the aquifer. Appendix 2.1 provides S^* as a function of (α, β) . The values of S^* computed by program MOUNDHT. The hydrogeologic setting and assumptions used for analytical solutions are obtained from the hydrogeological study, mean hydraulic conductivity of 32 m/d, specific yield of 0.24 and original water level about 1 m above sea level. A recharge value of 0.75 m/d, and the recharge basin schematized as a rectangular recharge basin of 175 by 450 m, the obtained results are as shown in Figure 5.3. At the center of the basin after 100 days, the height of groundwater mound rises to about 14 m above the present groundwater table.

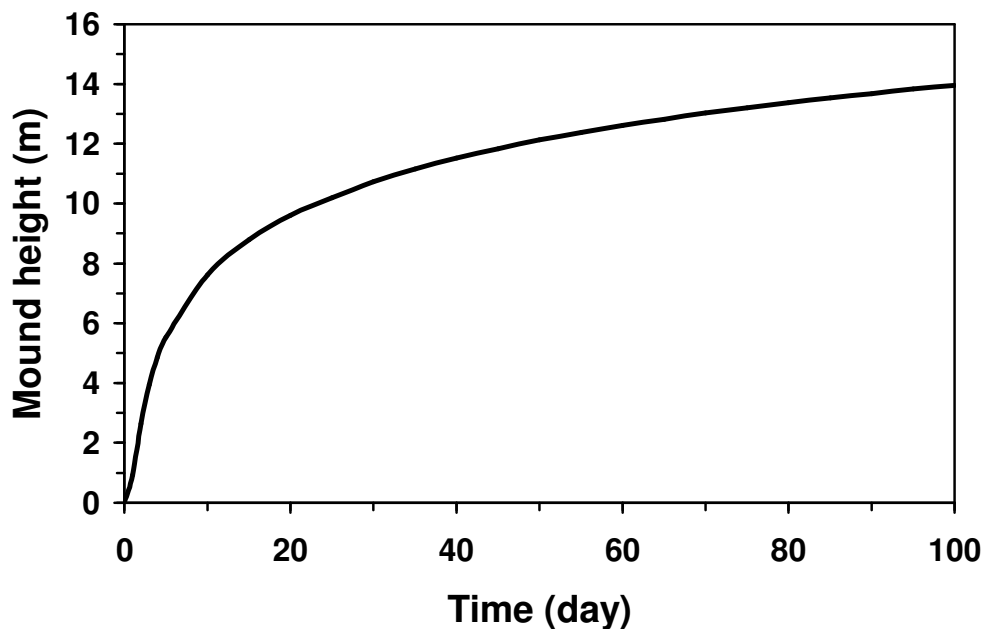


Figure 5.3 Height of the groundwater mound under the center of the basin

5.2 Numerical modeling

5.2.1 The conceptual model and grid design

Grid is chosen with in order to simulate the groundwater mounding by means of a numerical model, a regular cell size of 25 m by 25 m, such that the aquifer system is discretised with square grids as shown in Figure 5.4. The modeled area consists of 100 columns and 100 rows. The model domain encloses a square area of 2.5 km x 2.5 km centered around the infiltration ponds.

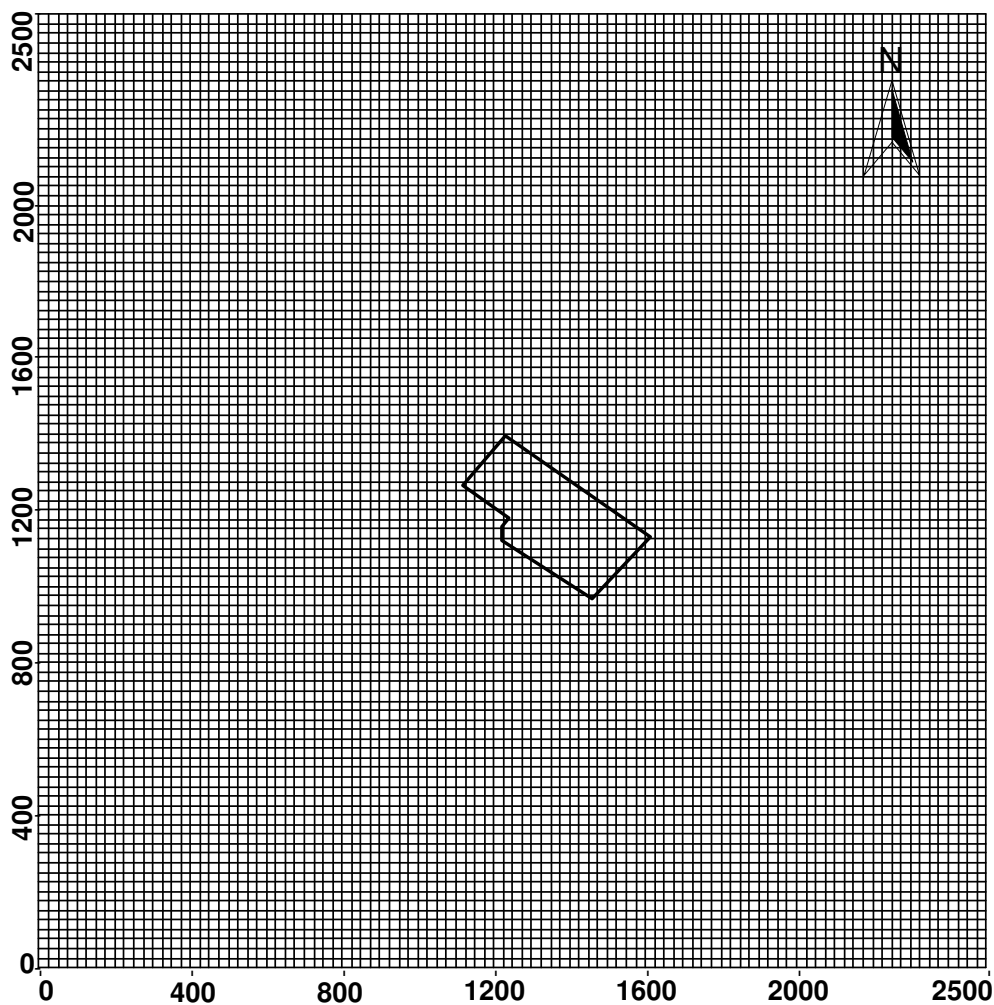


Figure 5.4 Conceptual model and grid design

5.2.2 Model construction

The aquifer is considered as an unconfined aquifer with a stratigraphy of 7 layers with alternating finer and coarser unconsolidated sediments belonging to the sandstone (Kurkar) formation. The layers are approximately horizontal, with a small inclination towards the sea as shown in Figure 5. 5. The cross-section is passing through $Y = 1200$ m in Figure5.7. The aquifer extends to areas far outside the chosen model domain. The boundary conditions are assigned as no-flow boundaries in all sides of the model. The initial water level is 1 m above sea level, as measured in boreholes within the site and in the private wells in the vicinity of the site.

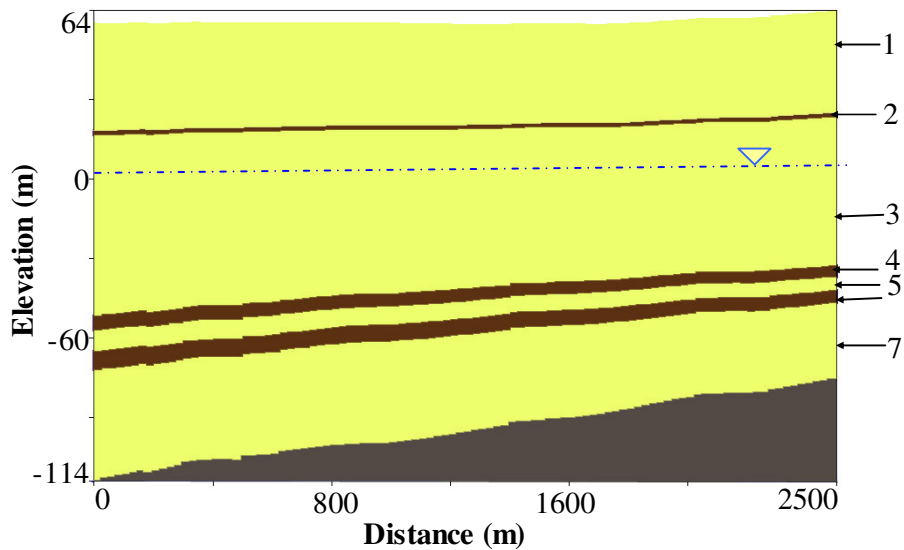


Figure 5.5 Model layers: 1- Sand with fine gravel, 2- Clay, 3- Sandstone, 4- Clay, 5-Sandstone, 6- Clay and 7- Sandstone

5.2.3 Model input parameters

Hydraulic property values are assigned based on the hydrogeological investigation. The hydraulic conductivity is assumed to be constant for each layer. The vertical hydraulic conductivity of the unsaturated zone for the soil types investigated is 18 m/d for sand with fine gravel and 0.3 m/d for clay. The horizontal hydraulic conductivity of the sandstone aquifer and the phreatic storage coefficient are taken from the pumping test. The vertical conductivity was set to 10% of the horizontal hydraulic conductivity. The recharge rate is 0.75 m/d similar as in the analytical solution. Other model inputs are shown in Table 5.1.

Table 5.1 Hydraulic parameters value for model inputs

Parameter	Sand with fine gravel	Sandstone	Clay
Hydraulic conductivity (m/d) K_h, K_v	18, 18	32, 3.2	0.3, 0.3
Specific storage (m^{-1}) S_s	$1 \cdot 10^{-5}$	$1 \cdot 10^{-5}$	$1 \cdot 10^{-5}$
Specific yield S_y	0.24	0.24	0.10
Effective porosity	0.25	0.25	0.40
Total porosity	0.30	0.30	0.45

5.2.4 Results

For representing the rise of the resulting groundwater mound, five observation points (wells) in the center and at the edges of the recharge area are considered, with results as shown in Figure 5.7. The simulation shows that the groundwater mound beneath the center of an infiltration area can be expected to rise to above around 14 m and at the edges to about 11 m to 12.5 m after 100 days, as shown in Figure 5.6.

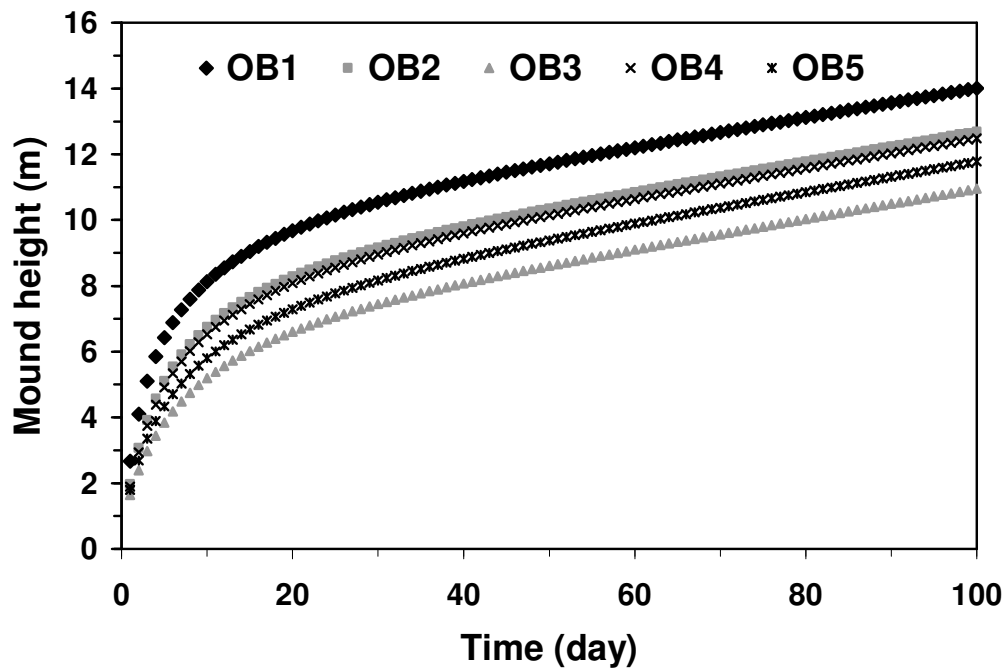


Figure 5.6 Height of the groundwater mound beneath the recharge basin calculated with the numerical model

Chapter 5 : Groundwater mound modeling

The shape and spread of the groundwater mound after 100 days in the immediate surroundings of the infiltration ponds is depicted in Figure 5.7.

Obviously the groundwater mound reaches the edge of the model domain, exceed 4 m above sea level and will be influenced by model boundaries. It would be better to extend the model laterally with course cells for a distance of at least 2500 m to be the total model domain 5000 by 5000 m.

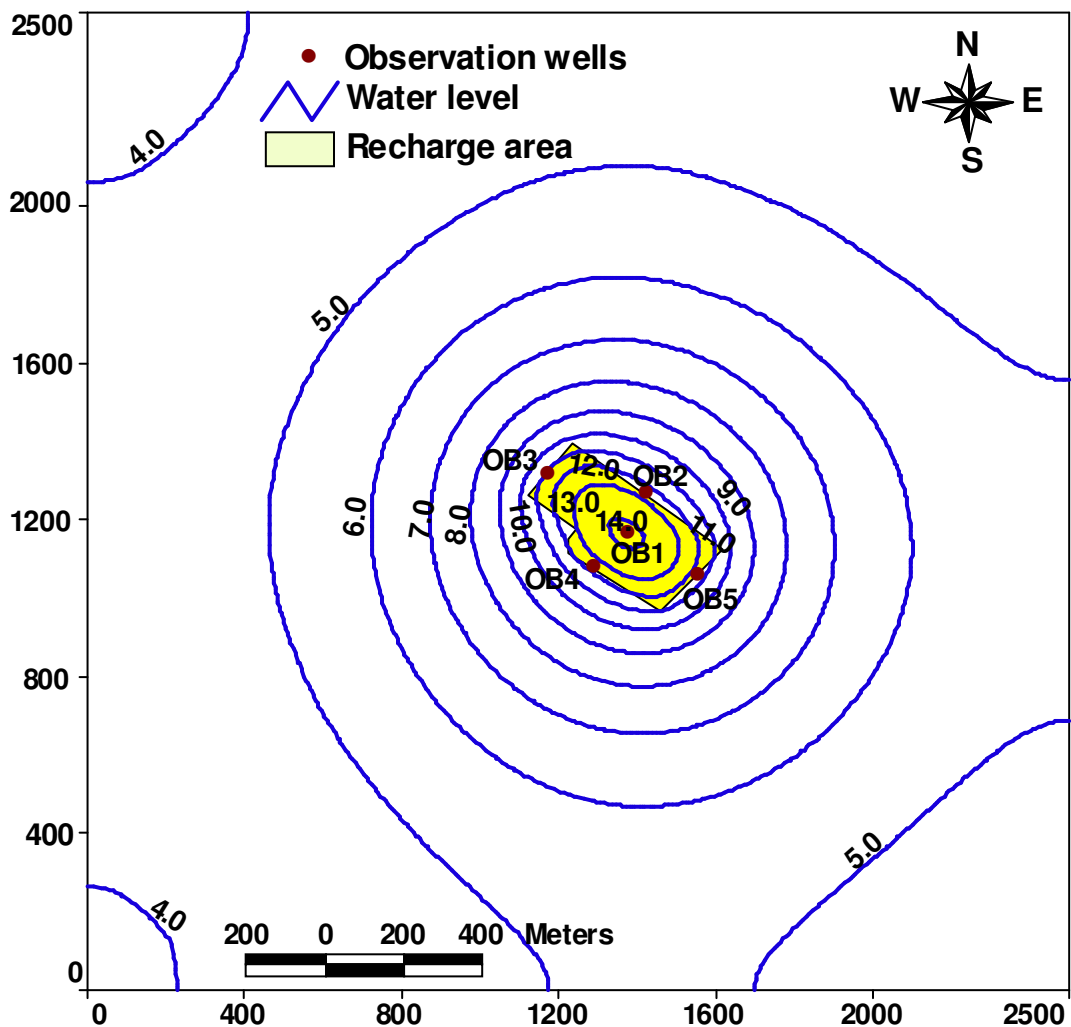


Figure 5.7 Groundwater mound after 100 days beneath recharge basin with five observation wells

5.3 Comparison of numerical and analytical results

The growth of the groundwater mound obtained with the model simulation is compared to the analytical solution as shown, in Figure 5.8. One can notice a very good agreement. The small differences can be explained by the assumptions that were made in case of the analytical solution, i.e. a rectangular basin and an average groundwater table elevation to calculate the aquifer transmissivity. However, at 100 days both methods give similar results, which indicate that the rise of the groundwater mound is about 14 m, which will not cause any problem to the site or surrounding areas.

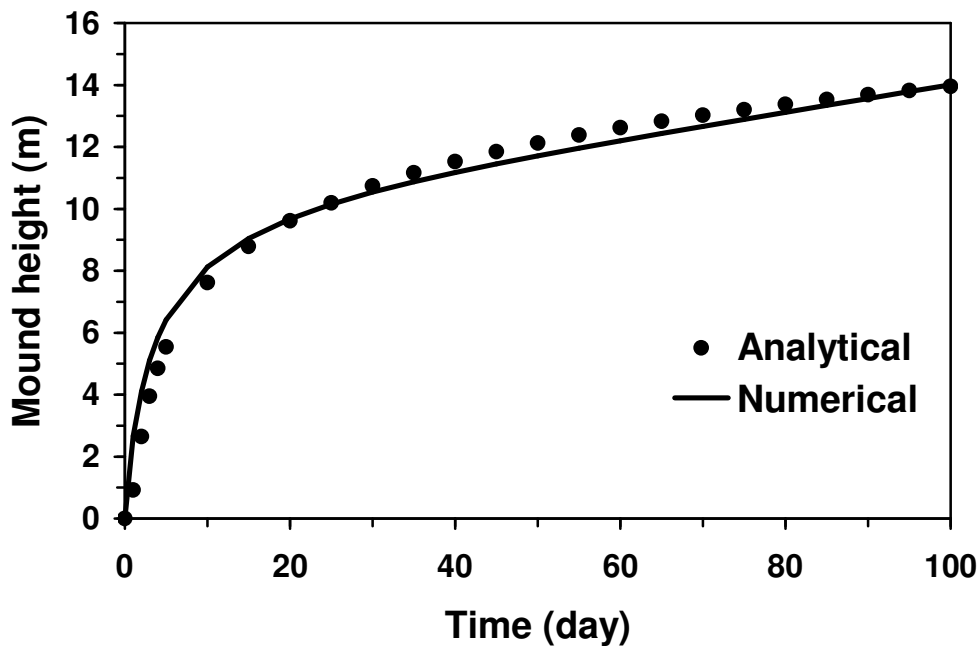


Figure 5.8 Comparison of numerical and analytical results showing the rise of the groundwater mound in the center of the infiltration basin

5.4 Summary

Planning and feasibility studies for artificial recharge of groundwater must include estimates of infiltration rates, and rise and extend of the resulting groundwater mound.

The hydrogeological field and laboratory analysis were used to develop an analytical and a numerical model of the study area in the Gaza Strip, where artificial groundwater recharge system has been planned. The unconfined aquifer receiving the recharge is assumed to have constant properties in time and space.

The results of the numerical model simulations are compared with an analytical solution; both are found to be in good agreement. It is shown that the groundwater mound will rise to about 14 m after 100 days. As the unsaturated zone is about 60 m thick, the artificial infiltration is considered to be feasible with infiltration rate of 0.75 m/d and maximum amount of treated wastewater about 60,000 m³/d. The treated wastewater quality should be according to Palestinian treated wastewater reuses guidelines. However, to get a more correct picture of the effect of the groundwater mounding and water flow on regional scale, a simulation with a large regional groundwater flow model of the whole Gaza Strip will be explained in chapter 6.

Chapter 6: Regional groundwater modeling

The purpose of the regional groundwater modeling is to study the influence on the groundwater of artificial recharge planned in the Gaza strip and to get a more comprehensive view of the effect of the groundwater mounding on regional scale.

6.1 Conceptual model and grid design

As shown in Figure 6.1, the regional model grid consists of a finite difference mesh of 184 columns and 60 rows. The grid is a regular with a cell size of 250 m by 250 m, but in the artificial recharge area the cell size of 25 m by 25 m.

The boundary conditions in the model are assigned as no- flow boundaries in the north and the south where the groundwater flow is perpendicular to the coast line. A constant head boundary was assigned in the east, when the groundwater levels along the boundary are assigned according to the data from a contour map of groundwater level for the year 2000.

In a small region near the artificial recharge area the constant head boundary is replaced by a general (third type) head boundary condition, with the same head value and conductance of $454 \text{ m}^2/\text{d}$. This will allow the head value along the boundary to be adjusted according to the impact of the artificial recharge.

The western boundary is assigned a zero constant head formed by the Mediterranean Sea. The outer areas are inactive cells. For the purpose of model construction, the aquifer system is schematized in 7 layers as shown in Figure 6.1. There are 4 subaquifers of sand with gravel (Kurkar formation) and 3 major clay layers. The base of the model consists of Saqiye group, assumed to be impermeable. General model stratigraphy is depicted as 3-D

Chapter 6 : Regional groundwater modeling

representation in Figure 6.2. The geological data were taken from Palestinian Water Authority and the Gaza coastal aquifer management program (Metcalf and Eddy, 2000).

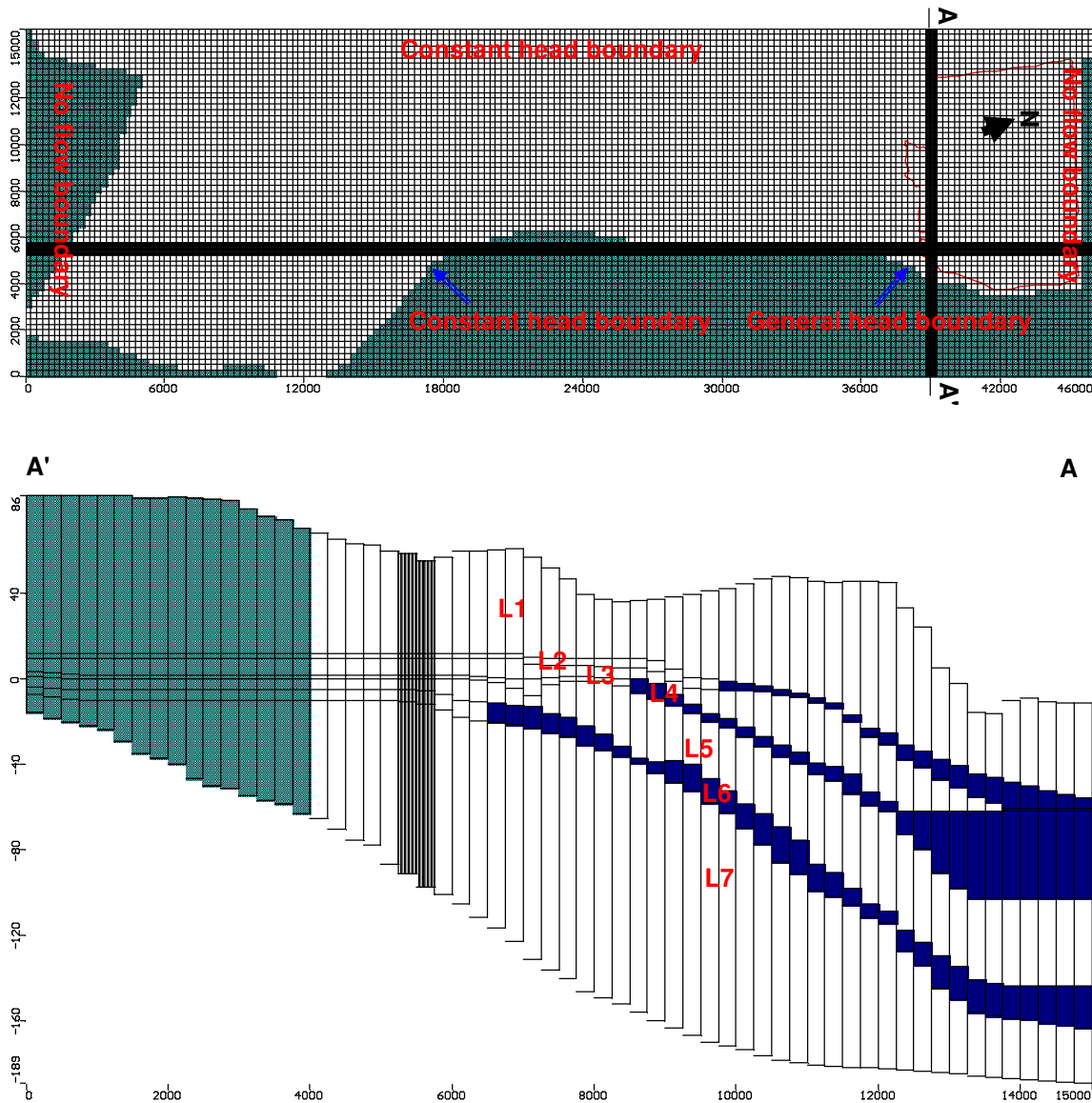


Figure 6.1 Plan of the model area showing the grid size and boundary conditions

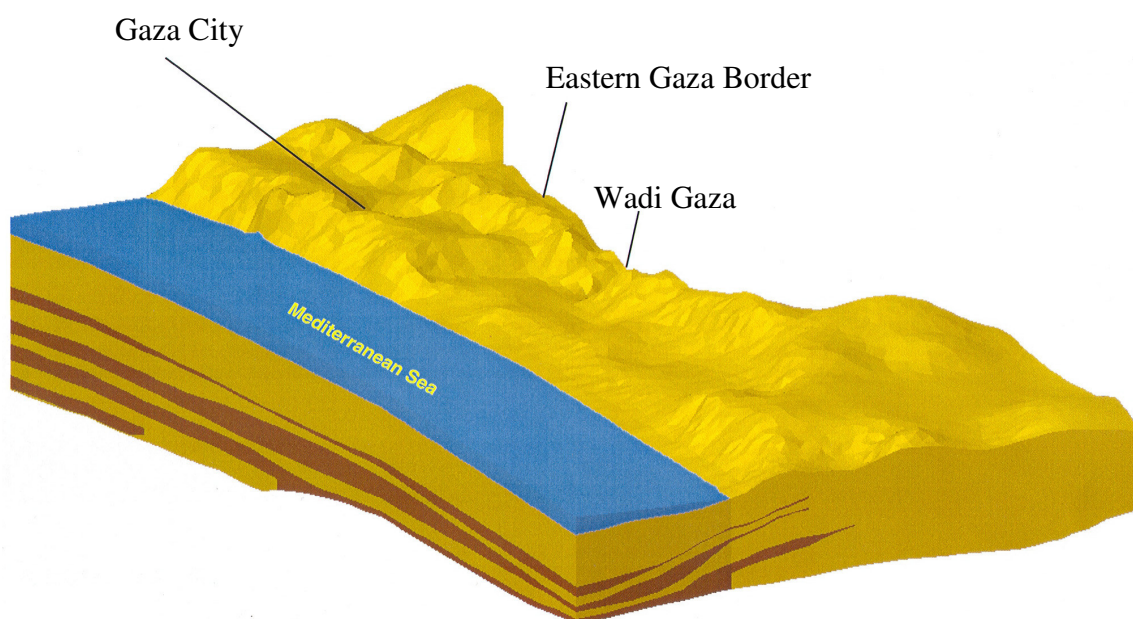


Figure 6.2 Model topography and 3-D view of stratigraphy in Gaza Strip

6.2 Model input

6.2.1 Hydraulic parameters

Hydraulic property values are assigned in the model based upon geologic and aquifer testing data and previous studies. In the model the hydraulic values have been assumed constant for each layer. The ranges of hydraulic values assumed or estimated in the model are summarized in the Table 6.1.

Table 6.1 Hydraulic parameters value for model inputs

Parameter	Sandstone	Clay
Hydraulic conductivity (m/d) K_h, K_v	32, 3.2	0.3, 0.3
Specific storage (m^{-1}) S_s	$1. 10^{-5}$	$1. 10^{-5}$
Specific yield S_y	0.24	0.10
Effective porosity	0.25	0.40
Total porosity	0.30	0.45

The hydraulic parameters values adopted in the groundwater model are chosen based on pumping test in hydrogeological study and on reported groundwater studies (Yakirevich, 1998).

6.2.2 Pumping wells

According to the Palestinian Water Authority, there are around 78 municipal wells within the Gaza Strip. The estimated municipal abstraction totals about 51 Mm³/year. Agricultural wells have not been metered since 1994. The total average annual abstraction for the 1500 metered wells over the period of records (1988-1993) was approximately 34 Mm³/year.

Extrapolation prorating this average over the estimated about 3800 wells in operation at present, yields an estimated total agricultural abstraction of about 90 Mm³/year (+/-10%).

Data from Israeli reports on the Gaza Strip in the 1970s would suggest that agricultural abstraction has been relatively stable since the late- 1960s to present. Bachmat and Melloul (1975) estimated the total agricultural pumping of about 90 Mm³/year in 1973/74.

Melloul (1992) also reported a total agricultural pumping of about 82 Mm³/year in 1990. Municipal and agricultural wells located within the Gaza Strip are shown in Figure 6.3.

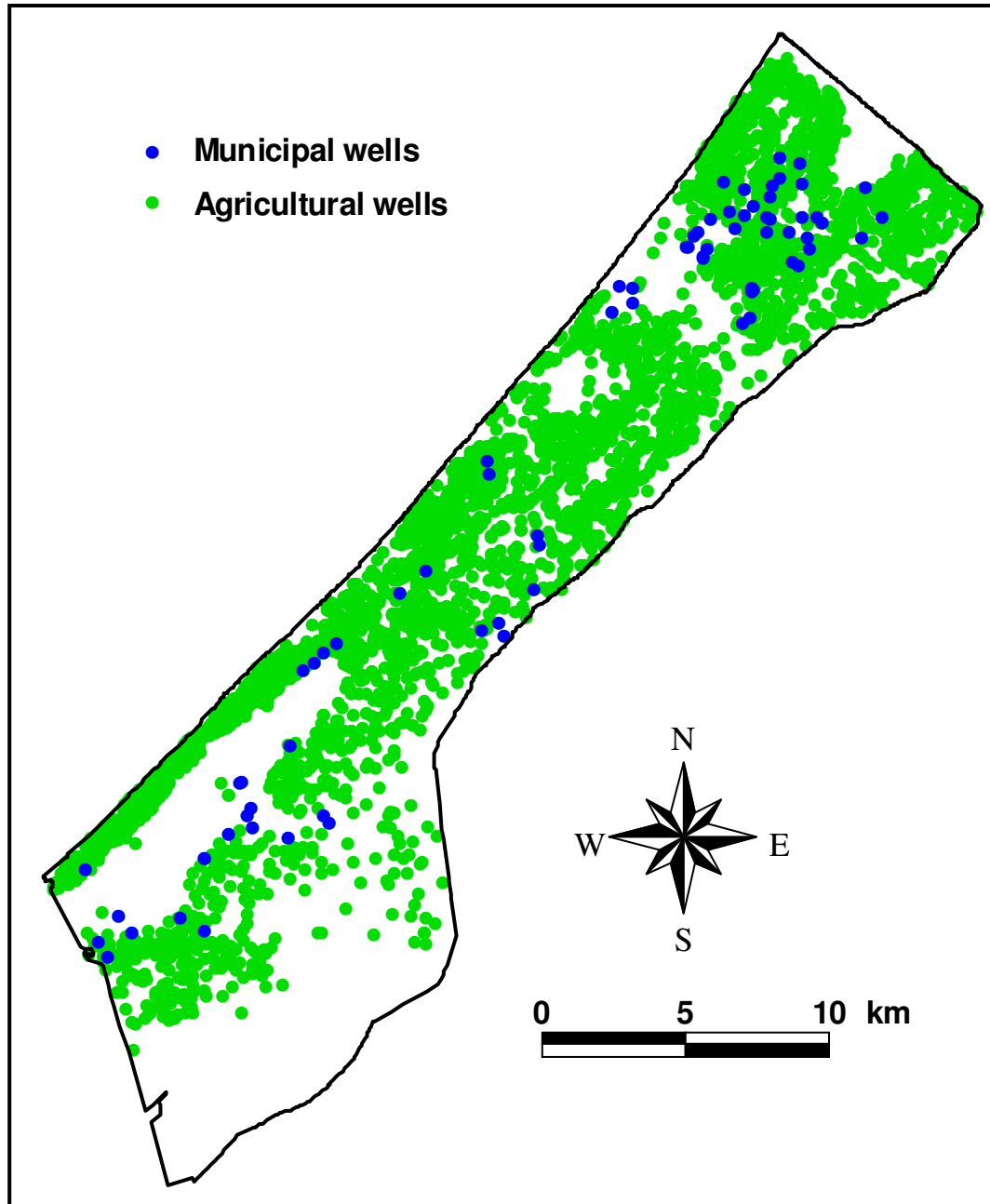


Figure 6.3 Location of Municipal and agricultural wells

6.2.3 Settlements abstraction

There are around 20 settlements in the Gaza Strip. Fink (1989) indicated that the total quantity pumped in the settlements in 1988/89, was 4.5 Mm³/year. The total annual abstraction used in the model was estimated as 5 Mm³/year.

Figure 6.4 shows the settlements location in the Gaza Strip.

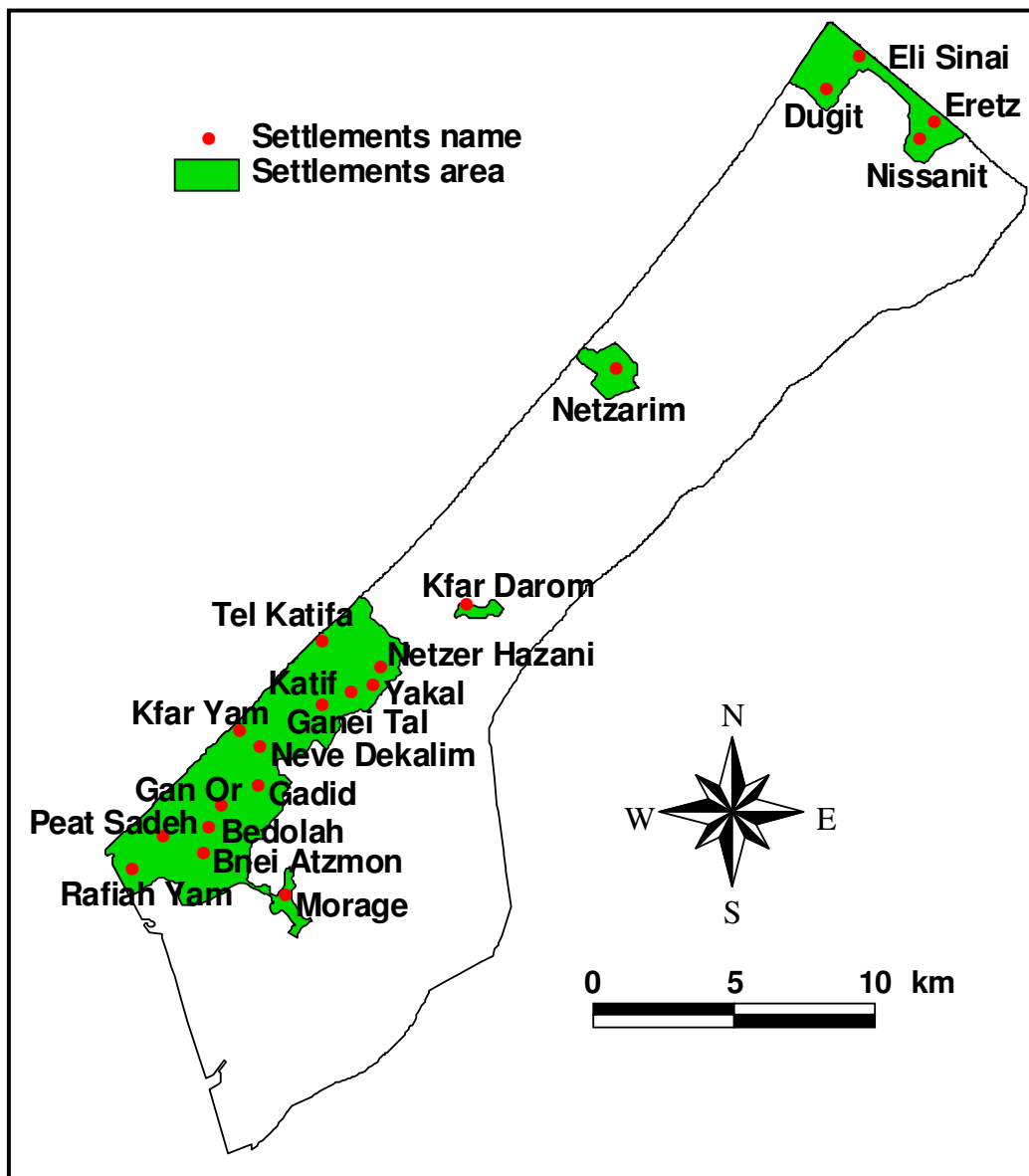


Figure 6.4 Settlements locations in the Gaza Strip

6.2.4 Recharge

Recharge from rainfall accounts for most of the renewable resources of the Gaza coastal aquifer. The recharge was calculated using the WetSpass model; the average annual recharge was estimated to be about 41 Mm³/year; the recharge map is presented in Figure 6.5. In WetSpass, some physical and hydrological parameters of the area, namely, the topography, the soil type, wind speed and potential evapotranspiration are needed as input. Some of used maps in WetSpass model are shown in appendix 2.2.

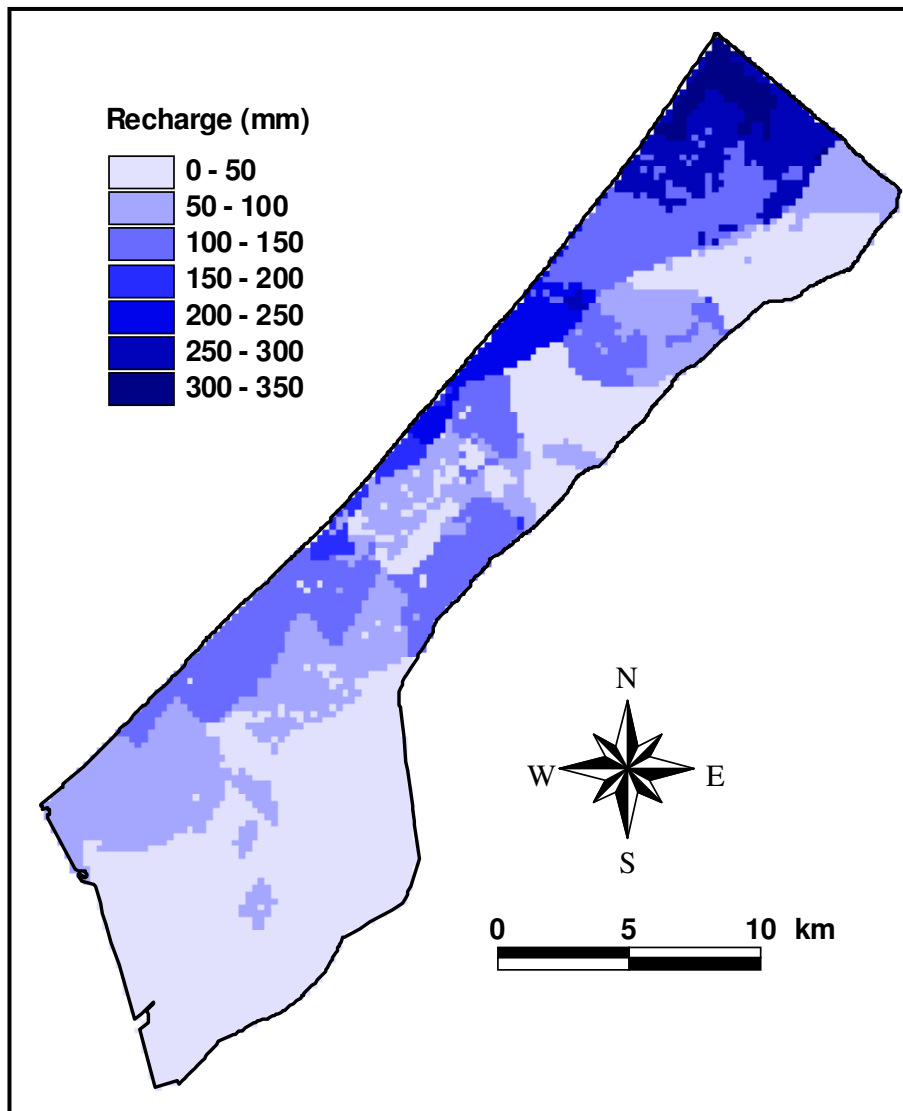


Figure 6.5 Annual groundwater recharge, calculated by the WetSpass model

In previous studies as part of the coastal aquifer management program, different approaches to calculate recharge were investigated. The average annual recharge was estimated as 40-45 Mm³/year, from calibration and sensitivity analysis of numerical flow and transport modeling of the Gaza coastal aquifer, and with the land use recharges coefficients method as 37 Mm³/year (Metcalf and Eddy, 2000).

6.2.5 Return flows

There are three primary sources of return flow in the Gaza Strip: leakage from municipal water distribution system, wastewater return flows and irrigation return flow. According to the Palestinian Water authority, the leakage from municipal water distribution system was estimated as 29 % of the total abstraction (51.0 Mm³/year). Wastewater return flows from Jabalia WWTP in the north and Gaza WWTP in the Gaza City has been estimated to about 25% of the total disposal (18.0 Mm³/year). Irrigation return flow has been estimated to be about 25 % of the total agricultural abstraction (90.0 Mm³/year) (Metcalf and Eddy, 2000).

6.3 Model calibration

Model calibration consists of successive refinement of model input parameters from the initial estimates to improve the fit between observed and model-predicted results. A solution of a steady-state groundwater flow problem requires information including: hydraulic conductivity, boundary conditions, and the location and magnitude of applied sources/sinks such as wells. The calibration procedure typically begins with selective definition of parameters/inputs based on available data and/or an initial conceptual model of the hydrogeologic system. Those parameters that are known or can be reasonably estimated/ assumed are initially specified as part of the input data set.

The steady state model was simulated for the year 2000. This year was selected because it represents a year when rainfall records were close to the long-term average and a relatively comprehensive set of municipal and agricultural abstraction data are available.

It is important to note that true steady state conditions don't exist in the Gaza coastal aquifer. Spatial and seasonal change in groundwater fluxes and rainfall, as well as seawater intrusion, combine to make the coastal aquifer a dynamic system. The model was therefore calibrated against average water levels for the specified hydrological year. Calibration involved comparison of the model results and observed heads at 53 target monitoring wells as shown in Figure 6.6.

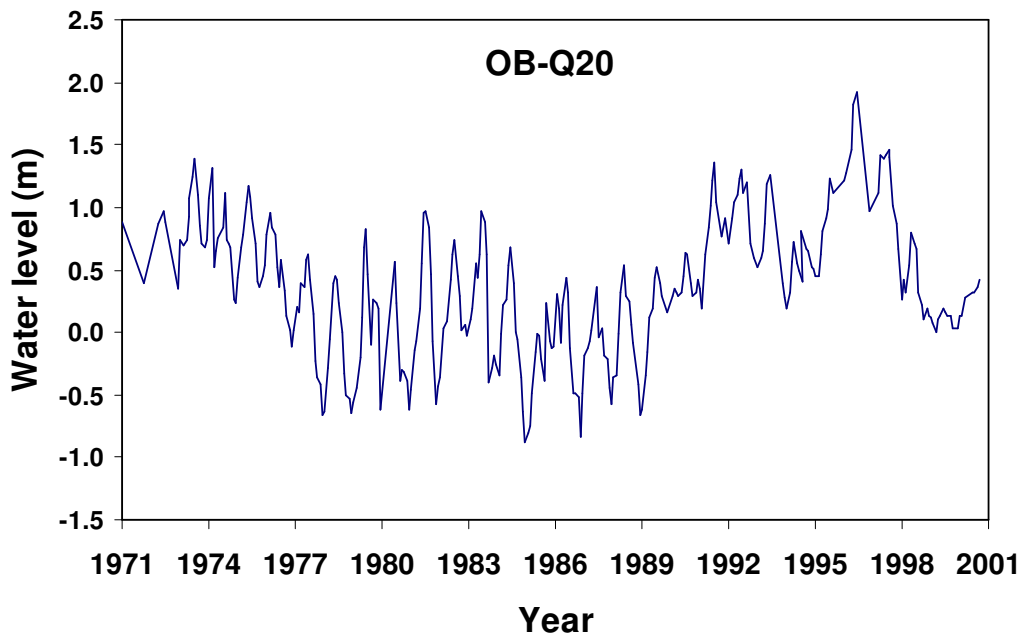


Figure 6.7 Long-term records of water levels (m.s.l.) near the study area

Visual MODFLOW post-processing features allow for a graphical comparison of model-predicted and observed heads, enabling calibration proceeded by trial and error. The obtained calibration residual values are used to calculate statistics such as mean error, mean absolute error, and root mean squared error. Steady- state calibration results and statistics are summarized in Table 6.2.

Table 6.2 Summary of steady-state calibration statistics

Num. points:	53
Max. Residual: at OB-S/50	0.762 m
Standard error of the estimate:	0.053 m
Min. Residual: at OB-C/78	0.004 m
Root mean squared:	0.392 m
Residual Mean:	-0.074 m
Normalized RMS:	7.20 %
Absolute Residual Mean:	0.344 m

Table 6.2 shows that the largest discrepancies occur at well OB-S/50 with overestimate water level by 0.76 m. The model-wide average discrepancy between observed and calculated water level is 0.34 m, and the normalized root mean square error of the estimate is 7.2%. The final calibration graph for the model is shown in Figure 6.8.

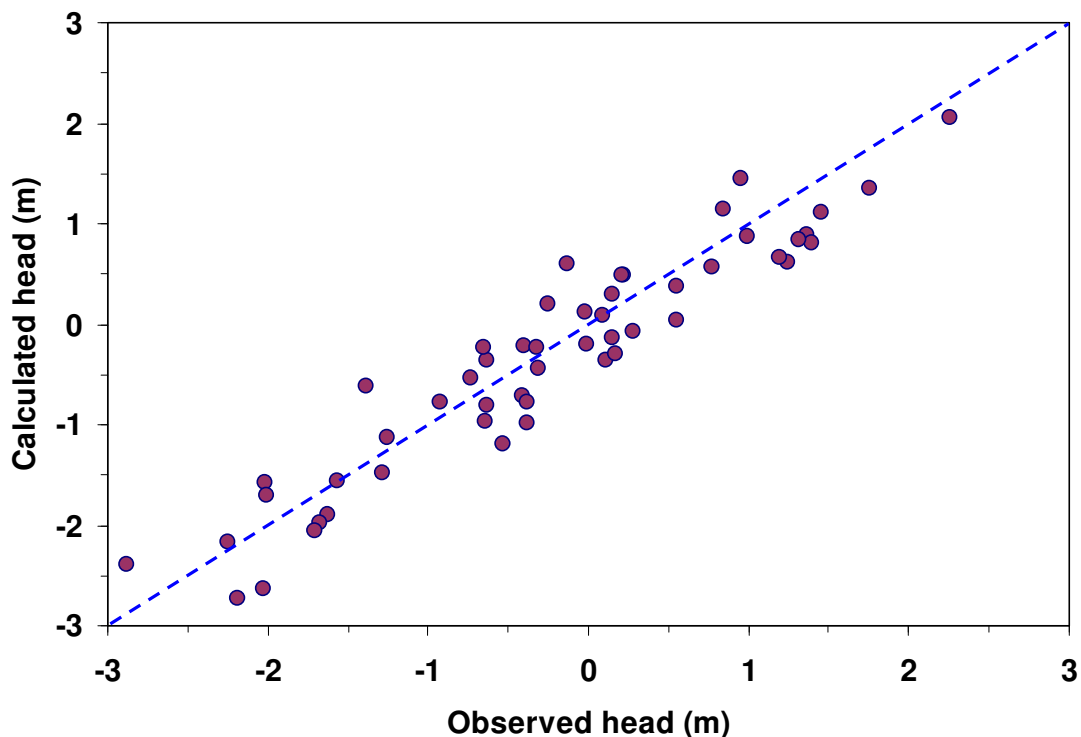


Figure 6.8 Calibration graph of observed vs. calculated water levels in observation Wells

The Gaza coastal aquifer is a dynamic system, with continuously changing inflows and outflows. The aquifer balance in the Gaza Strip is negative; that is, there is a water deficit. Under defined average climatic conditions and pumpage and return flows, the deficit is about 16.0 Mm³/year. Implication of the deficit include: lowering of water levels, reduction in availability of fresh groundwater and seawater intrusion, and potentially upcoming of deep brines.

Chapter 6 : Regional groundwater modeling

Lateral inflow is an important parameter in the overall water balance of the Gaza Strip; however, this is subject to considerable variation from one year to another depending on the hydraulic regime in Israel. It was estimated from the model about 51.8 Mm³/year from north and east. Summary of water balance shown in Table 6.3.

Table 6.3 Summary of water balance in the Gaza Strip for year 2000

Inflows (Mm ³ /year)	
Recharge from precipitation	41.0
Irrigation return flows	22.5
Municipal return flows	14.8
Wastewater return flows	4.1
Lateral inflow from Israel	51.8
Total Inflow	134.2
Outflows (Mm ³ /year)	
Municipal abstraction	51.0
Agricultural abstraction	90.0
Settlements abstraction	5.0
Discharge to the Sea	4.2
Total Outflows	150.2
Net balance (deficit)	-16.0
Seawater intrusion	16.0

6.4 Artificial recharge simulation

6.4.1 Groundwater mound

The groundwater mound is simulated with the regional model adding an extra input a constant recharge of 60,000 m³/d and an infiltration rate of 0.75 m/d, while all hydrogeological conditions, such as groundwater abstractions, remain constant within the model domain. The simulation shows that the groundwater mound beneath the center of an infiltration area can be expected to rise to about 14.1 m after 100 days as shown in Fig 6.9.

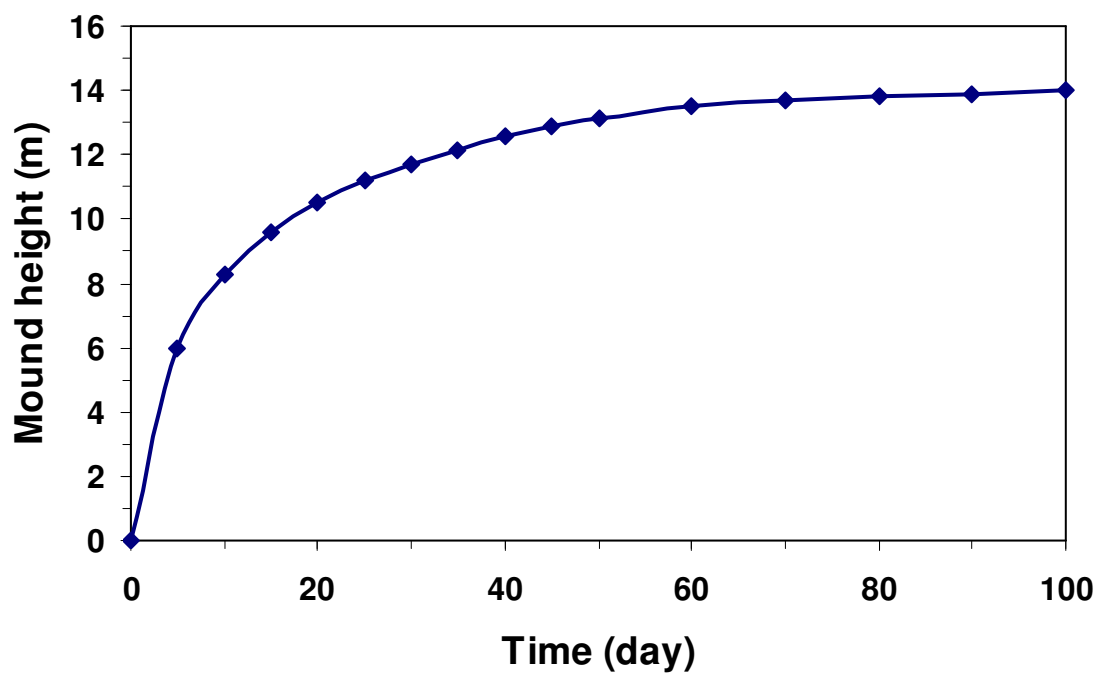


Figure 6.9 Height of the groundwater mound beneath the recharge basin for the first 100 days, simulated with the regional model

Chapter 6 : Regional groundwater modeling

The shape and spread of the groundwater mound after 100 days in the immediate surrounding of the infiltration ponds is depicted in Figure 6.10, from which we conclude that the groundwater mounding will be noticeable over a distance of about 1 km around the infiltration site.

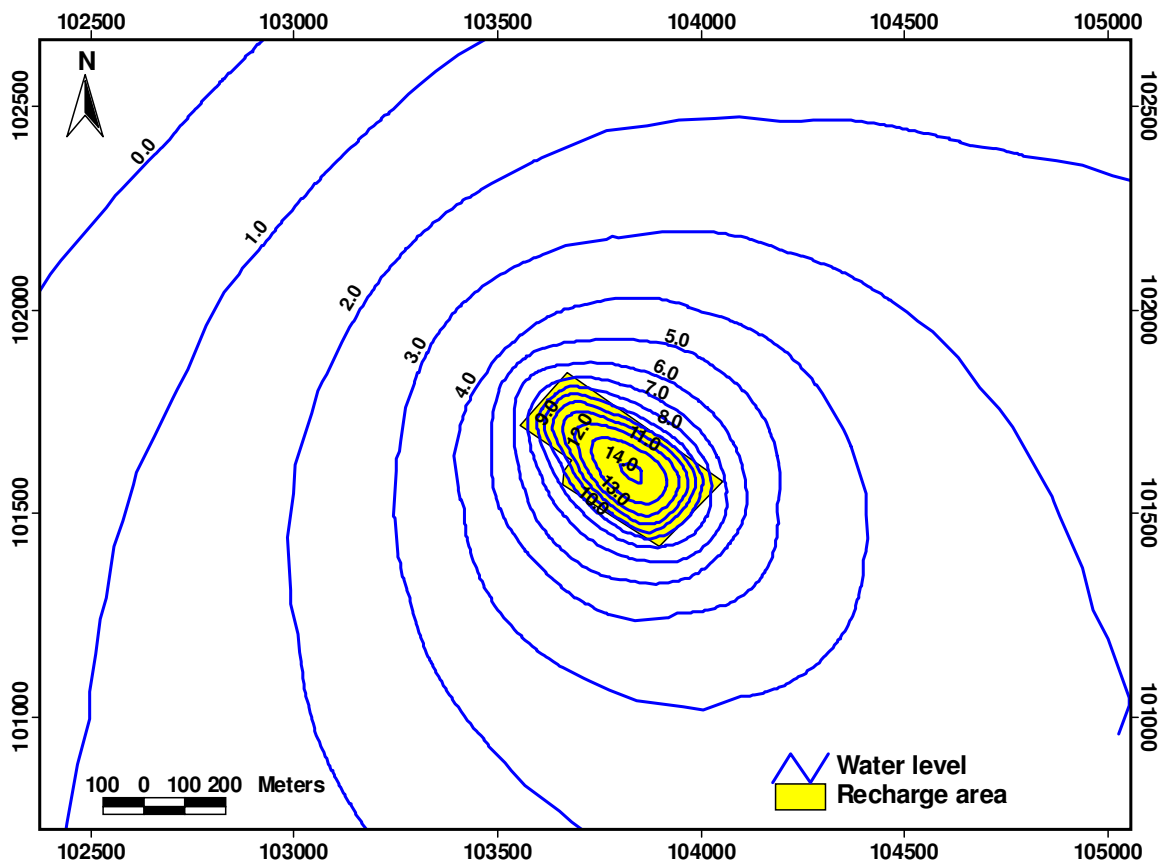


Figure 6.10 Groundwater mound after 100 days beneath the recharge area

After that, the groundwater mound will continue to rise gradually and after 2 years will be a slight increase in the groundwater mound, as shown in Figure 6.11, assuming full constant continues recharge of 60,000 m³/d from the time zero onwards, while keeping all other inputs and outputs constant in time.

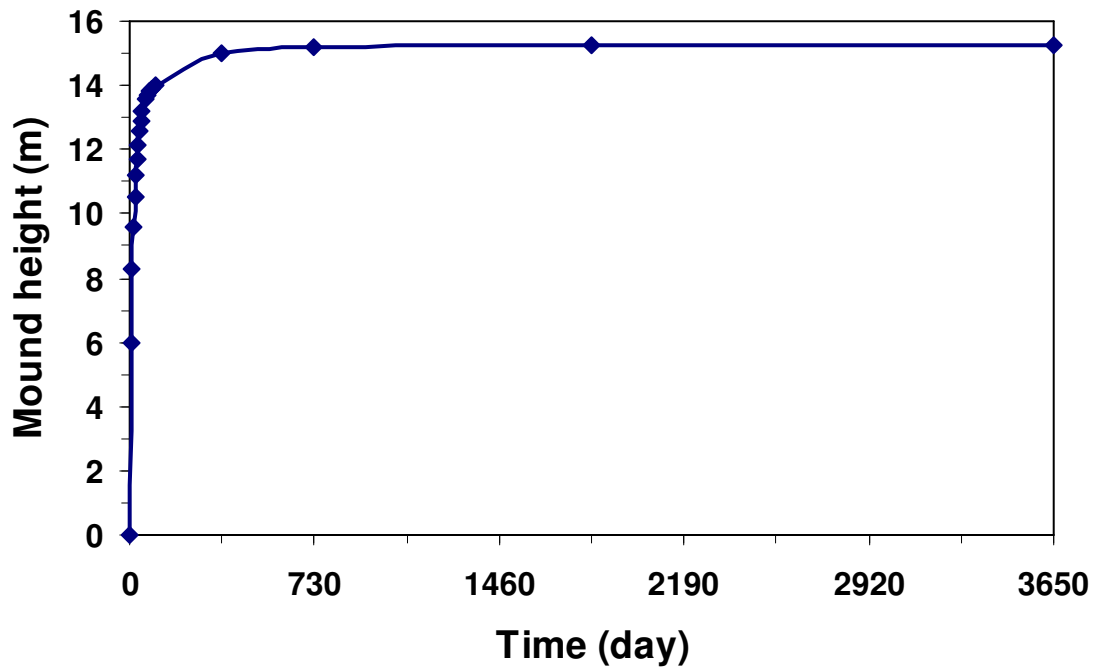


Figure 6.11 Groundwater mound beneath the recharge basin

6.4.2 Predicted groundwater table

The infiltration will result in a rising groundwater table in the north part of the Gaza Strip. The rise will be gradual and the full effect will be seen after 5-10 years. Figure 6.12a shows the groundwater levels of initial heads (steady state conditions). The groundwater levels with when the infiltration has given full effect on the groundwater level change as shown from transient simulation after 1 year, 2 years, 5 years and 10 years in Figure 6.12b, Figure 6.12c, Figure 6.12d and Figure 6.1e respectively. The model simulations indicate that the water level will be increased in the area and the cone of depression will diminish substantially due to the infiltration.

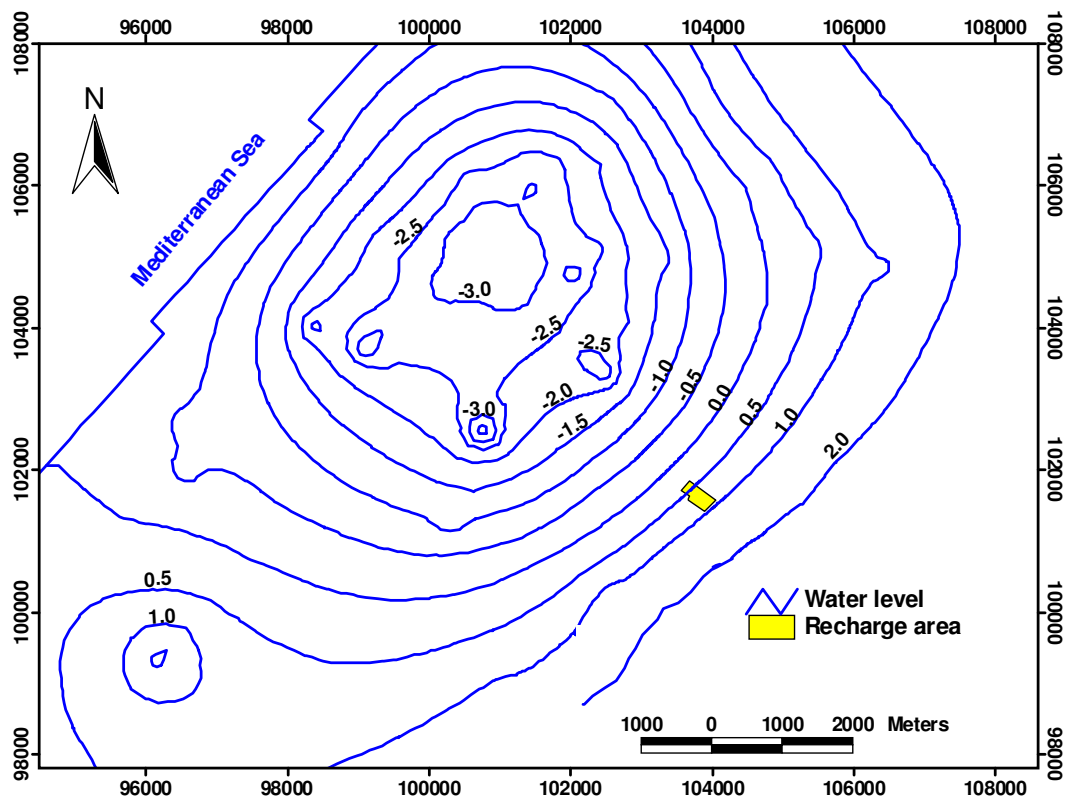


Figure 6.12a Simulated water levels in the north of the Gaza Strip (year 2000)

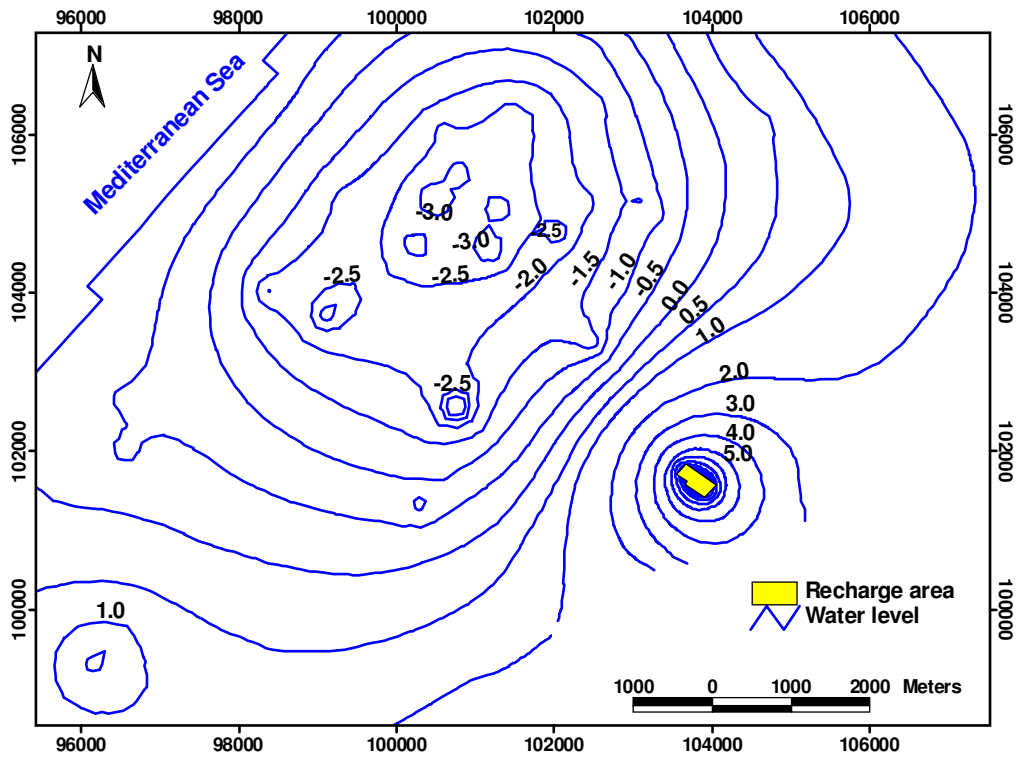


Figure 6.12b Simulated groundwater levels with infiltration after 1 year

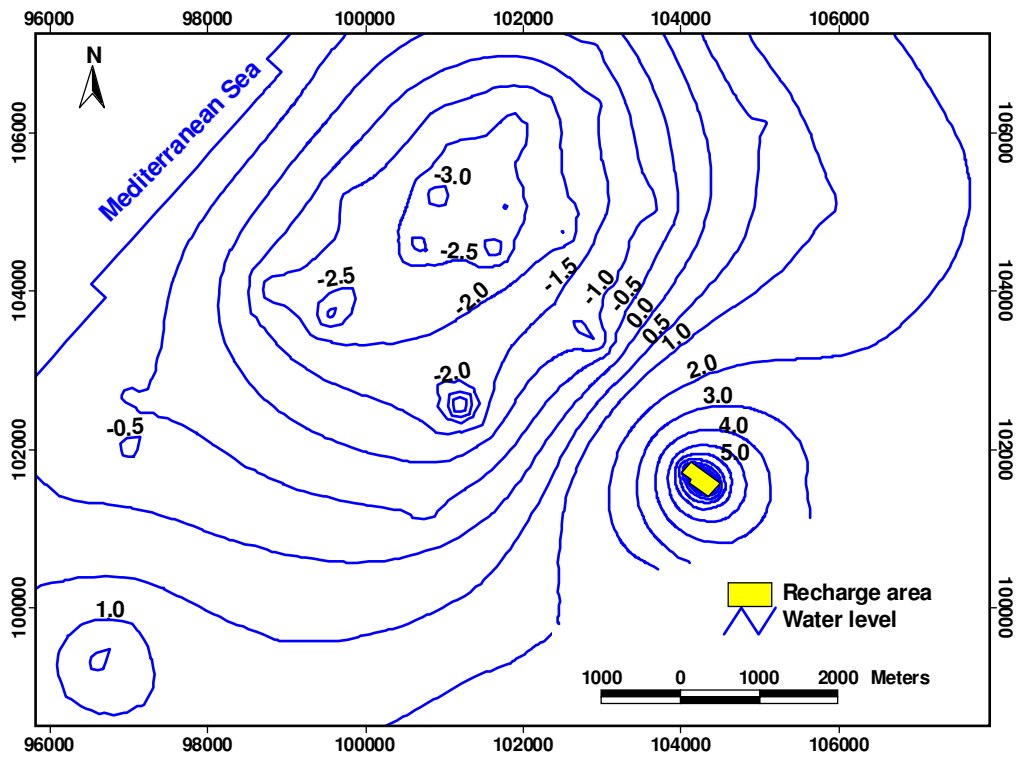


Figure 6.12c Simulated groundwater levels with infiltration after 2 years

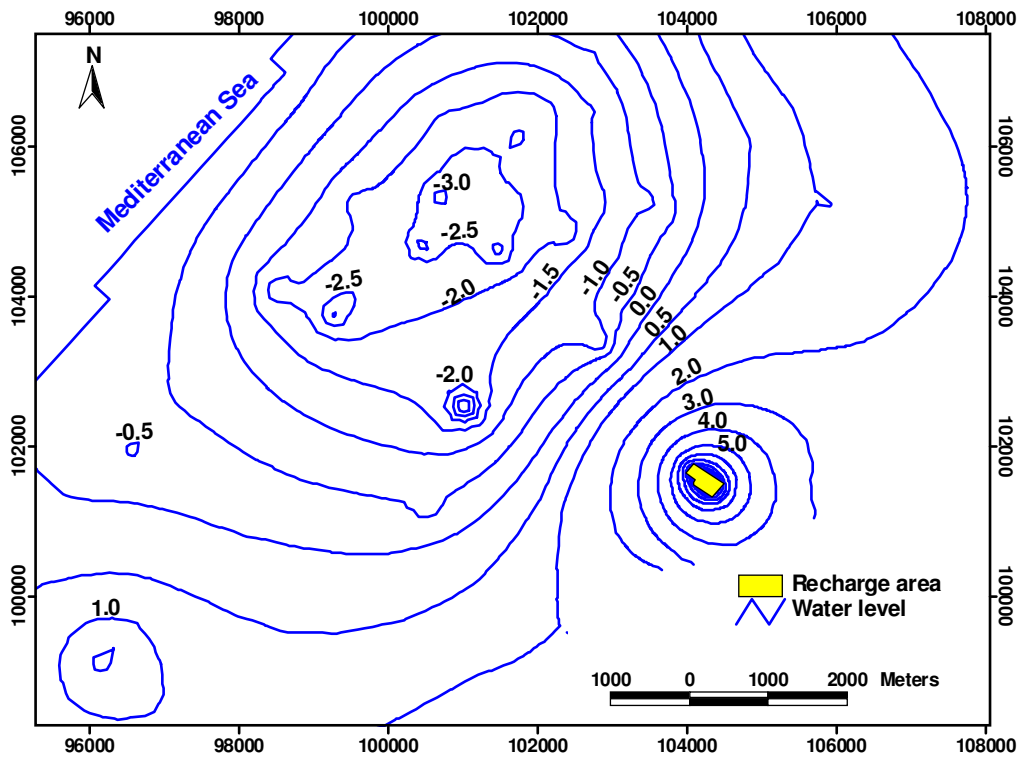


Figure 6.12d Simulated groundwater levels with infiltration after 5 years

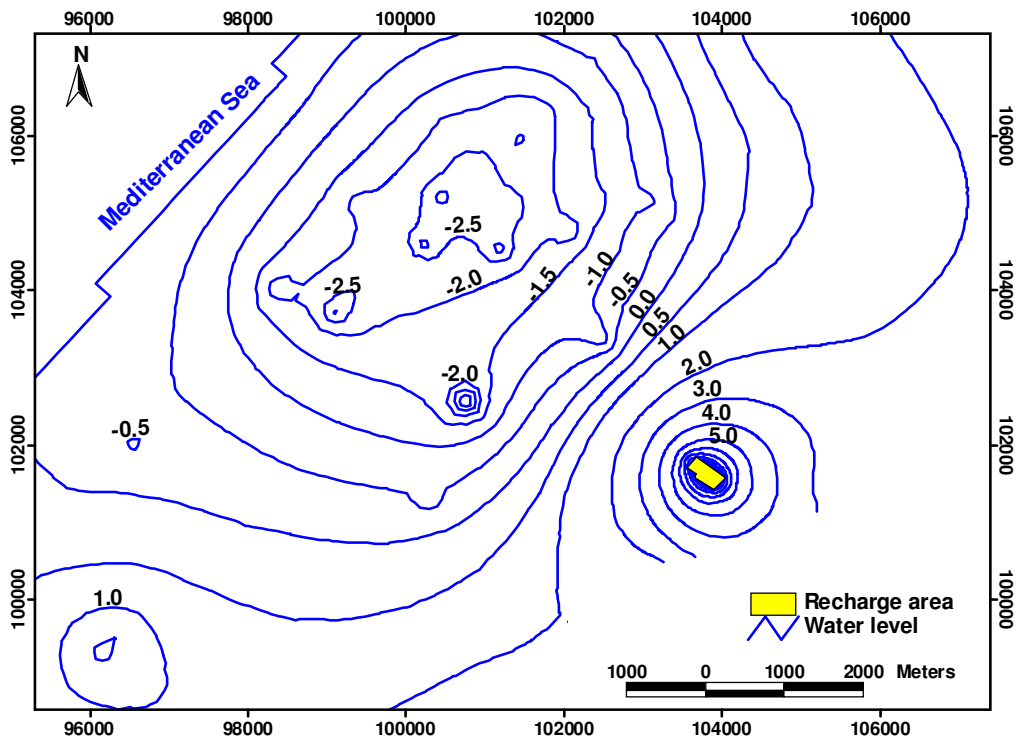


Figure 6.12e Simulated groundwater levels with infiltration after 10 years

6.4.3 Particles pathlines

In order to simulate the penetration of the injected water in the original groundwater layer, we will make use of MODPATH for tracking of flow lines from the injection site. The pathlines for imaginary particles that are infiltrated in the recharge area will spread radially about 500 m after 1 year, 750 m after 2 years, 1000 m after 5 years, and 1500 m after 10 years, as shown in Figure 6.13a, Figure 6.13b, Figure 6.13c, and Figure 6.13d respectively.

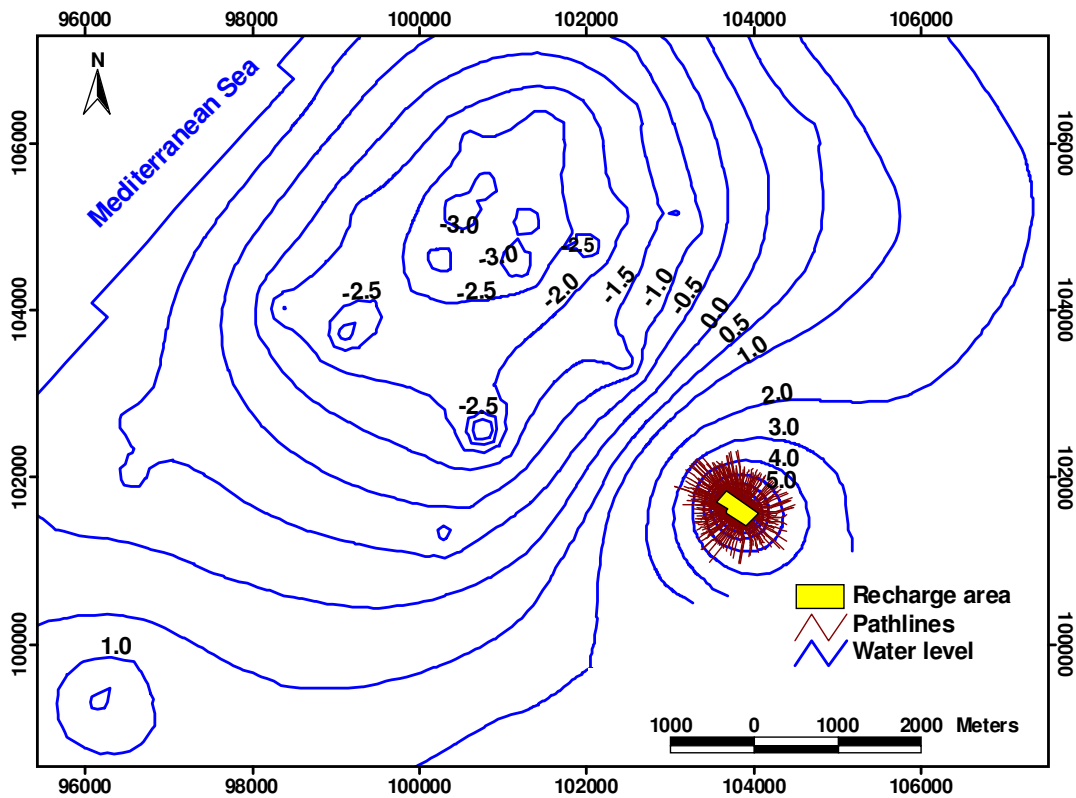


Figure 6.13a Pathlines for virtual particles infiltrated after 1 year.

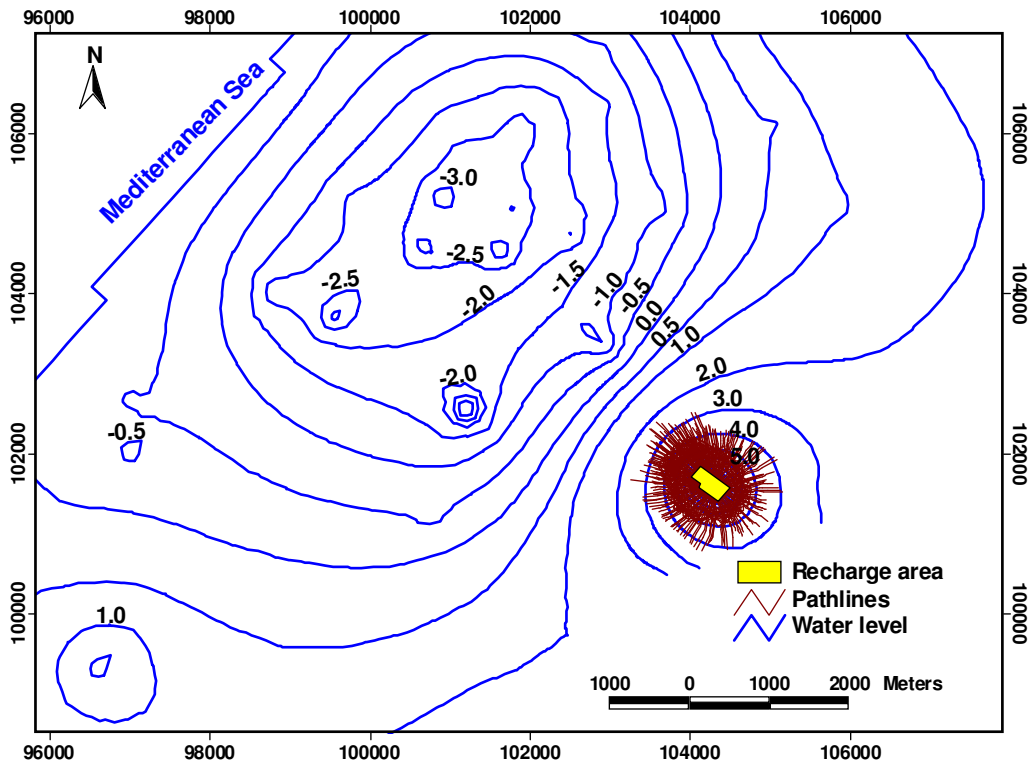


Figure 6.13b Pathlines for virtual particles infiltrated after 2 years

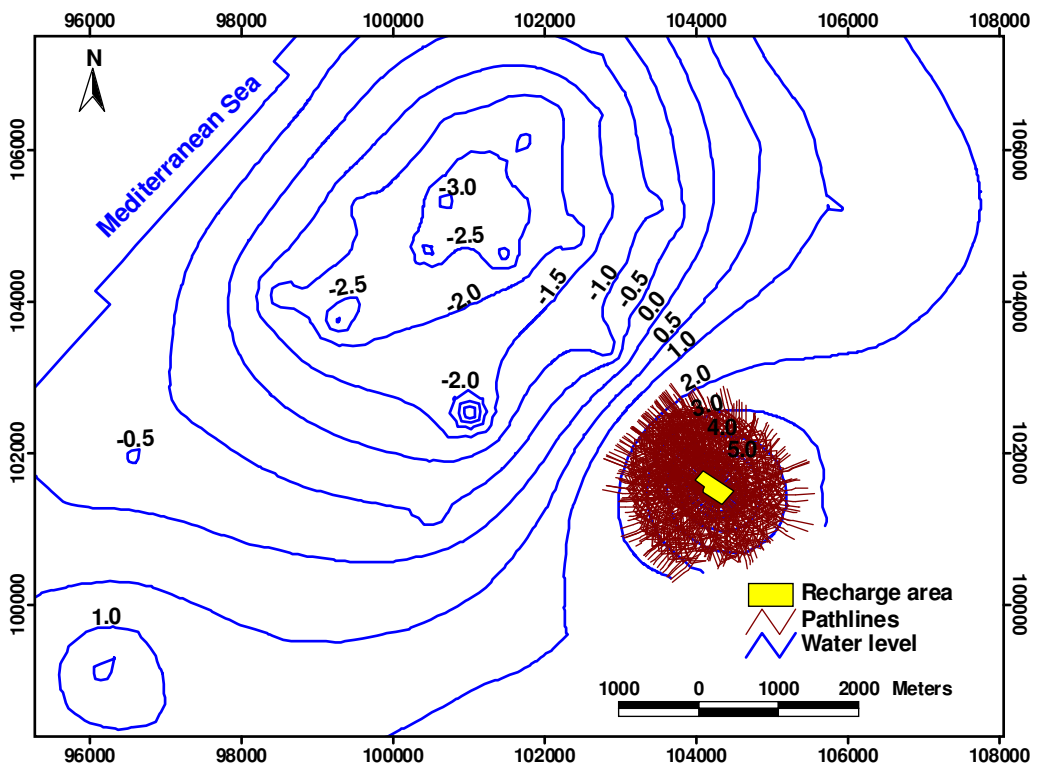


Figure 6.13c Pathlines for virtual particles infiltrated after 5 years

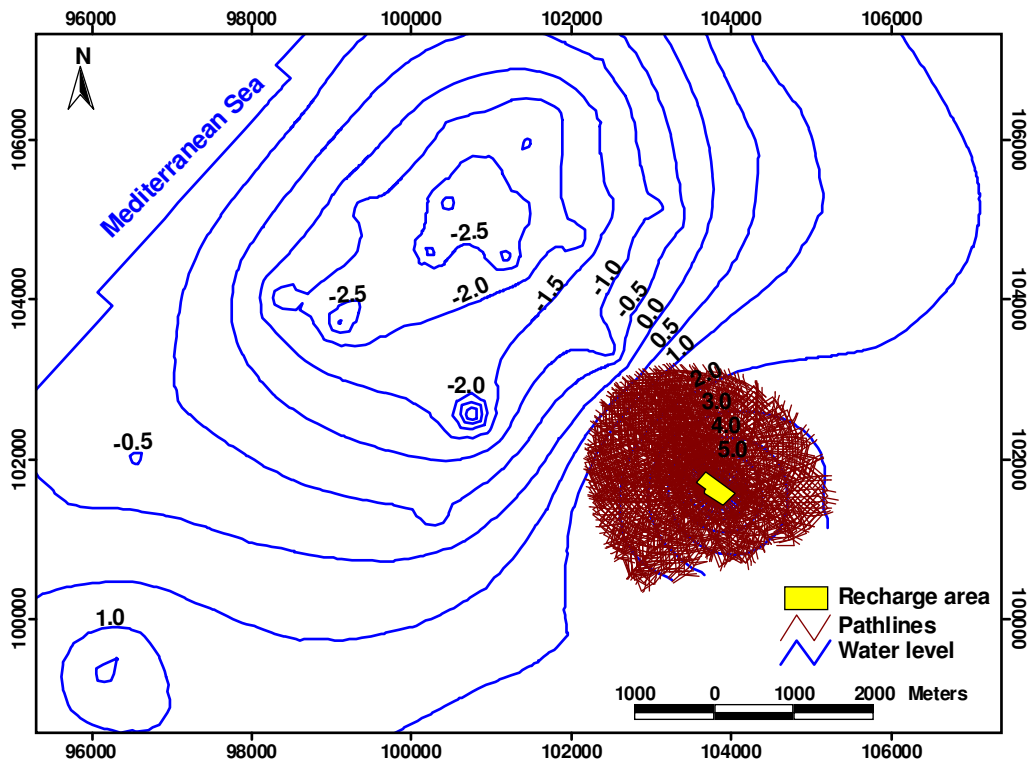


Figure 6.13d Pathlines for virtual particles infiltrated after 10 years

6.4.4 Solute transport model

The solute transport model MT3D (Zheng, 1994) describe the process of advection, dispersion-diffusion and chemical reactions. The model set-up was conducted based on the results of the regional flow model. The parameters values adopted in the solute transport model are chosen based on reported studies (Yakirevich, 1998), The longitudinal dispersivity is about 50 m, horizontal dispersivity ratio 0.1, vertical transverse dispersivity ratio 0.1 and molecular diffusion coefficient 10^{-4} m²/day.

In order to study the solute transport due to dispersion, we assumed that a conservative trace does not degrade or not absorbed or adsorbed. It is assumed that is the infiltration water, a concentration of 100 mg/l is present, while the material concentration in the aquifer is set to 0 mg/l. In the analysis of the results, the 100 mg/l will be considered as the reference concentration (100% injected water) and the simulated concentration in the aquifer well be expressed relative to this values. i.e. in percentage. Hence this percentage tells us how much of the original groundwater has been replaced by invading infiltration water at a particular site.

The results indicate that 90% of the infiltrated water will be mixed with the aquifer water after 1 year beneath the recharge area and will spread outward with decreasing percentages in the surrounding area, as shown in Figure 6.14a, Figures 6.14b, 6.14c, and 6.14d, show similar results after 2, 5, and 10 years respectively. The groundwater quality of the groundwater downstream of the recharge area eventually will be a result of the infiltration water quality.

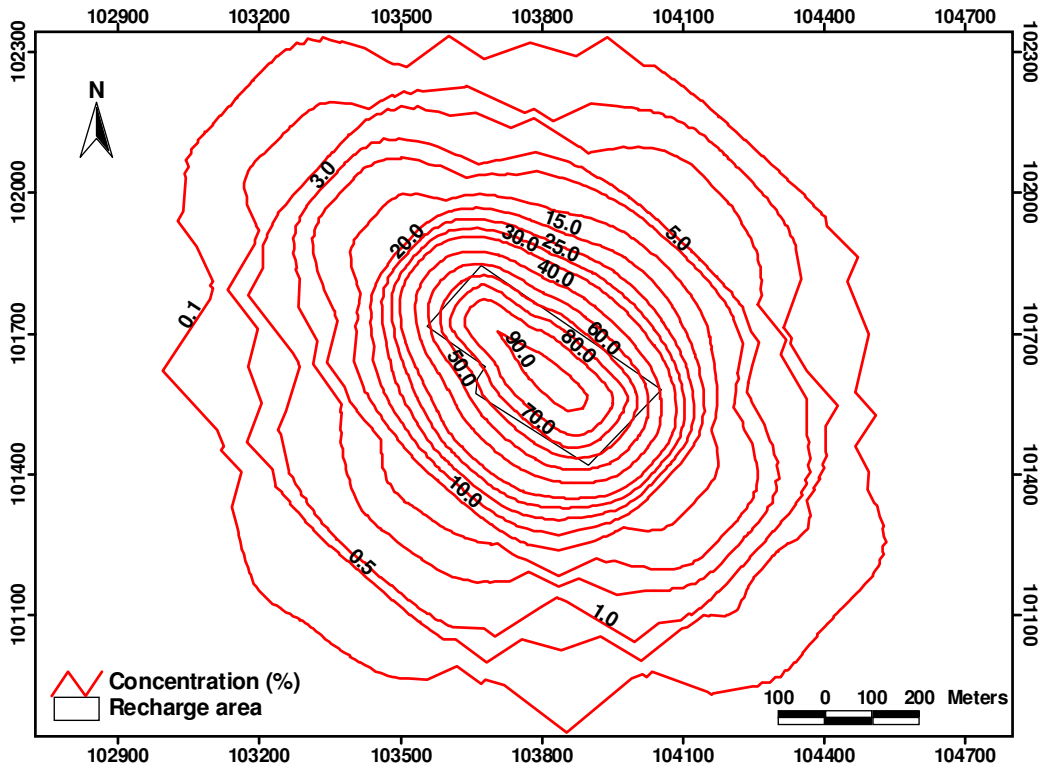


Figure 6.14a Simulation of mass transport after 1 year

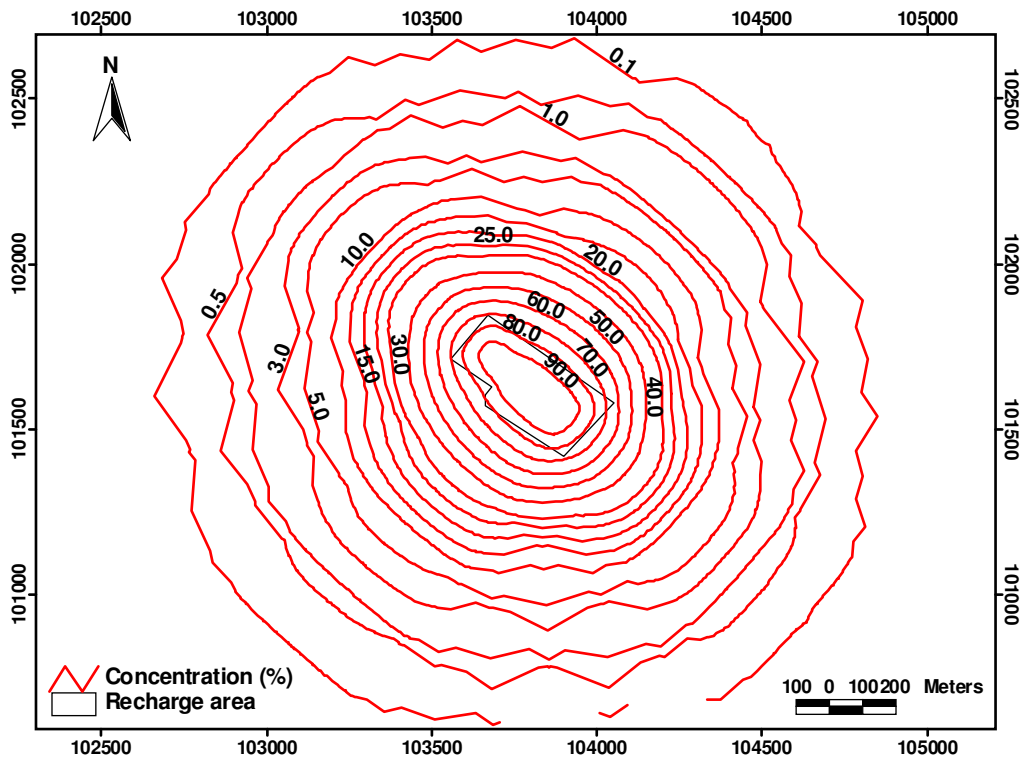


Figure 6.14b Simulation of mass transport after 2 years

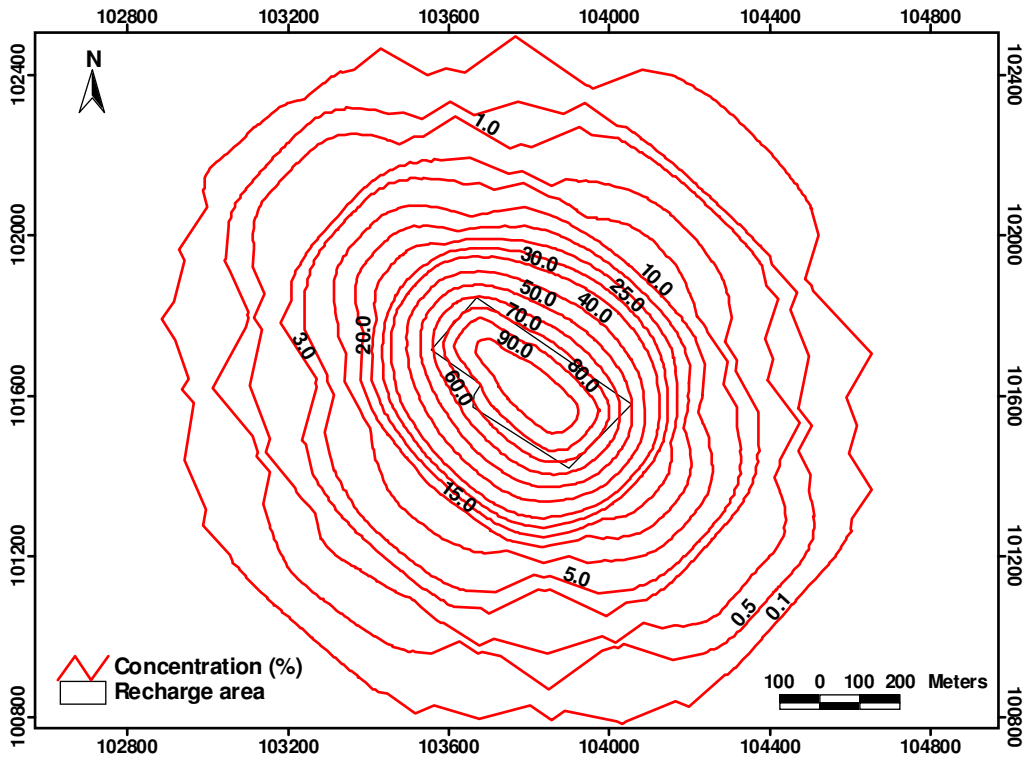


Figure 6.14c Simulation of mass transport after 5 years

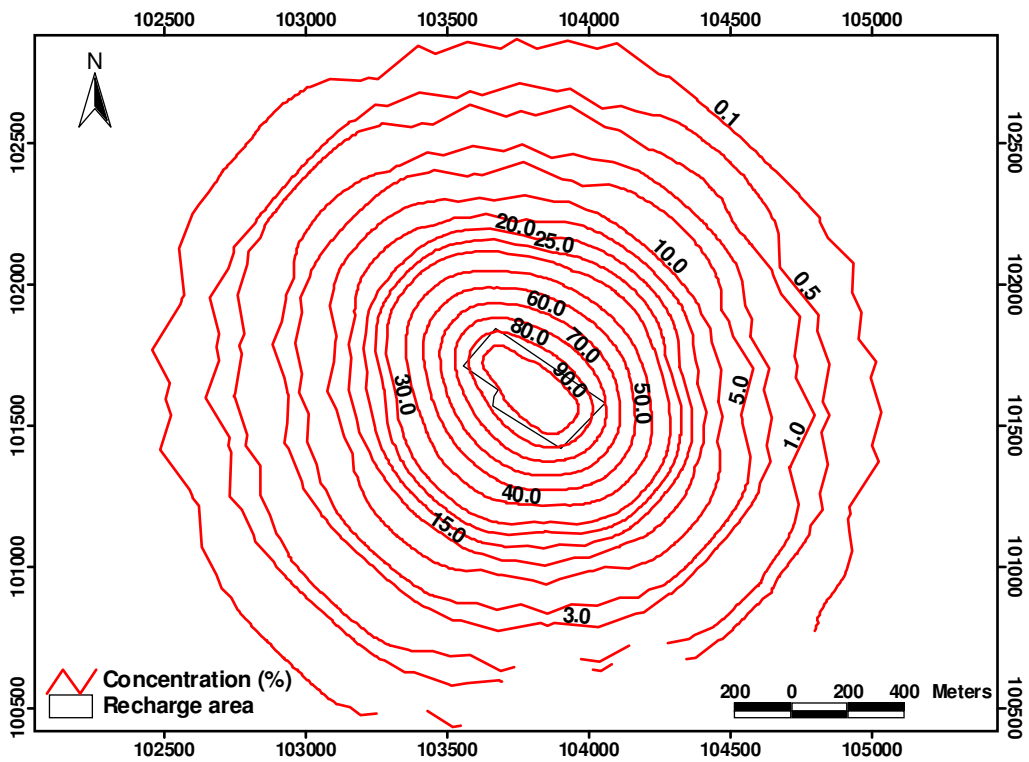


Figure 6.14d Simulation of mass transport after 10 years

6.5 Summary

The results from the regional groundwater flow simulation may be summarized as follows. The native groundwater under and around the recharge area will eventually completely be exchanged with water originating from the infiltrated water. The area around the infiltration site will be affected by the infiltration water within a distance of 1500 m from the recharge area. These results are based on the assumption that all hydrogeological conditions, such as groundwater abstraction from wells and land-use remain constant as today.

Chapter 7: Conclusions and Recommendations

In this chapter, the main results and findings of the research work will be presented following closely the contents of the dissertation. This research study focused on the hydrogeological investigation and artificial recharge modeling.

7.1 Conclusion about the hydrogeological study

The drilling methods used were rotary auger and cable percussion drillings. For the shallow boreholes and the semi-deep boreholes, the drilling methods were rotary air flush and rotary water circulation drilling. In the deep boreholes, auger and cable tool percussion methods were used.

During the drillings, disturbed samples (bulk samples) were collected for each 1-2 m drilling and/or at the change of formation. The samples were checked ocular at the site with regards of the soil texture and color.

The drillings and mechanical analysis of soil revealed that the topsoil consists of a continuous silty clay layer, with a thickness of 3 to 14 m. The clay can be described as a brownish, slightly moist to moist, very stiff to hard, and slightly sandy and silty.

In the semi-deep and deep boreholes, coarser material underlays the clay layer; consisting of sand and kurkar (sand with fine gravels of sandstone). Within the kurkar and sand formations, the degree of packing varies as well as texture. Normally, the sand varies between fines to coarse, while the gravel usually is fine to medium. Also brownish clayey or silty layers of

Chapter 7 : Conclusions and Recomendations

variable thickness and at different depths are found. In all of these boreholes, except for DB2, one or more layers of clayey to silty material are found between 20 to 40 m above the mean sea level. Clayey formations are also found below 40 m under the mean sea level.

The hydraulic conductivity from the field permeability test (Packer test) for the clay varies between 0.003 m/d and 0.86 m/d, with an average of 0.3 m/d. The K-values for the coarser material (sand with fine gravel) range from 1.4 m/d to 39 m/d with an average of 11.6 m/d.

The hydraulic conductivity from grain size was interpreted using Hazen formulae related to the effective grain size of the soil. The values range from 2.2 m/d to 22 m/d with an average value of 6 m/d for the lowest value $C = 0.004$ and range from 6 m/d to 65 m/d, with an average value of 18 m/d for the maximum value $C = 0.012$.

The infiltration rate of the sand with fine gravel materials obtained from infiltration test varies between 9.9 m/d and 15.1 m/d, with an average of 12.0 m/d. The hydraulic conductivity obtained from Philip equation varies between 5.6 m/d and 10.9 m/d with an average 7.8 m/d.

The hydrologic properties from pumping test are showing small variations in the different methods used. The transmissivity ranged between 2150 m²/d to 2800 m²/d and the hydraulic conductivity ranged between 28 m/d to 38 m/d. The highest value of transmissivity and hydraulic conductivity were found in the observation borehole DB2. The storativity varies from 0.22 to 0.27 with the highest value were found in the observation borehole SD4.

A statistical analysis and the comparison of the hydraulic conductivity of the sand with fine gravel material (Kurkar) from Packer test, Hazen formula, infiltration test and pumping test show the variation of hydraulic conductivity with depth. The variation of hydraulic conductivity at the same depth in different boreholes indicates the nonhomogeneity of the soil and soil drainage from poor to good.

Generally, we conclude that the field investigation gives clear information about the study area and the hydrogeological conditions.

7.2 Conclusion about the groundwater modeling

A three-dimensional groundwater flow model was developed. The model was calibrated by adjusting model input parameters until a best fit was achieved between simulated and observed water levels. Simulated water levels compared favorably to observed average water levels measured in observation wells in year 2000.

The Gaza Strip is an area with political boundaries, and no real aquifer boundaries. In hydrogeological terms this area forms part of the coastal aquifer that extends far beyond the study area. Hence, the decision was made to take a constant head boundary in the east from the water level contour map of the year 2000. The western boundary was assigned a zero constant head formed by the Mediterranean Sea. The northern and southern boundaries were assigned as no flow boundary.

The goal of constructing hydrologic and hydrogeological models, through which we can understand the behavior of the Gaza coastal aquifer, is reached

and provides a complete insight of the groundwater flow in the coastal aquifer.

The models (groundwater flow, solute transport and hydrologic model from WetSpass) as well as all automated data (such as geological cross-sections, land-use map, rainfall, depth of water table and slope of the topography, etc,) will be very useful for the responsible for further regional development.

7.3 Conclusion about the artificial recharge simulation

Infiltration from a recharge basin produces a groundwater mound above the original water table. In the local model, the obtained results from analytical analysis at the center of the basin after 100 days, the height of groundwater mound rises to about 14 m above the present groundwater table. In the numerical model the simulation shows that the groundwater mound beneath the center of an infiltration area can be expected to rise to above around 14 m and at the edges to about 11 m to 12.5 m after 100 days.

In the regional groundwater modeling, the simulation shows that the groundwater mound beneath the center of an infiltration area can be expected to rise to about 14.1 m after 100 days

The growth of the groundwater mound obtained with the local model, regional model simulation and the analytical solution are compared together as shown in Figure 7 .1; one can notice a very good agreement. The small differences can be explained by the assumptions that were made in the case of the analytical solution, i.e. a rectangular basin and an average groundwater table elevation to calculate the aquifer transmissivity. Anyway, at 100 days both

methods give similar results, which indicate that the rise of the groundwater mound is about 14 m, which will not cause any problem to the site or surrounding areas.

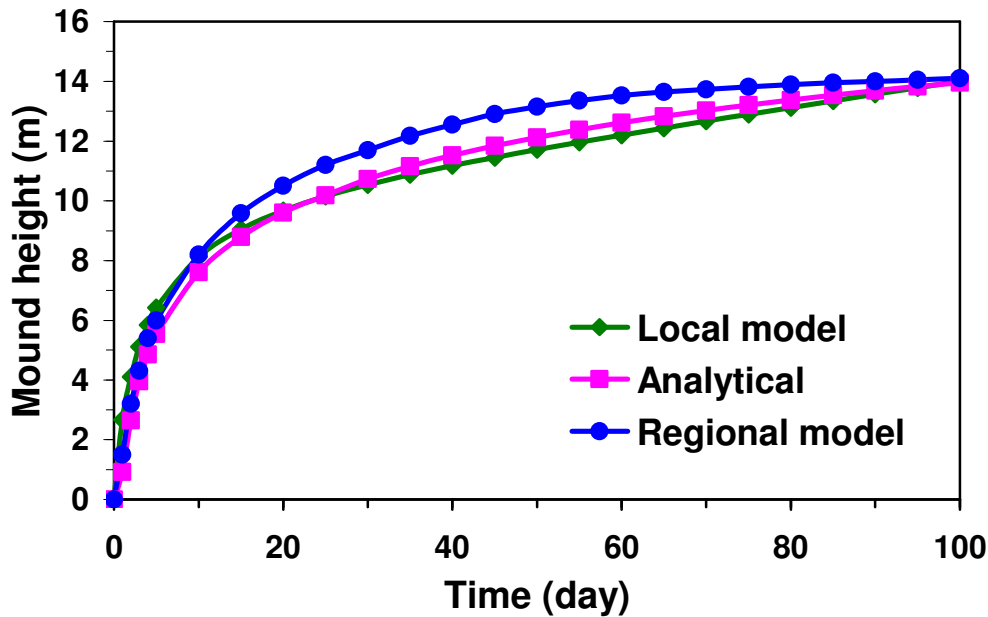


Figure 7.1 Comparison of numerical and analytical results

7.4 Conclusion about water migration and solute transport

The expected groundwater mound will continue to rise gradually and after 2 years there will be a slight increment in the groundwater mound, assuming full constant continuous recharge of 60,000 m³/d from the time zero onwards, while keeping all other inputs and outputs constant in time.

The infiltration will result in a rising groundwater table in the northern part of the Gaza Strip. The rise will be gradual and the full effect will be seen after

Chapter 7 : Conclusions and Recomendations

5-10 years. The model simulations indicate that the groundwater flow is toward the sea and the water level will be increased in the area and the cone of depression will diminish substantially due to the infiltration. This will prevent seawater intrusion into the aquifer, thus protecting the quality and replenishing the supply of the inland groundwater.

In order to simulate the penetration of the injected water in the original groundwater layer, we used MODPATH for tracking of flow lines from the injection site. The pathlines for imaginary particles that are infiltrated in the recharge area spread radially about 500 m after 1 year, 750 m after 2 years, 1000 m after 5 years, and 1500 m after 10 years.

In order to study the transport due to dispersion, we assumed conservative traces that do not degrade or are not absorbed on solid material. It is assumed that in the infiltration water, a concentration of 100 mg/l is present, while the material concentration in the aquifer is set to 0 mg/l. In the analysis of the results, the 100 mg/l will be considered as the reference concentration (100% injected water) and the simulated concentration in the aquifer will be expressed relative to this values. i.e. in percentage. Hence this percentage tells us how much of the original groundwater has been replaced by invading infiltration water at a particular site.

The results indicate that 90% of the infiltrated water will be mixed with the aquifer water after 1 year beneath the recharge area and will spread outward with decreasing percentages in the surrounding area.

7.5 Recommendations

- Comprehensive environmental impact assessment (EIA) should be done before implementing the artificial recharge of the treated wastewater project.
- Water levels should be closely monitored during the start-up of the infiltration at the site and vicinity wells to confirm that the aquifer responds as predicted.
- The monitoring program for groundwater quality should be designed with a selection of parameters and frequency that allows the effect on the groundwater to be observed.

Long-term recommendations

- Pumping ground water from pumping well DB# 4 in the site for agricultural use.
- Establishment and applied research program to support and enhance the work in the recharge area as:
 - Geochemical transformation during artificial groundwater recharge.
 - Integrated modeling of clogging processes in artificial groundwater recharge
 - Tracer and isotope investigation of groundwater recharge

References

Allen, R., Pereira, L., Raes, D., and Smith, M., 1998. Crop evapotranspiration (Guidelines for computing crop water requirements). FAO irrigation and drainage paper, No. 56. Italy, Rome. 297p.

Anderson, M. P., and Woessner, W. W., 1992. Applied groundwater modeling: simulation of flow and advective transport. Academic Press, Inc.

Bachmat, Y., and Melloul, A., 1975. An appraisal of the hydrogeological situation in the Gaza Strip as a basis to operation of the aquifer. Hydrological services of Israel report HYDRO/3/1975.

Batelaan, O., and De Smedt, F., "WetSpass: a flexible, GIS based, distributed recharge methodology for regional groundwater recharge", Gehrels, H., Peters, J., Hoehn, E., Jensen, K., Leibundgut, C., Griffioen, J., Webb, B. and Zaadnoordijk, W.-J. (Eds.), Impact of Human Activity on Groundwater Dynamics, IAHS Publ. No. 269, 2001, pp. 11-17.

Baveye, P., Vandervivere, P., Hoyle, B. L., Deleo, P. C., Sanchez, D. E., and Lozada, D., 1998. Environmental impact and mechanisms of the biological clogging of saturated soils and aquifer materials. Crit. Rev. Environ. Sci. Technol. CRC press 28 (2): 123-191.

Bianchi, W. C., and Muckel, D. C., 1970. Groundwater recharge hydrology, ARS 41-161, USDA, 62 pp.

British Standard Institution (B.S.), 1981. Code of practice for site investigations. B. S. 5930, London.

Clarke, K., 1999. Getting started with geographic information systems. University of California, Santa Barbara, Prentice Hall, New Jersey, ISBN: 0-13-9238891

References

Cuyk, S., Siegrist, R., Logan, A., and Figueroa, L., 2001. Hydraulic and purification behavior and their interactions during wastewater treatment in soil infiltration systems. *Wat. Res.* Vol. 35, No. 4, pp. 953-964.

De Smedt, F., 1999. Two-and three dimensional flow of groundwater. In: Deleur, J. W. (editor), *The handbook of groundwater engineering*. M. C. Graw-Inc. New York.

De Smedt, F., 2003. Groundwater modeling, course notes.

De Smedt, F., Belhadi, M., and Nural I. K., 1985. Study of spatial variability of the hydraulic conductivity with different measurement techniques, in *Proceeding of the International Symposium on " the stochastic approach to subsurface flow"*, edited by Marsily, G. De., International Association for Hydraulic Research, Monvillargenne, France, Jun 3-6.

Dillon, P., Pavelic P., 1996. Guidelines on the quality of stormwater and treated and treated wastewater for injection into aquifers for storage and reuse. Research Report No 109, Urban Water Research Association of Australia, Melbourne.

Dillon, P. J., 2002. Management of aquifer recharge for sustainability. *Proceedings 4th international symposium on artificial recharge of groundwater*, Adelaide, September. Balkema, Rotterdam.

Domenico, P., and Schwartz, F., 1990. *Physical and chemical hydrogeology*. John Willy and Sons, Inc., New York.

Fetter, C. W., 2001. *Applied Hydrogeology*, fourth edition, Merrill Pupliching Company, ISBN 0-13-088239-9.

Fink, M. A., 1989. Survey for groundwater in the coastal area of northern Sinai: preliminary report. Tahal P. M. 727.

Fink, M., 1970. *The hydrogeology of the Gaza Strip*, Tahal report 3, Tel-Aviv (in Hebrew).

References

Finnemore, E. J., 1993. Estimation of groundwater mounding beneath septic drain fields, *Groundwater*, Vo. 31, No. 6, 884 -889.

Finnemore, E. J., 1995. A program to calculate groundwater mound heights, *Groundwater*, Vo. 33, No. 1, 139-143.

Flint, A., 2003. The role of unsaturated flow in artificial recharge projects. Proceedings, TOUGH Symposium.

GEP, 1994. Gaza environmental profile, part I. Inventory of resources. Palestinian Environmental Protection Authority. Euroconsult and IWACO, the Netherlands, pp 7-10.

Glover, R. E., 1961. Mathematical derivations as pertain to groundwater recharge. Mimeographed report, Agricultural Research Service, U.S. Dept. Agriculture, Ft. Collins, Colo., 81 pp.

Goldenberg, L. C., 1992. Evaluation of the water balance in the Gaza Strip. Geological survey, Report TR-GSI/16/92 (in Hebrew).

Greitzer, Y. and Dan, J., 1967. The effect of soil landscape and Quaternary geology on the distribution of saline and fresh water aquifers in the coastal plain of Israel: tahal water planning for Israel, Ltd, 45pp.

Gvirtzman, G., et al, 1984. Stratigraphy of the Kurkar group (Quaternary) of the coastal plain of Israel: geological survey of Israel research, 64pp.

Hantush, M. S., 1967. Growth and decay of groundwater mounds in response to uniform percolation. *Water Resources Research*, 3: 227-234.

Harbaugh, A., and McDonald, M., 1996. User's documentation for MODFLOW-96, an update to the US Geological Survey modular finite-difference groundwater flow model. Open-file report 96-485, US Geological Survey.

References

Harbaugh, A., Banata, E., Hill, M., and McDonald M., 2000. The U.S. geological survey modular groundwater model-user guide to modularization concepts and the groundwater flow process.

Hem, J. D., 1989. Study and interpretation of the chemical characteristics of natural waters. USGS water supply paper 2254.

Herman, B., 1996. Issues in artificial recharge. *Water Science Technology*, Vol. 33, No. 10 – 11, pp. 381 – 390.

Herman, B., 2002. Artificial recharge of groundwater: hydrogeology and engineering. *Hydrogeology Journal*, 10: 121- 142.

Houston, S., Duryea, P., and Hong, R., 1999. Infiltration considerations for groundwater recharge with waste effluent. *Journal of Irrigation and Drainage Engineering*, Vol. 125, No. 5, pp. 264-272.

Issar, A., 1981. The rate of flushing as a major factor in deciding the chemistry of water in fossil aquifer in southern Israel: *Journal of hydrology*, vol, 54, 285-295.

Jacobus, J., and Simmers, I., 2002. Groundwater recharge: an overview of processes and challenges. *Hydrogeology Journal*, 10:5-17.

Jos, H. P., 1996. Artificial recharge of groundwater. Proceedings of an international symposium, June 3 – 5, 1996, in Helsinki, Finland. *Nordic hydrological program*, 38: 256 – 269.

Jury, W., Gardner, W., 1991. *Soil physics*. Fifth edition. ISBN: 0-471-83108-5, pp 4-18.

Kanarek, A., and Michail, M., 1996. Groundwater recharge with municipal effluent: Dan region reclamation project, Israel. *Wat. Sci. Tech.* Vol. 34, No. 11, pp. 227-233.

References

Kresic, N., 1997. Quantitative solutions in Hydrogeology and groundwater modeling. CRC press LLC, ISBN 0-56670-219-4.

Lallana, C., and Krinner, W., et al, 2001. Sustainable water use in Europe. Part 2: Demand management. Environmental issue report No. 19, pp 47.

Latinopoulos, P., 1981. The effect of infiltration distribution on artificial recharge schemes. Journal of Hydrology, 49: 279-286.

Latinopoulos, P., 1986. Analytical solutions for strip basin recharge to aquifers with auchy boundary conditions. Journal of Hydrology 83: 197-206.

Lenore S. Clescerl, et al 1999. Standard methods for examination of water and wastewater, 20th edition, ISBN 0-87553-235-7.

Lugeon, M., 1933. Barrages et Geologie. Dunod, Paris.

Manglik, A., and Rai, S. N., 2000. Modeling of water table fluctuation in response to time-varying recharge and withdrawal. Water Resources Management 14: 339-347.

Marino, M. A., 1967. Hele-Shaw model study of the growth and decay of groundwater ridges. Journal of Geophysics Research 72: 1195-1205.

Marino, M. A., 1974. Water table fluctuations in response to recharge. American Society of Civil Engineers, Journal of Irrigation and Drainage Division, 100: 117-125.

Marino, M. A., 1975. Artificial Groundwater recharge, II. Rectangular recharging area. J. Hydrol., 26:29-37.

Marmion, K. R., 1962. Hydraulics of artificial recharge in non homogeneous formations. Water Resources Center Contribution No. 48, Univ. of California, Berkeley, Calif., 88 pp.

Mazor, E., 1991. Applied chemical and isotopic groundwater hydrology. Halstead Press, New York.

References

McDonald, M. G., and Harbaugh A.W., 1988. A modular three-dimensional finite difference groundwater flow model. USGS Techniques of water Resources Investigation Report, book 6, ch A1: 586 pp.

Melloul, A. J. and Collin, M., 1994. The hydrological malaise of the Gaza Strip. *Isr. J. Earth Sci.* 43(2): 105-116.

Melloul, A., 1992. Hydrological situation in the coastal aquifer of the Gaza Strip from 1985 to 1990. Water commission report HYDRO 1992/7.

Metcalf and Eddy, 2000. The Gaza coastal aquifer management plan – Task 3 Appendix A, USAID, Contract No. 294-C-99-00038-00.

Mollah, M. A., and Sayed, A. S., 1995. Assessment of in situ permeability with emphasis on packer testing in Kuwait. *Engineering Geology* 39: 217-231.

Mukhopadhyay, E., and Al-Awadi, E., 2003. Laboratory investigations of compatibility of the Kuwait group aquifer with possible injection waters. *Journal of Hydrology*, article in press.

N. N., 1994. Groundwater recharge using waters of impaired quality. National Academy Press Washington, 12pp.

Nutbrown, D. A., 1976. A model study of the effects of artificial recharge, *Journal of Hydrology*, 31: 57-65.

Palestinian Central Bureau of Statistics (P. C. B. S.), 2002. Projected population in the Palestinian territory. Establishments report, Ramallah, Palestine, 5pp.

Palestinian Water Authority (PWA), 2003. Hydrogeological data bank department, Gaza Strip.

Peter, J. H., et al. 1998. Proceedings of the third international symposium on artificial recharge of groundwater. Amsterdam, September 21-25.

References

- Philip, J. R., 1969. Theory of infiltration in *Advances in Hydrosience*, vol. 5, ed. V.T. Chow, 215-96. New York: Academic Press.
- Prabhata, K., and Chandra, S., 1995. Groundwater mound equation for rectangular recharge area. *Journal of Irrigation and Drainage Engineering*, Vol. 123, No. 3, pp. 215-217.
- Rai, S. N., and Singh, R. N., 1995. Two-dimensional modeling of water table fluctuation in response to localized transient recharge. *Journal of Hydrology* 167: 167-174.
- Rai, S. N., Ramana, D. V., Thiagarajan, S., and Manglik, A., 2001. Modeling of groundwater mound formation resulting from transient recharge. *Hydrol. Process*: 15, 1507-1514.
- Rao, N. H. and Sarma, P. B. S., 1983. Recharge to finite aquifer from strip basins. *Journal of Hydrology* 66: 245-252.
- Rastogi, A., and Pandey, S., 1998. Modeling of artificial recharge basins of different shapes and effect on underlying aquifer system. *Journal of Hydrologic Engineering*, Vol.. 3, No. 1, pp. 62-68.
- Recharged, H. M., 1992. *Microcomputer applications in statistical hydrology*. Englewood Cliffs, New Jersey, ISBN 0-13-585290-0.
- Rinck, P. S., and Vandavelde, T., 2000. Interrelationships between biological, chemical, and physical processes as an analog to clogging in aquifer storage and recovery wells. *Water Research* Vol. 34, No. 7, pp. 2110-2118.
- Scanlon, B., Healy, R., and Cook, P., 2002. Choosing appropriate techniques for quantifying groundwater recharge. *Hydrogeology Journal* 10: 18-39.
- Schwartz, F., and Zhang, H., 2002. *Fundamentals of groundwater*. Published by John Willy and Sons, Inc.

References

Stormwater and sewerage project, Northern Gaza- Study D, new WWTP, environmental impact assessment report-final, September 1999. Montgomery WatsonBoliden Contech.

Sumner, M. E., Stewart B. A., 1992. Soil crusting: chemical and physical processes, Lewis publishers, Boca Raton, Florida, 372 pp.

Tompson, A., Carle, S., and Rosenberg, N., 1999. Analysis of groundwater migration from artificial recharge in a large urban aquifer: A simulation perspective, *Water Resources Research*, Vol. 35, No. 10, pp. 2981-2998.

Tsay, T., and Hoopes, J., 1998. Numerical simulation of groundwater mounding and its verification by hele-shaw. *Computer and Geosciences* Vol. 24, No. 10, pp. 979-990.

United States Bureau of Reclamation, 1974. Earth manual, water resources technical publication. 2nd ed. Washington.

Vengosh, A., and Keren, R., 1996. Chemical modifications of groundwater contaminated by recharge of treated sewage effluent. *Journal of Contaminant Hydrology* 23: 347-360.

Wang, H. F., and Anderson, M. P., 1982. Introduction to groundwater modeling finite difference and finite element methods. W. H. Freeman and Company, San Francisco.

Washington Department of Ecology, 2001. Storm water management manual, publication numbers 99-11 through 99-15.

Wood, W. W., and Sanford W. E., 1995. Chemical and isotopic methods for quantifying groundwater recharge in a regional, semiarid environment. *Ground Water* 33, no. 3: 58-68

Yakirevich, A., Melloul, A., Sorek, S., Shaath, S., and Borisov, V., 1998. Simulation of seawater intrusion into the Khan-Yunis area of the Gaza Strip coastal aquifer. *Hydrogeology Journal* 6: 549-559

References

Zheng, C., and Wang, P., 1998. MT3DMS, a modular three-dimensional multispecies transport model. Technical report, the hydrogeology group, the University of Alabama.

Zheng, C., 1994. MT3D, a modular three-dimensional transport model, S. S. Papadopoulos and Associates, Inc., Rockville, Maryland.

Zheng, C., 1993. MT3D, a modular three –dimensional transport model, S.S. Papadopoulos and Associates, Inc., Rockville, Maryland.

Zheng, C., and Bennett, G. D., 1995. Applied contaminant transport modeling, theory and practice, 440 pp, Van Nostrand Reinhold, New York.

Zubiller, C., et al. 2002. Policy guidelines for sustainable wastewater management in the Gaza Strip. Part I, LIFE/CY/99/GA/141, legal and institutional issues.

Appendix: 1

Appendices

Appendix 1.1

Selected data for the boreholes that were drilled on the site

BH No.	X	Y	Drilling Depth(m)	Ground Elevation (m)
B1	103570.0	101715.9	15.0	50.91
B2	103559.3	101590.0	18.6	52.06
B3	103674.5	101664.7	14.5	54.09
B4	103751.3	101714.4	13.4	56.25
B5	103625.5	101513.9	15.8	54.11
B6	103779.4	101613.3	7.5	58.73
B7	103856.3	101663.0	11.0	60.31
B8	103768.7	101487.4	17.5	56.56
B9	103864.8	101549.6	14.5	60.4
B10	103911.9	101460.9	11.5	61.58
B11	103988.8	101510.7	6.0	64.43
CD1	103666.5	101719.0	8.0	53.41
CD2	103743.3	101768.7	12.5	54.12
CD3	103682.1	101610.0	9.0	54.49
CD4	103771.3	101667.6	8.5	57.84
CD5	103890.1	101507.3	13.5	60.76
CD6	104035.3	101600.3	6.5	67.15
CD7	103981.3	101426.6	10.0	63.86
CD8	104091.7	101458.2	8.5	69.53
SD1	104020.9	101580.1	73.0	66.88
SD2	103794.8	101556.1	70.0	57.82
SD3	103888.8	101616.9	66.0	61.78
SD4	103919.9	101693.8	66.0	60.19
SB1	103955.5	101548.5	71.0	63.55
DB1	103699.2	101651.9	100.0	54.94
DB2	103842.0	101499.4	118.0	58.85
DB3	103912.9	101582.0	120.0	62.25
DB4	103826.3	101642.6	156.0	59.53

Appendices

Appendix 1.2

Sieve analysis data sheet and grain size distribution graphs

Total sample dry weight: 217.40 g			Borehole no. : B #1 (12-13)m	
Sieve no.	Size (mm)	Cumulative Weight Retained (g)	Cumulative % Retained	Cumulative % Passing
3/4"	19.0		0.0	100.0
1/2"	12.5		0.0	100.0
3/8"	9.5		0.0	100.0
No. 4	4.75	3.0	1.38	98.62
No. 10	2.00	40.1	18.45	81.55
No. 40	0.425	142.7	65.64	34.36
No. 200	0.075	216.9	99.77	0.23

Total sample dry weight: 171.20 g			Borehole no. : B #1 (14-15)m	
Sieve no.	Size (mm)	Cumulative Weight Retained (g)	Cumulative % Retained	Cumulative % Passing
3/4"	19.0		0.0	100.0
1/2"	12.5		0.0	100.0
3/8"	9.5		0.0	100.0
No. 4	4.75	0.64	0.37	99.63
No. 10	2.00	62.19	36.33	63.67
No. 40	0.425	134.22	78.40	21.60
No. 200	0.075	166.62	97.32	2.68

Total sample dry weight: 136.80 g			Borehole no. : B# 2 (15-16)m	
Sieve no.	Size (mm)	Cumulative Weight Retained (g)	Cumulative % Retained	Cumulative % Passing
3/4"	19.0		0.0	100.0
1/2"	12.5		0.0	100.0
3/8"	9.5		0.0	100.0
No. 4	4.75	14.1	10.31	89.69
No. 10	2.00	29.3	21.42	78.58
No. 40	0.425	67.4	49.27	50.73
No. 200	0.075	123.8	90.50	9.50

Total sample dry weight: 280.30 g			Borehole no. : B# 3 (10-11)m	
Sieve no.	Size (mm)	Cumulative Weight Retained (g)	Cumulative % Retained	Cumulative % Passing
3/4"	19.0		0.0	100.0
1/2"	12.5		0.0	100.0
3/8"	9.5		0.0	100.0
No. 4	4.75	3.9	1.39	98.61
No. 10	2.00	8.7	3.10	96.90
No. 40	0.425	44.5	15.88	84.12
No. 200	0.075	199.0	71.00	29.00

Appendices

Appendix 1.2

Total sample dry weight: 361.60 g			Borehole no. : B# 3 (13-14)m	
Sieve no.	Size (mm)	Cumulative Weight Retained (g)	Cumulative % Retained	Cumulative % Passing
3/4"	19.0		0.0	100.0
1/2"	12.5		0.0	100.0
3/8"	9.5		0.0	100.0
No. 4	4.75	14.4	3.98	96.02
No. 10	2.00	45.0	12.44	87.56
No. 40	0.425	104.8	28.98	71.02
No. 200	0.075	350.8	97.01	2.99

Total sample dry weight: 140.45 g			Borehole no. : B# 4 (14-14.5)m	
Sieve no.	Size (mm)	Cumulative Weight Retained (g)	Cumulative % Retained	Cumulative % Passing
3/4"	19.0		0.0	100.0
1/2"	12.5		0.0	100.0
3/8"	9.5		0.0	100.0
No. 4	4.75	0.0	0.0	100.0
No. 10	2.00	2.64	1.88	98.12
No. 40	0.425	17.92	12.76	87.24
No. 200	0.075	124.6	88.71	11.29

Total sample dry weight: 169.10 g			Borehole no. : B# 5 (15-15.5)m	
Sieve no.	Size (mm)	Cumulative Weight Retained (g)	Cumulative % Retained	Cumulative % Passing
3/4"	19.0		0.0	100.0
1/2"	12.5		0.0	100.0
3/8"	9.5		0.0	100.0
No. 4	4.75	0.4	0.24	99.76
No. 10	2.00	9.5	5.62	94.38
No. 40	0.425	85	50.27	49.73
No. 200	0.075	166.3	98.34	1.66

Total sample dry weight: 195.00 g			Borehole no. : B# 6 (7-7.5)m	
Sieve no.	Size (mm)	Cumulative Weight Retained (g)	Cumulative % Retained	Cumulative % Passing
3/4"	19.0		0.0	100.0
1/2"	12.5		0.0	100.0
3/8"	9.5		0.0	100.0
No. 4	4.75	16.1	8.26	91.74
No. 10	2.00	36.7	18.82	81.18
No. 40	0.425	75.9	38.92	61.08
No. 200	0.075	182.8	93.74	06.26

Appendices

Appendix 1.2

Total sample dry weight: 136.90 g			Borehole no. : B# 7 (8-8.5)m	
Sieve no.	Size (mm)	Cumulative Weight Retained (g)	Cumulative % Retained	Cumulative % Passing
3/4"	19.0		0.0	100.0
1/2"	12.5		0.0	100.0
3/8"	9.5		0.0	100.0
No. 4	4.75	6.5	4.75	95.25
No. 10	2.00	20.5	14.97	85.03
No. 40	0.425	52.6	38.40	61.60
No. 200	0.075	129.7	94.74	5.26

Total sample dry weight: 143.50 g			Borehole no. : B# 8 (13-13.5)m	
Sieve no.	Size (mm)	Cumulative Weight Retained (g)	Cumulative % Retained	Cumulative % Passing
3/4"	19.0		0.0	100.0
1/2"	12.5		0.0	100.0
3/8"	9.5		0.0	100.0
No. 4	4.75	6.1	4.25	95.75
No. 10	2.00	9.4	6.55	93.45
No. 40	0.425	30.0	20.91	79.09
No. 200	0.075	94.2	65.64	34.36

Total sample dry weight: 132.70 g			Borehole no. : B# 9 (9.5-9.8)m	
Sieve no.	Size (mm)	Cumulative Weight Retained (g)	Cumulative % Retained	Cumulative % Passing
3/4"	19.0		0.0	100.0
1/2"	12.5		0.0	100.0
3/8"	9.5		0.0	100.0
No. 4	4.75	3.0	2.26	97.74
No. 10	2.00	4.8	3.62	96.38
No. 40	0.425	18.4	13.87	86.13
No. 200	0.075	88.8	66.62	33.38

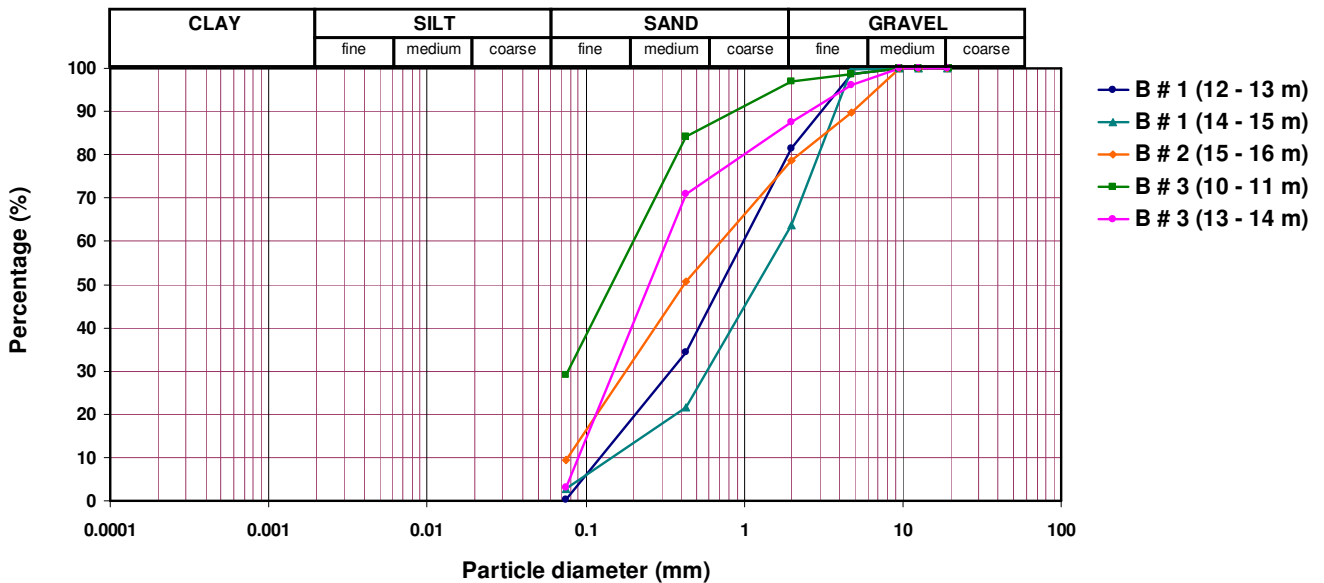
Total sample dry weight: 130.60 g			Borehole no. : B# 10 (11.5-12)m	
Sieve no.	Size(mm)	Cumulative Weight Retained (g)	Cumulative % Retained	Cumulative % Passing
3/4"	19.0		0.0	100.0
1/2"	12.5		0.0	100.0
3/8"	9.5		0.0	100.0
No. 4	4.75	0.2	0.15	99.85
No. 10	2.00	1.1	0.84	99.16
No. 40	0.425	27.0	20.67	79.33
No. 200	0.075	112.0	85.76	14.24

Appendices

Appendix 1.2

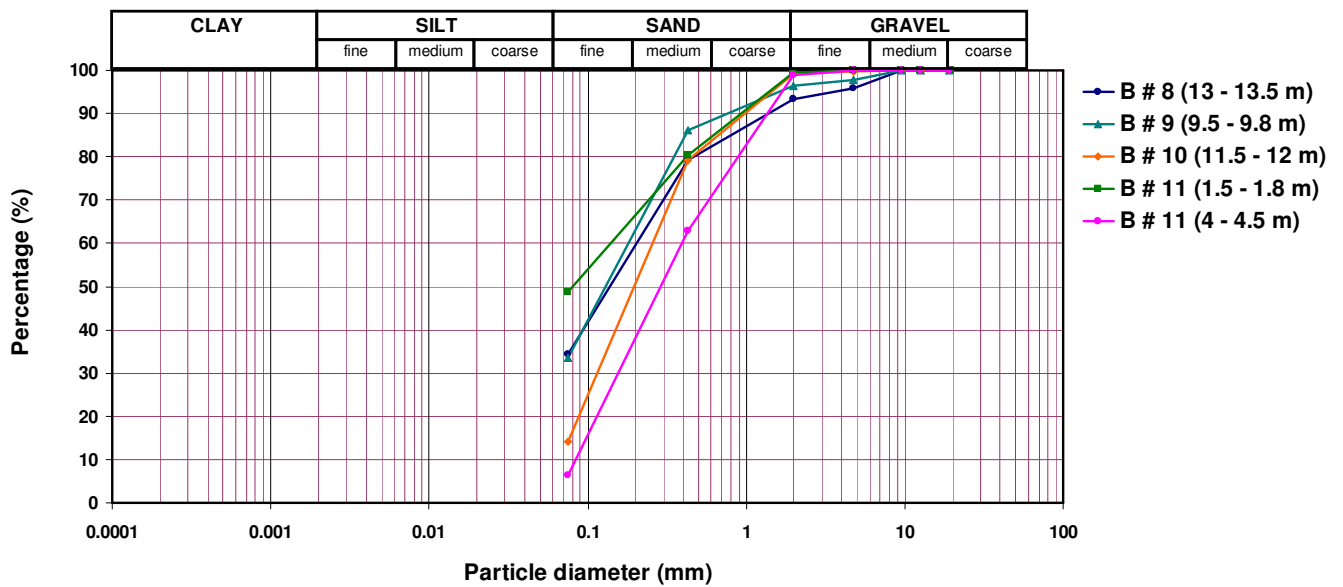
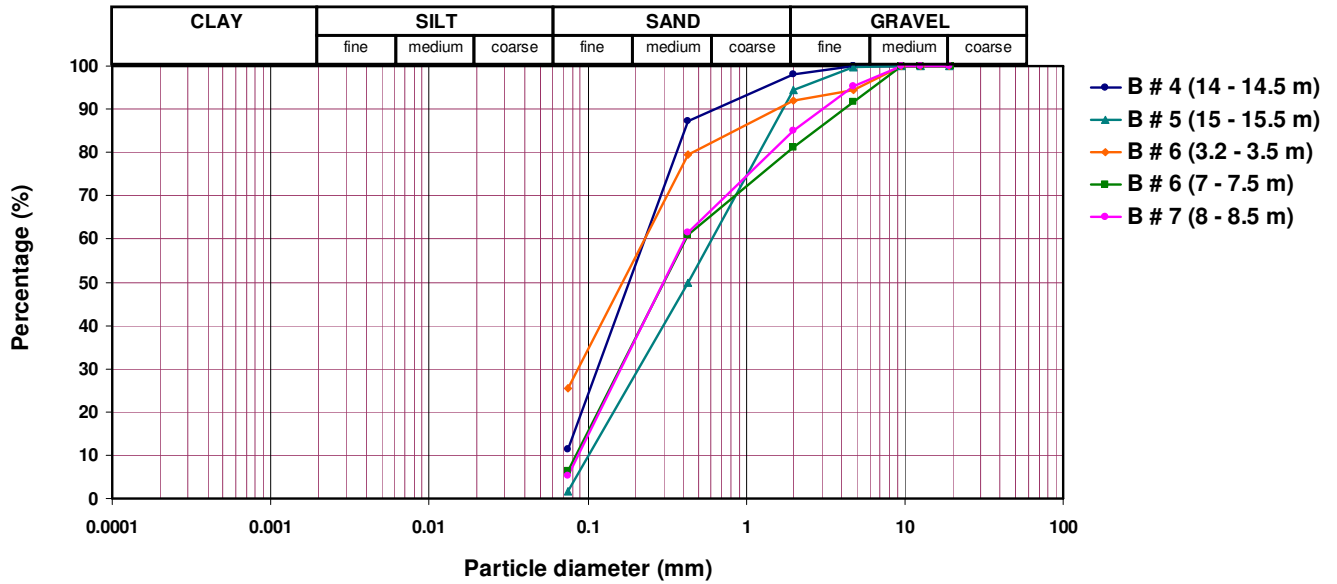
Total sample dry weight : 104.60 g			Borehole no. : B# 11 (1.5-1.8)m	
Sieve no.	Size (mm)	Cumulative Weight Retained (g)	Cumulative % Retained	Cumulative % Passing
3/4"	19.0		0.0	100.0
1/2"	12.5		0.0	100.0
3/8"	9.5		0.0	100.0
No. 4	4.75	0.0	0.0	100.0
No. 10	2.00	0.5	0.48	99.52
No. 40	0.425	20.6	19.69	80.31
No. 200	0.075	53.7	51.30	48.70

Total sample dry weight: 124.10 g			Borehole no. : B# 11 (4-4.5)m	
Sieve no.	Size (mm)	Cumulative Weight Retained (g)	Cumulative % Retained	Cumulative % Passing
3/4"	19.0		0.0	100.0
1/2"	12.5		0.0	100.0
3/8"	9.5		0.0	100.0
No. 4	4.75	0.0	0.0	100.0
No. 10	2.00	1.5	1.21	98.79
No. 40	0.425	46.0	37.07	62.93
No. 200	0.075	116.3	93.71	6.29



Appendices

Appendix 1.2



Appendices

Appendix 1.2

Total sample dry weight: 169.70 g			Borehole no. : SD# 1 (4-4.5)m	
Sieve no.	Size (mm)	Cumulative Weight Retained (g)	Cumulative % Retained	Cumulative % Passing
3/4"	19.0		0.0	100.0
1/2"	12.5		0.0	100.0
3/8"	9.5		0.0	100.0
No. 4	4.75	39.7	23.39	76.61
No. 10	2.00	47.0	27.70	72.30
No. 40	0.425	73.3	43.19	56.81
No. 200	0.075	114.9	67.71	32.29

Total sample dry weight: 146.80 g			Borehole no. : SD# 1 (6-6.5)m	
Sieve no.	Size (mm)	Cumulative Weight Retained (g)	Cumulative % Retained	Cumulative % Passing
3/4"	19.0		0.0	100.0
1/2"	12.5		0.0	100.0
3/8"	9.5		0.0	100.0
No. 4	4.75	10.8	7.36	92.64
No. 10	2.00	13.2	8.99	91.01
No. 40	0.425	33.0	22.48	77.52
No. 200	0.075	130.1	88.62	11.38

Total sample dry weight: 140.40 g			Borehole no. : SD# 1 (8-9)m	
Sieve no.	Size (mm)	Cumulative Weight Retained (g)	Cumulative % Retained	Cumulative % Passing
3/4"	19.0		0.0	100.0
1/2"	12.5		0.0	100.0
3/8"	9.5		0.0	100.0
No. 4	4.75	2.7	1.92	98.08
No. 10	2.00	9.1	6.48	93.52
No. 40	0.425	57.8	41.17	58.83
No. 200	0.075	130.4	92.88	7.12

Total sample dry weight: 173.40 g			Borehole no. : SD# 1 (10-10.5)m	
Sieve no.	Size (mm)	Cumulative Weight Retained (g)	Cumulative % Retained	Cumulative % Passing
3/4"	19.0		0.0	100.0
1/2"	12.5		0.0	100.0
3/8"	9.5		0.0	100.0
No. 4	4.75	29.6	17.07	82.93
No. 10	2.00	37.3	21.51	78.49
No. 40	0.425	64.3	37.08	62.92
No. 200	0.075	157.7	90.95	9.05

Appendices

Appendix 1.2

Total sample dry weight: 159.40 g			Borehole no. : SD# 1 (11-12)m	
Sieve no.	Size (mm)	Cumulative Weight Retained (g)	Cumulative % Retained	Cumulative % Passing
3/4"	19.0		0.0	100.0
1/2"	12.5		0.0	100.0
3/8"	9.5		0.0	100.0
No. 4	4.75	13.4	8.41	91.59
No. 10	2.00	20.3	12.74	87.26
No. 40	0.425	59.1	37.08	62.92
No. 200	0.075	153.2	96.11	3.89

Total sample dry weight: 146.40 g			Borehole no. : SD# 1 (14-14.5)m	
Sieve no.	Size (mm)	Cumulative Weight Retained (g)	Cumulative % Retained	Cumulative % Passing
3/4"	19.0		0.0	100.0
1/2"	12.5		0.0	100.0
3/8"	9.5		0.0	100.0
No. 4	4.75	17.8	12.16	87.84
No. 10	2.00	23.2	15.85	84.15
No. 40	0.425	49.0	33.47	66.53
No. 200	0.075	140.1	95.70	4.30

Total sample dry weight: 164.00 g			Borehole no. : SD# 1 (16.5-17)m	
Sieve no.	Size (mm)	Cumulative Weight Retained (g)	Cumulative % Retained	Cumulative % Passing
3/4"	19.0		0.0	100.0
1/2"	12.5		0.0	100.0
3/8"	9.5		0.0	100.0
No. 4	4.75	21.5	13.11	86.89
No. 10	2.00	37.7	22.99	77.01
No. 40	0.425	66.8	40.73	59.27
No. 200	0.075	149.4	91.10	8.90

Total sample dry weight: 163.70 g			Borehole no. : SD# 1 (20-20.5)m	
Sieve no.	Size (mm)	Cumulative Weight Retained (g)	Cumulative % Retained	Cumulative % Passing
3/4"	19.0		0.0	100.0
1/2"	12.5		0.0	100.0
3/8"	9.5		0.0	100.0
No. 4	4.75	49.0	29.93	70.07
No. 10	2.00	54.2	33.11	66.89
No. 40	0.425	73.8	45.08	54.92
No. 200	0.075	154.1	94.14	5.86

Appendices

Appendix 1.2

Total sample dry weight: 174.50 g			Borehole no. : SD# 1 (26-27)m	
Sieve no.	Size (mm)	Cumulative Weight Retained (g)	Cumulative % Retained	Cumulative % Passing
3/4"	19.0		0.0	100.0
1/2"	12.5		0.0	100.0
3/8"	9.5		0.0	100.0
No. 4	4.75	28.5	16.33	83.67
No. 10	2.00	62.7	35.93	64.07
No. 40	0.425	95.3	54.61	45.39
No. 200	0.075	169.3	97.02	2.98

Total sample dry weight: 178.00 g			Borehole no. : SD# 1 (30-31)m	
Sieve no.	Size (mm)	Cumulative Weight Retained (g)	Cumulative % Retained	Cumulative % Passing
3/4"	19.0		0.0	100.0
1/2"	12.5		0.0	100.0
3/8"	9.5		0.0	100.0
No. 4	4.75	34.8	19.55	80.45
No. 10	2.00	75.2	42.25	57.75
No. 40	0.425	116.0	65.17	34.83
No. 200	0.075	172.4	96.85	3.15

Total sample dry weight: 171.40 g			Borehole no. : SD# 1 (35-36)m	
Sieve no.	Size (mm)	Cumulative Weight Retained (g)	Cumulative % Retained	Cumulative % Passing
3/4"	19.0		0.0	100.0
1/2"	12.5		0.0	100.0
3/8"	9.5		0.0	100.0
No. 4	4.75	1.5	0.88	99.12
No. 10	2.00	12.2	7.12	92.88
No. 40	0.425	40.9	23.86	76.14
No. 200	0.075	143.1	83.49	16.51

Total sample dry weight: 178.00 g			Borehole no. : SD# 1 (37-38)m	
Sieve no.	Size (mm)	Cumulative Weight Retained (g)	Cumulative % Retained	Cumulative % Passing
3/4"	19.0		0.0	100.0
1/2"	12.5		0.0	100.0
3/8"	9.5		0.0	100.0
No. 4	4.75	3.1	1.74	98.26
No. 10	2.00	48.0	26.97	73.03
No. 40	0.425	95.2	53.48	46.52
No. 200	0.075	163.6	91.91	8.09

Appendices

Appendix 1.2

Total sample dry weight: 238.80 g		Borehole no. : SD# 1 (44-45)m		
Sieve no.	Size (mm)	Cumulative Weight Retained (g)	Cumulative % Retained	Cumulative % Passing
3/4"	19.0		0.0	100.0
1/2"	12.5		0.0	100.0
3/8"	9.5		0.0	100.0
No. 4	4.75	28.3	11.85	88.15
No. 10	2.00	42.2	17.67	82.33
No. 40	0.425	85.0	35.59	64.41
No. 200	0.075	228.2	95.56	4.44

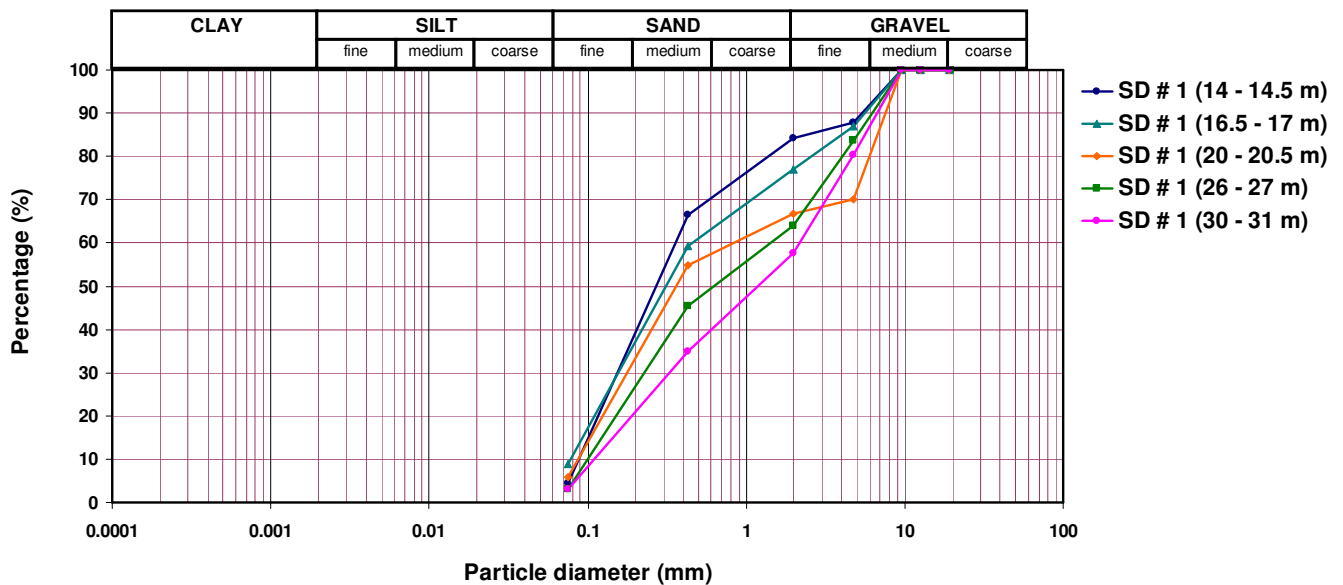
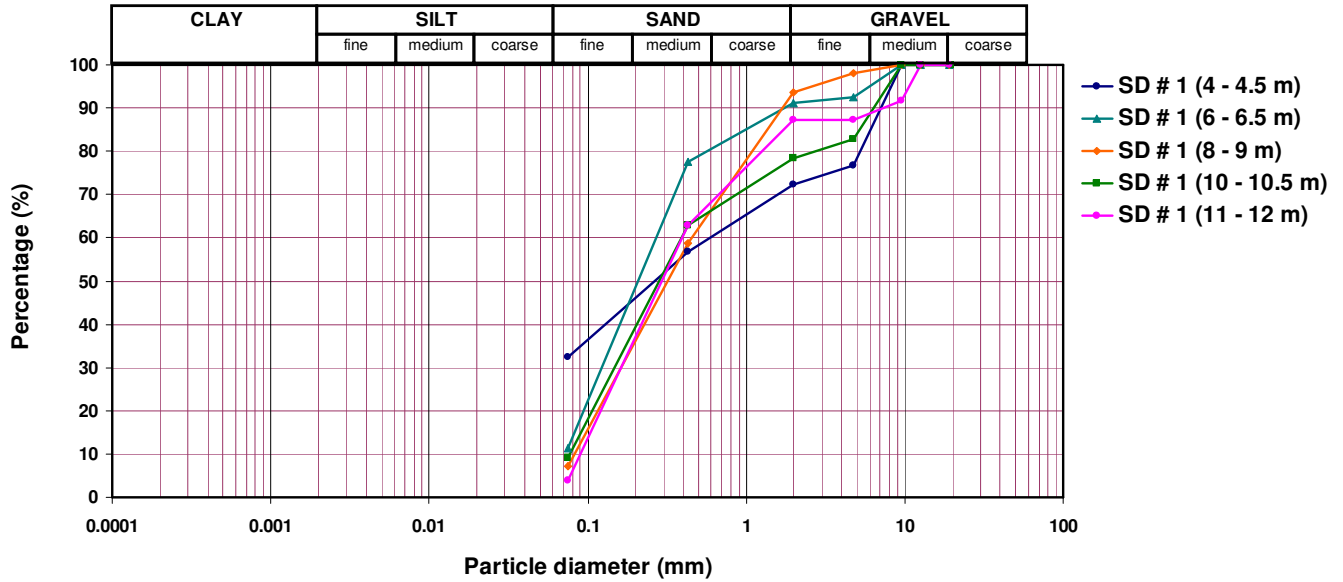
Total sample dry weight: 252.10 g		Borehole no. : SD# 1 (49-50)m		
Sieve no.	Size (mm)	Cumulative Weight Retained (g)	Cumulative % Retained	Cumulative % Passing
3/4"	19.0		0.0	100.0
1/2"	12.5		0.0	100.0
3/8"	9.5		0.0	100.0
No. 4	4.75	0.0	0.0	100.0
No. 10	2.00	0.2	0.08	99.92
No. 40	0.425	19.3	7.66	92.34
No. 200	0.075	237.7	94.29	5.71

Total sample dry weight: 238.70 g		Borehole no. : SD# 1 (56-57)m		
Sieve no.	Size (mm)	Cumulative Weight Retained (g)	Cumulative % Retained	Cumulative % Passing
3/4"	19.0		0.0	100.0
1/2"	12.5		0.0	100.0
3/8"	9.5		0.0	100.0
No. 4	4.75	0.7	0.29	99.71
No. 10	2.00	4.0	1.68	98.32
No. 40	0.425	31.2	13.07	86.93
No. 200	0.075	234.3	98.16	1.84

Total sample dry weight: 217.50 g		Borehole no. : SD# 1 (63-64)m		
Sieve no.	Size (mm)	Cumulative Weight Retained (g)	Cumulative % Retained	Cumulative % Passing
3/4"	19.0		0.0	100.0
1/2"	12.5		0.0	100.0
3/8"	9.5		0.0	100.0
No. 4	4.75	0.0	0.0	100.0
No. 10	2.00	0.7	0.32	99.68
No. 40	0.425	33.5	15.40	84.60
No. 200	0.075	214.4	98.57	1.43

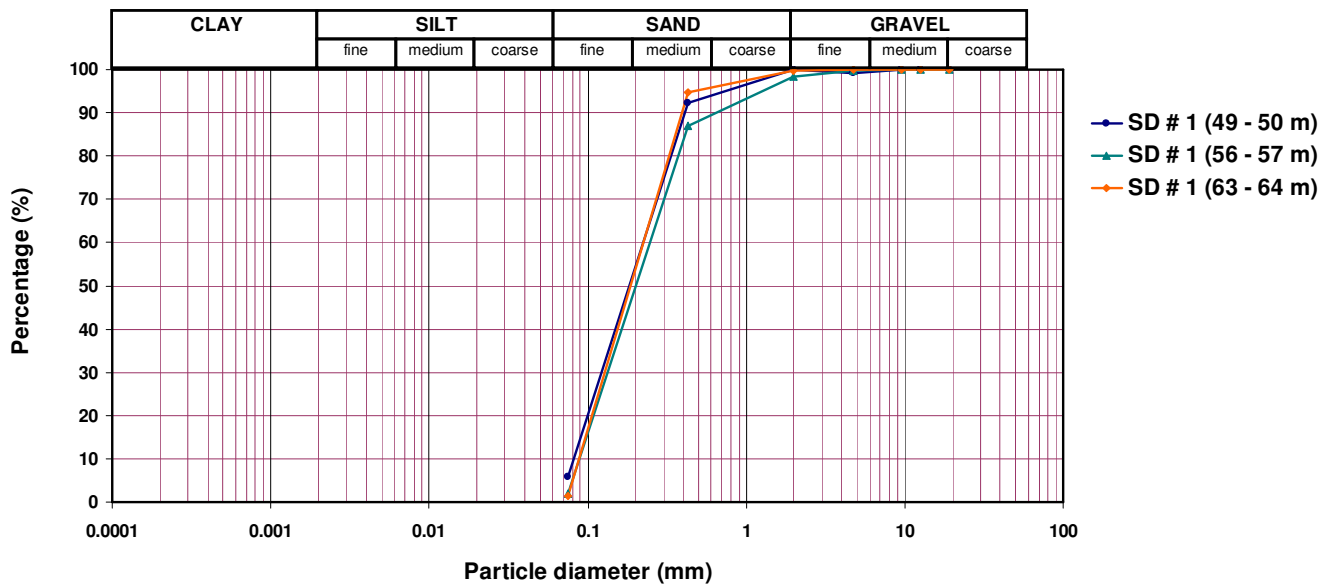
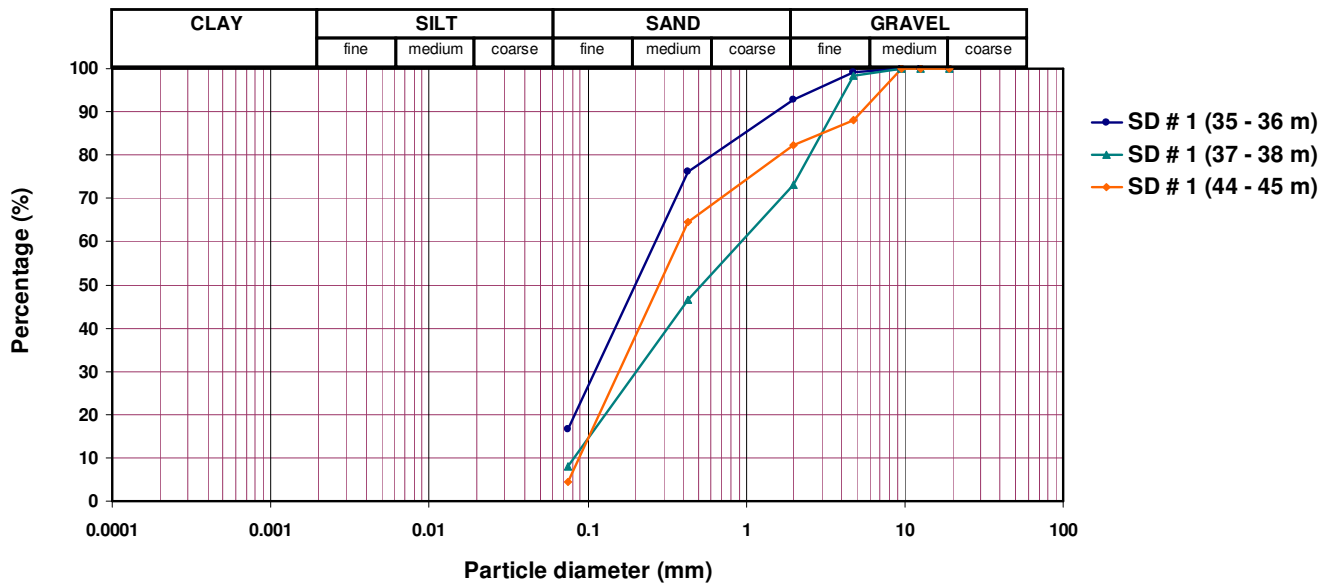
Appendices

Appendix 1.2



Appendices

Appendix 1.2



Appendices

Appendix 1.2

Total sample dry weight: 254.70 g		Borehole no. : SD# 2 (7-7.5)m		
Sieve no.	Size (mm)	Cumulative Weight Retained (g)	Cumulative % Retained	Cumulative % Passing
3/4"	19.0		0.0	100.0
1/2"	12.5		0.0	100.0
3/8"	9.5		0.0	100.0
No. 4	4.75	18.7	7.34	92.66
No. 10	2.00	34.0	13.35	86.65
No. 40	0.425	65.8	25.83	74.17
No. 200	0.075	220.8	86.69	13.31

Total sample dry weight: 234.20 g		Borehole no. : SD# 2 (12-12.5)m		
Sieve no.	Size (mm)	Cumulative Weight Retained (g)	Cumulative % Retained	Cumulative % Passing
3/4"	19.0		0.0	100.0
1/2"	12.5		0.0	100.0
3/8"	9.5		0.0	100.0
No. 4	4.75	2.8	1.2	98.80
No. 10	2.00	7.2	3.07	96.93
No. 40	0.425	42.5	18.15	81.85
No. 200	0.075	219.6	93.77	6.23

Total sample dry weight: 246.30 g		Borehole no. : SD# 2 (14-15)m		
Sieve no.	Size (mm)	Cumulative Weight Retained (g)	Cumulative % Retained	Cumulative % Passing
3/4"	19.0		0.0	100.0
1/2"	12.5		0.0	100.0
3/8"	9.5		0.0	100.0
No. 4	4.75	1.7	0.69	99.31
No. 10	2.00	13.2	5.36	94.64
No. 40	0.425	79.5	32.28	67.72
No. 200	0.075	239.7	97.32	2.68

Total sample dry weight: 249.60 g		Borehole no. : SD# 2 (17-18)m		
Sieve no.	Size (mm)	Cumulative Weight Retained (g)	Cumulative % Retained	Cumulative % Passing
3/4"	19.0		0.0	100.0
1/2"	12.5		0.0	100.0
3/8"	9.5		0.0	100.0
No. 4	4.75	0.3	0.12	99.88
No. 10	2.00	7.2	2.88	97.12
No. 40	0.425	69.7	27.92	72.08
No. 200	0.075	239.7	96.03	3.97

Appendices

Appendix 1.2

Total sample dry weight: 284.30 g		Borehole no. : SD# 2 (19-20)m		
Sieve no.	Size (mm)	Cumulative Weight Retained (g)	Cumulative % Retained	Cumulative % Passing
3/4"	19.0		0.0	100.0
1/2"	12.5		0.0	100.0
3/8"	9.5		0.0	100.0
No. 4	4.75	0.0	0.0	100.0
No. 10	2.00	5.4	1.90	98.10
No. 40	0.425	71.7	25.22	74.78
No. 200	0.075	278.9	98.10	1.90

Total sample dry weight: 218.10 g		Borehole no. : SD# 2 (22-23)m		
Sieve no.	Size (mm)	Cumulative Weight Retained (g)	Cumulative % Retained	Cumulative % Passing
3/4"	19.0		0.0	100.0
1/2"	12.5		0.0	100.0
3/8"	9.5		0.0	100.0
No. 4	4.75	0.0	0.0	100.0
No. 10	2.00	2.5	1.15	98.85
No. 40	0.425	43.8	20.08	79.92
No. 200	0.075	148.5	68.09	31.91

Total sample dry weight: 273.10 g		Borehole no. : SD# 2 (24-25)m		
Sieve no.	Size (mm)	Cumulative Weight Retained (g)	Cumulative % Retained	Cumulative % Passing
3/4"	19.0		0.0	100.0
1/2"	12.5		0.0	100.0
3/8"	9.5		0.0	100.0
No. 4	4.75	2.3	0.84	99.16
No. 10	2.00	15.3	5.60	94.40
No. 40	0.425	82.6	30.25	69.75
No. 200	0.075	255.3	93.48	6.52

Total sample dry weight: 223.30 g		Borehole no. : SD# 2 (29-30)m		
Sieve no.	Size (mm)	Cumulative Weight Retained (g)	Cumulative % Retained	Cumulative % Passing
3/4"	19.0		0.0	100.0
1/2"	12.5		0.0	100.0
3/8"	9.5		0.0	100.0
No. 4	4.75	4.0	1.79	98.21
No. 10	2.00	67.3	30.14	69.86
No. 40	0.425	178.0	79.71	20.29
No. 200	0.075	218.1	97.67	2.33

Appendices

Appendix 1.2

Total sample dry weight: 234.50 g			Borehole no. : SD# 2 (34-35)m	
Sieve no.	Size (mm)	Cumulative Weight Retained (g)	Cumulative % Retained	Cumulative % Passing
3/4"	19.0		0.0	100.0
1/2"	12.5		0.0	100.0
3/8"	9.5		0.0	100.0
No. 4	4.75	3.2	1.36	98.64
No. 10	2.00	31.5	13.43	86.57
No. 40	0.425	87.2	37.19	62.81
No. 200	0.075	234	99.79	0.21

Total sample dry weight: 364.40 g			Borehole no. : SD# 2 (40-41)m	
Sieve no.	Size (mm)	Cumulative Weight Retained (g)	Cumulative % Retained	Cumulative % Passing
3/4"	19.0		0.0	100.0
1/2"	12.5		0.0	100.0
3/8"	9.5		0.0	100.0
No. 4	4.75	0.0	0.0	100.0
No. 10	2.00	1.1	0.30	99.70
No. 40	0.425	85.6	23.49	76.51
No. 200	0.075	361	99.07	0.93

Total sample dry weight: 305.30 g			Borehole no. : SD# 2 (45-46)m	
Sieve no.	Size (mm)	Cumulative Weight Retained (g)	Cumulative % Retained	Cumulative % Passing
3/4"	19.0		0.0	100.0
1/2"	12.5		0.0	100.0
3/8"	9.5		0.0	100.0
No. 4	4.75	0.0	0.0	100.0
No. 10	2.00	0.0	0.0	100.0
No. 40	0.425	37.3	12.22	87.78
No. 200	0.075	302.8	99.18	0.82

Total sample dry weight: 250.30 g			Borehole no. : SD# 2 (51-52)m	
Sieve no.	Size (mm)	Cumulative Weight Retained (g)	Cumulative % Retained	Cumulative % Passing
3/4"	19.0		0.0	100.0
1/2"	12.5		0.0	100.0
3/8"	9.5		0.0	100.0
No. 4	4.75	7.4	2.96	97.04
No. 10	2.00	63.3	25.29	74.71
No. 40	0.425	155.5	62.13	37.87
No. 200	0.075	249.3	99.60	0.40

Appendices

Appendix 1.2

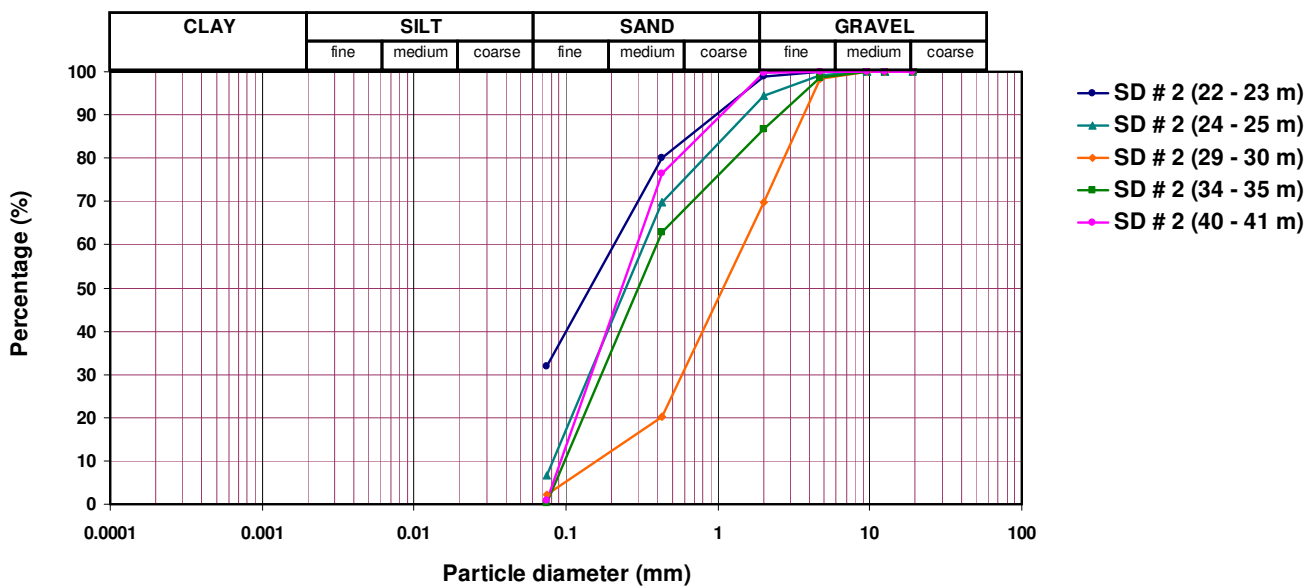
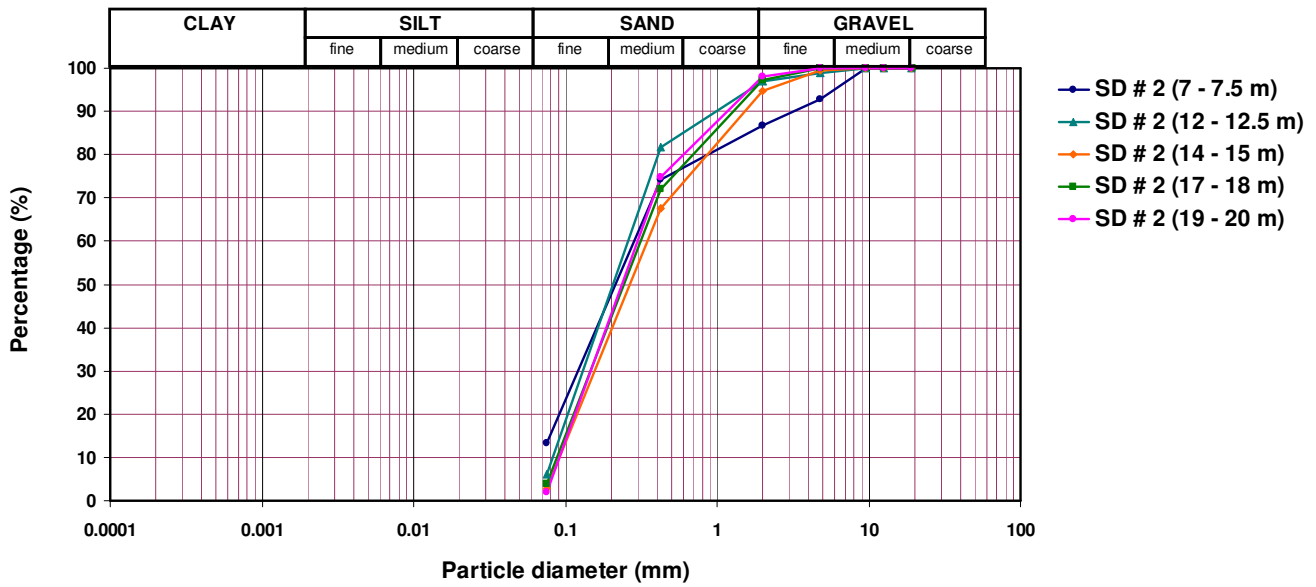
Total sample dry weight: 229.10 g			Borehole no. : SD# 2 (55-56)m	
Sieve no.	Size (mm)	Cumulative Weight Retained (g)	Cumulative % Retained	Cumulative % Passing
3/4"	19.0		0.0	100.0
1/2"	12.5		0.0	100.0
3/8"	9.5		0.0	100.0
No. 4	4.75	0.0	0.0	100.0
No. 10	2.00	1.9	0.83	99.17
No. 40	0.425	59.8	26.10	73.90
No. 200	0.075	228.2	99.61	0.39

Total sample dry weight: 249.60 g			Borehole no. : SD# 2 (60-61)m	
Sieve no.	Size (mm)	Cumulative Weight Retained (g)	Cumulative % Retained	Cumulative % Passing
3/4"	19.0		0.0	100.0
1/2"	12.5		0.0	100.0
3/8"	9.5		0.0	100.0
No. 4	4.75	0.0	0.0	100.0
No. 10	2.00	7.4	2.96	97.04
No. 40	0.425	73.4	29.41	70.59
No. 200	0.075	249.0	99.76	0.24

Total sample dry weight: 299.00 g			Borehole no. : SD# 2 (62-63)m	
Sieve no.	Size (mm)	Cumulative Weight Retained (g)	Cumulative % Retained	Cumulative % Passing
3/4"	19.0		0.0	100.0
1/2"	12.5		0.0	100.0
3/8"	9.5		0.0	100.0
No. 4	4.75	2.9	0.97	99.03
No. 10	2.00	11.4	3.81	96.19
No. 40	0.425	83.3	27.86	72.14
No. 200	0.075	297.4	99.46	0.54

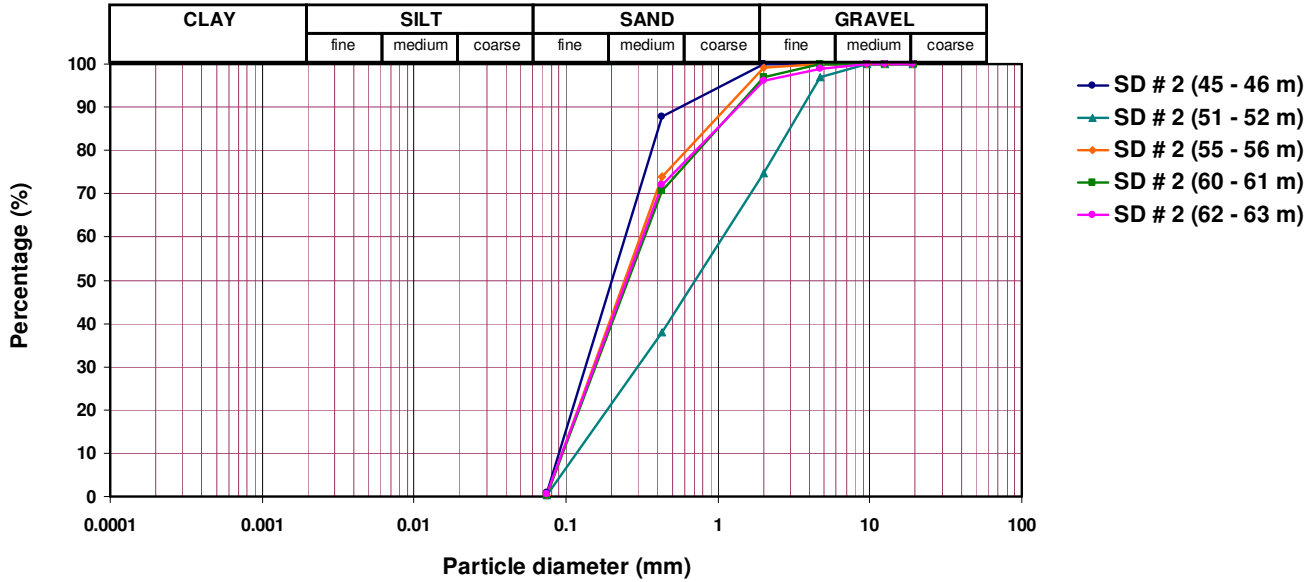
Appendices

Appendix 1.2



Appendices

Appendix 1.2



Total sample dry weight: 185.00 g		Borehole no. : SD# 3 (6.5-7.5)m		
Sieve no.	Size (mm)	Cumulative Weight Retained (g)	Cumulative % Retained	Cumulative % Passing
3/4"	19.0		0.0	100.0
1/2"	12.5		0.0	100.0
3/8"	9.5		0.0	100.0
No. 4	4.75	1.8	0.97	99.03
No. 10	2.00	3.2	1.73	98.27
No. 40	0.425	21.1	11.41	88.59
No. 200	0.075	128.9	69.68	30.32

Total sample dry weight: 175.80 g		Borehole no. : SD# 3 (9-9.5)m		
Sieve no.	Size (mm)	Cumulative Weight Retained (g)	Cumulative % Retained	Cumulative % Passing
3/4"	19.0		0.0	100.0
1/2"	12.5		0.0	100.0
3/8"	9.5		0.0	100.0
No. 4	4.75	21.5	12.23	87.77
No. 10	2.00	28.6	16.27	83.73
No. 40	0.425	55.3	31.46	68.54
No. 200	0.075	158.3	90.05	9.95

Appendices

Appendix 1.2

Total sample dry weight: 145.20 g		Borehole no. : SD# 3 (12-12.5)m		
Sieve no.	Size (mm)	Cumulative Weight Retained (g)	Cumulative % Retained	Cumulative % Passing
3/4"	19.0		0.0	100.0
1/2"	12.5		0.0	100.0
3/8"	9.5		0.0	100.0
No. 4	4.75	57.0	39.26	60.74
No. 10	2.00	74.0	50.96	49.04
No. 40	0.425	93.7	64.53	35.47
No. 200	0.075	131.7	90.70	9.30

Total sample dry weight: 182.40 g		Borehole no. : SD# 3 (15-15.5)m		
Sieve no.	Size (mm)	Cumulative Weight Retained (g)	Cumulative % Retained	Cumulative % Passing
3/4"	19.0		0.0	100.0
1/2"	12.5		0.0	100.0
3/8"	9.5		0.0	100.0
No. 4	4.75	13.0	7.13	92.87
No. 10	2.00	16.9	9.27	90.73
No. 40	0.425	28.2	15.46	84.54
No. 200	0.075	126.9	69.57	30.43

Total sample dry weight: 318.00 g		Borehole no. : SD# 3 (17-18)m		
Sieve no.	Size (mm)	Cumulative Weight Retained (g)	Cumulative % Retained	Cumulative % Passing
3/4"	19.0		0.0	100.0
1/2"	12.5		0.0	100.0
3/8"	9.5		0.0	100.0
No. 4	4.75	0.0	0.0	100.0
No. 10	2.00	11.4	3.58	96.42
No. 40	0.425	77.5	24.37	75.63
No. 200	0.075	312.6	98.30	1.70

Total sample dry weight: 287.00 g		Borehole no. : SD# 3 (20-21)m		
Sieve no.	Size (mm)	Cumulative Weight Retained (g)	Cumulative % Retained	Cumulative % Passing
3/4"	19.0		0.0	100.0
1/2"	12.5		0.0	100.0
3/8"	9.5		0.0	100.0
No. 4	4.75	0.0	0.0	100.0
No. 10	2.00	0.0	0.0	100.0
No. 40	0.425	173.3	60.38	39.62
No. 200	0.075	284.7	99.20	0.80

Appendices

Appendix 1.2

Total sample dry weight: 287.00 g		Borehole no. : SD# 3 (25-26)m		
Sieve no.	Size (mm)	Cumulative Weight Retained (g)	Cumulative % Retained	Cumulative % Passing
3/4"	19.0		0.0	100.0
1/2"	12.5		0.0	100.0
3/8"	9.5		0.0	100.0
No. 4	4.75	0.0	0.0	100.0
No. 10	2.00	2.2	0.77	99.23
No. 40	0.425	60.8	21.18	78.82
No. 200	0.075	284.7	99.20	0.80

Total sample dry weight: 248.80 g		Borehole no. : SD# 3 (27-28)m		
Sieve no.	Size (mm)	Cumulative Weight Retained (g)	Cumulative % Retained	Cumulative % Passing
3/4"	19.0		0.0	100.0
1/2"	12.5		0.0	100.0
3/8"	9.5		0.0	100.0
No. 4	4.75	0.0	0.0	100.0
No. 10	2.00	0.2	0.08	99.92
No. 40	0.425	49.5	19.90	80.10
No. 200	0.075	246.3	99.00	1.00

Total sample dry weight: 213.40 g		Borehole no. : SD# 3 (33-34)m		
Sieve no.	Size (mm)	Cumulative Weight Retained (g)	Cumulative % Retained	Cumulative % Passing
3/4"	19.0		0.0	100.0
1/2"	12.5		0.0	100.0
3/8"	9.5		0.0	100.0
No. 4	4.75	0.0	0.0	100.0
No. 10	2.00	0.0	0.0	100.0
No. 40	0.425	76.2	35.71	64.29
No. 200	0.075	211.4	99.06	0.94

Total sample dry weight: 235.60 g		Borehole no. : SD# 3 (39-40)m		
Sieve no.	Size (mm)	Cumulative Weight Retained (g)	Cumulative % Retained	Cumulative % Passing
3/4"	19.0		0.0	100.0
1/2"	12.5		0.0	100.0
3/8"	9.5		0.0	100.0
No. 4	4.75	0.0	0.0	100.0
No. 10	2.00	0.0	0.0	100.0
No. 40	0.425	185.9	78.90	21.10
No. 200	0.075	234.4	99.49	0.51

Appendices

Appendix 1.2

Total sample dry weight: 226.20 g		Borehole no. : SD# 3 (47-48)m		
Sieve no.	Size (mm)	Cumulative Weight Retained (g)	Cumulative % Retained	Cumulative % Passing
3/4"	19.0		0.0	100.0
1/2"	12.5		0.0	100.0
3/8"	9.5		0.0	100.0
No. 4	4.75	0.0	0.0	100.0
No. 10	2.00	0.0	0.0	100.0
No. 40	0.425	125.0	55.26	44.74
No. 200	0.075	225.7	99.78	0.22

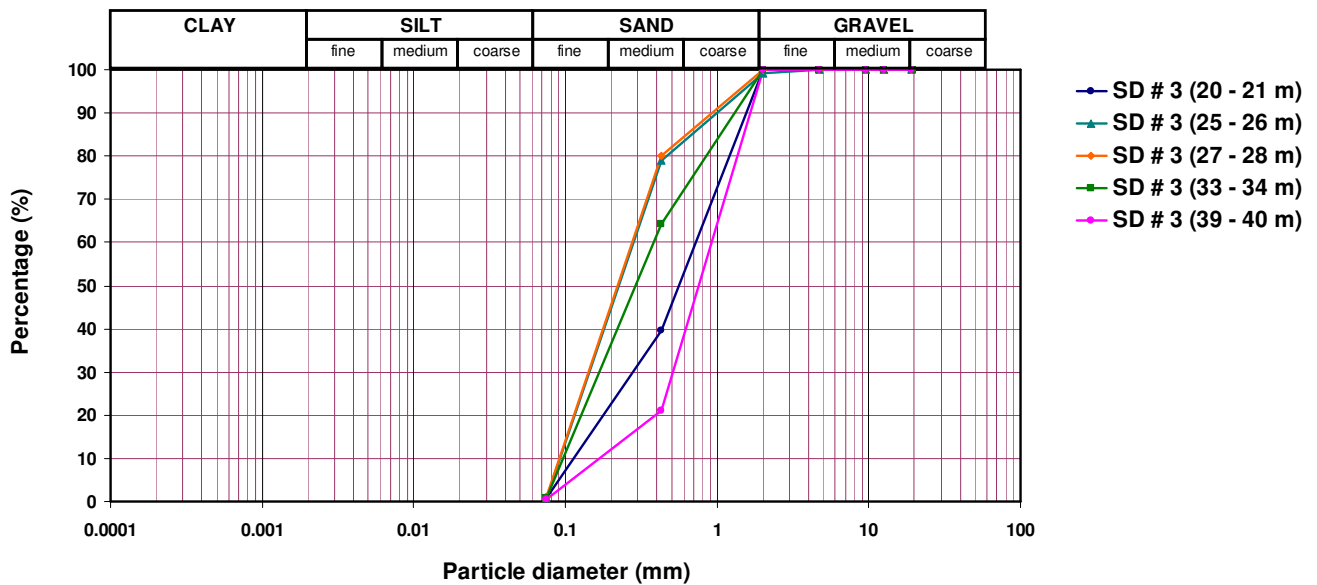
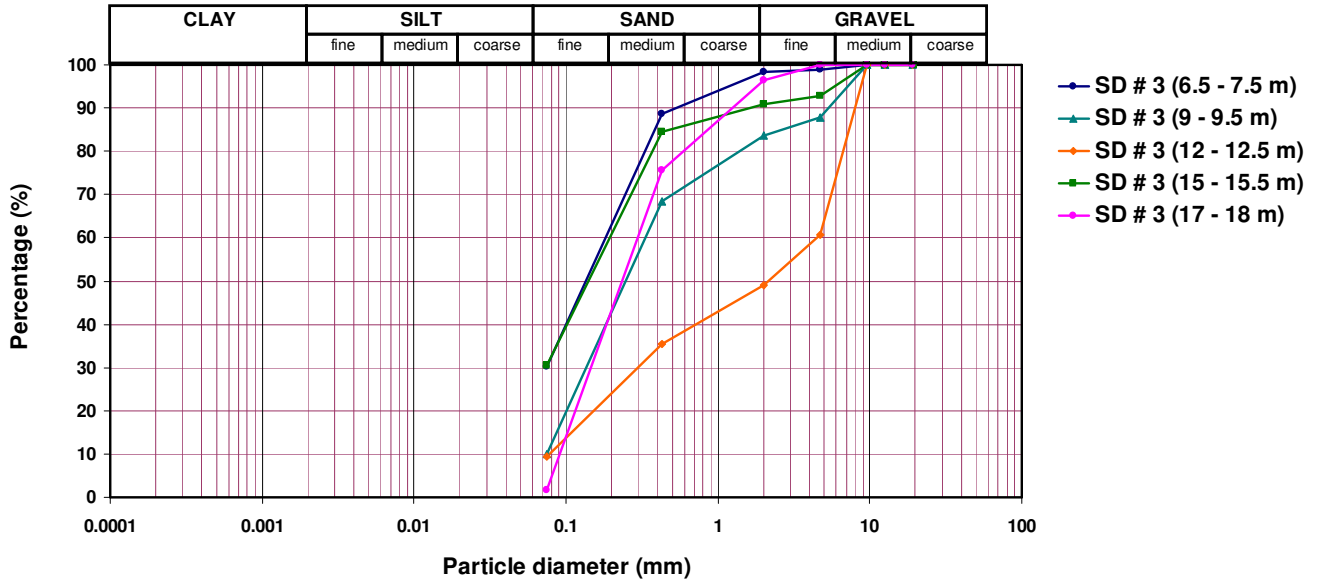
Total sample dry weight: 243.30 g		Borehole no. : SD# 3 (54-55)m		
Sieve no.	Size (mm)	Cumulative Weight Retained (g)	Cumulative % Retained	Cumulative % Passing
3/4"	19.0		0.0	100.0
1/2"	12.5		0.0	100.0
3/8"	9.5		0.0	100.0
No. 4	4.75	0.0	0.0	100.0
No. 10	2.00	0.0	0.0	100.0
No. 40	0.425	25.1	10.32	89.68
No. 200	0.075	242.0	99.47	0.53

Total sample dry weight: 252.20 g		Borehole no. : SD# 3 (59-60)m		
Sieve no.	Size (mm)	Cumulative Weight Retained (g)	Cumulative % Retained	Cumulative % Passing
3/4"	19.0		0.0	100.0
1/2"	12.5		0.0	100.0
3/8"	9.5		0.0	100.0
No. 4	4.75	0.0	0.0	100.0
No. 10	2.00	0.0	0.0	100.0
No. 40	0.425	11.7	4.64	95.36
No. 200	0.075	251.4	99.68	0.32

Total sample dry weight: 245.80 g		Borehole no. : SD# 3 (62-63)m		
Sieve no.	Size (mm)	Cumulative Weight Retained (g)	Cumulative % Retained	Cumulative % Passing
3/4"	19.0		0.0	100.0
1/2"	12.5		0.0	100.0
3/8"	9.5		0.0	100.0
No. 4	4.75	0.0	0.0	100.0
No. 10	2.00	0.0	0.0	100.0
No. 40	0.425	10.4	4.23	95.77
No. 200	0.075	244.4	99.43	0.57

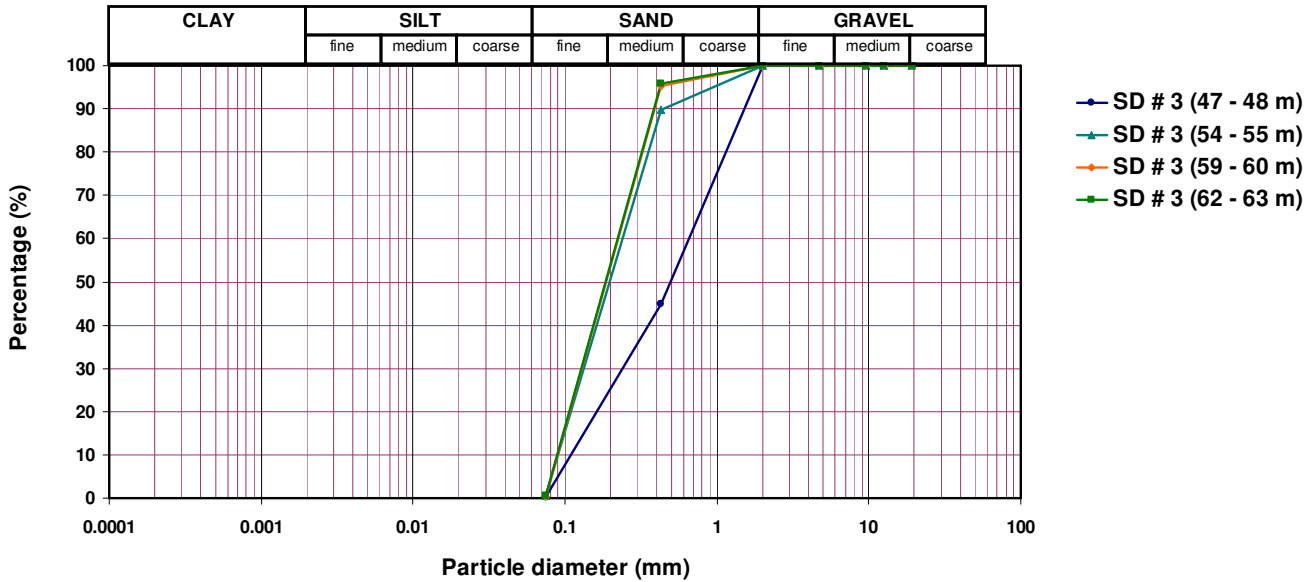
Appendices

Appendix 1.2



Appendices

Appendix 1.2



Total sample dry weight: 258.50 g		Borehole no. : SD# 4 (12-12.5)m		
Sieve no.	Size (mm)	Cumulative Weight Retained (g)	Cumulative % Retained	Cumulative % Passing
3/4"	19.0		0.0	100.0
1/2"	12.5		0.0	100.0
3/8"	9.5	3.4	1.32	98.68
No. 4	4.75	8.2	3.17	96.83
No. 10	2.00	20.0	7.74	92.26
No. 40	0.425	85.2	32.96	67.04
No. 200	0.075	220.8	85.42	14.58

Total sample dry weight: 209.30 g		Borehole no. : SD# 4 (15-15.5)m		
Sieve no.	Size (mm)	Cumulative Weight Retained (g)	Cumulative % Retained	Cumulative % Passing
3/4"	19.0		0.0	100.0
1/2"	12.5		0.0	100.0
3/8"	9.5	2.4	1.15	98.85
No. 4	4.75	8.9	4.25	95.75
No. 10	2.00	14.1	6.74	93.26
No. 40	0.425	40.0	19.11	80.89
No. 200	0.075	174.6	83.42	16.58

Appendices

Appendix 1.2

Total sample dry weight: 176.20 g			Borehole no. : SD# 4 (20-20.5)m	
Sieve no.	Size (mm)	Cumulative Weight Retained (g)	Cumulative % Retained	Cumulative % Passing
3/4"	19.0		0.0	100.0
1/2"	12.5		0.0	100.0
3/8"	9.5	0.0	0.0	100.0
No. 4	4.75	0.1	0.06	99.94
No. 10	2.00	9.2	5.22	94.78
No. 40	0.425	90.0	51.08	48.92
No. 200	0.075	166.6	94.55	5.45

Total sample dry weight: 158.90 g			Borehole no. : SD# 4 (23-23.5)m	
Sieve no.	Size (mm)	Cumulative Weight Retained (g)	Cumulative % Retained	Cumulative % Passing
3/4"	19.0		0.0	100.0
1/2"	12.5		0.0	100.0
3/8"	9.5	7.0	4.41	95.59
No. 4	4.75	12.9	8.12	91.88
No. 10	2.00	14.8	9.31	90.69
No. 40	0.425	59.4	37.38	62.62
No. 200	0.075	129.0	81.18	18.82

Total sample dry weight: 174.16 g			Borehole no. : SD# 4 (31-32)m	
Sieve no.	Size (mm)	Cumulative Weight Retained (g)	Cumulative % Retained	Cumulative % Passing
3/4"	19.0		0.0	100.0
1/2"	12.5		0.0	100.0
3/8"	9.5		0.0	100.0
No. 4	4.75	6.9	3.96	96.04
No. 10	2.00	23.0	13.21	86.79
No. 40	0.425	72.3	41.51	58.49
No. 200	0.075	170.0	97.71	2.39

Total sample dry weight: 211.60 g			Borehole no. : SD# 4 (34-35)m	
Sieve no.	Size (mm)	Cumulative Weight Retained (g)	Cumulative % Retained	Cumulative % Passing
3/4"	19.0		0.0	100.0
1/2"	12.5		0.0	100.0
3/8"	9.5		0.0	100.0
No. 4	4.75	0.0	0.0	100.0
No. 10	2.00	1.3	0.61	99.39
No. 40	0.425	55.7	26.32	73.68
No. 200	0.075	204.7	96.74	3.26

Appendices

Appendix 1.2

Total sample dry weight: 240.30 g		Borehole no. : SD# 4 (39-40)m		
Sieve no.	Size (mm)	Cumulative Weight Retained (g)	Cumulative % Retained	Cumulative % Passing
3/4"	19.0		0.0	100.0
1/2"	12.5		0.0	100.0
3/8"	9.5		0.0	100.0
No. 4	4.75	0.0	0.0	100.0
No. 10	2.00	0.1	0.04	99.96
No. 40	0.425	66.4	27.63	72.37
No. 200	0.075	231.0	96.13	3.87

Total sample dry weight: 276.40 g		Borehole no. : SD# 4 (46-47)m		
Sieve no.	Size (mm)	Cumulative Weight Retained (g)	Cumulative % Retained	Cumulative % Passing
3/4"	19.0		0.0	100.0
1/2"	12.5		0.0	100.0
3/8"	9.5		0.0	100.0
No. 4	4.75	0.0	0.0	100.0
No. 10	2.00	0.1	0.04	99.96
No. 40	0.425	156.8	56.73	43.27
No. 200	0.075	275.7	99.75	0.25

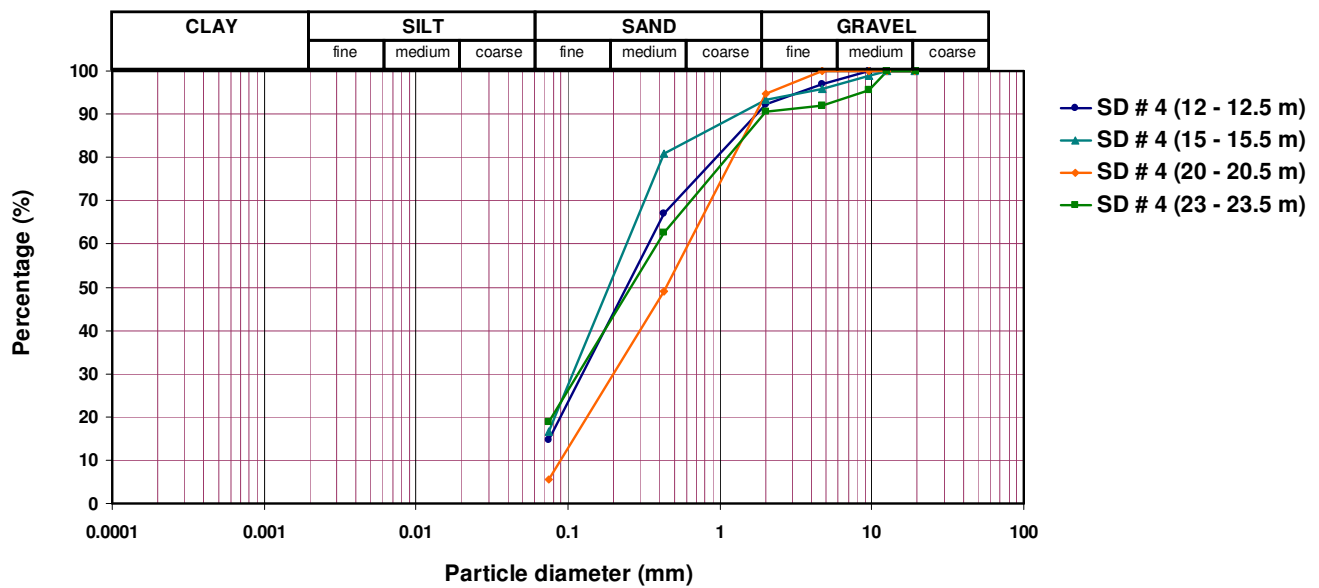
Total sample dry weight: 353.20 g		Borehole no. : SD# 4 (52-53)m		
Sieve no.	Size (mm)	Cumulative Weight Retained (g)	Cumulative % Retained	Cumulative % Passing
3/4"	19.0		0.0	100.0
1/2"	12.5		0.0	100.0
3/8"	9.5		0.0	100.0
No. 4	4.75	0.0	0.0	100.0
No. 10	2.00	0.0	0.0	100.0
No. 40	0.425	157.0	44.45	55.55
No. 200	0.075	348.7	98.73	1.27

Total sample dry weight: 268.10 g		Borehole no. : SD# 4 (56-57)m		
Sieve no.	Size (mm)	Cumulative Weight Retained (g)	Cumulative % Retained	Cumulative % Passing
3/4"	19.0		0.0	100.0
1/2"	12.5		0.0	100.0
3/8"	9.5		0.0	100.0
No. 4	4.75	0.0	0.0	100.0
No. 10	2.00	0.0	0.0	100.0
No. 40	0.425	5.1	1.90	98.10
No. 200	0.075	266.4	99.37	0.63

Appendices

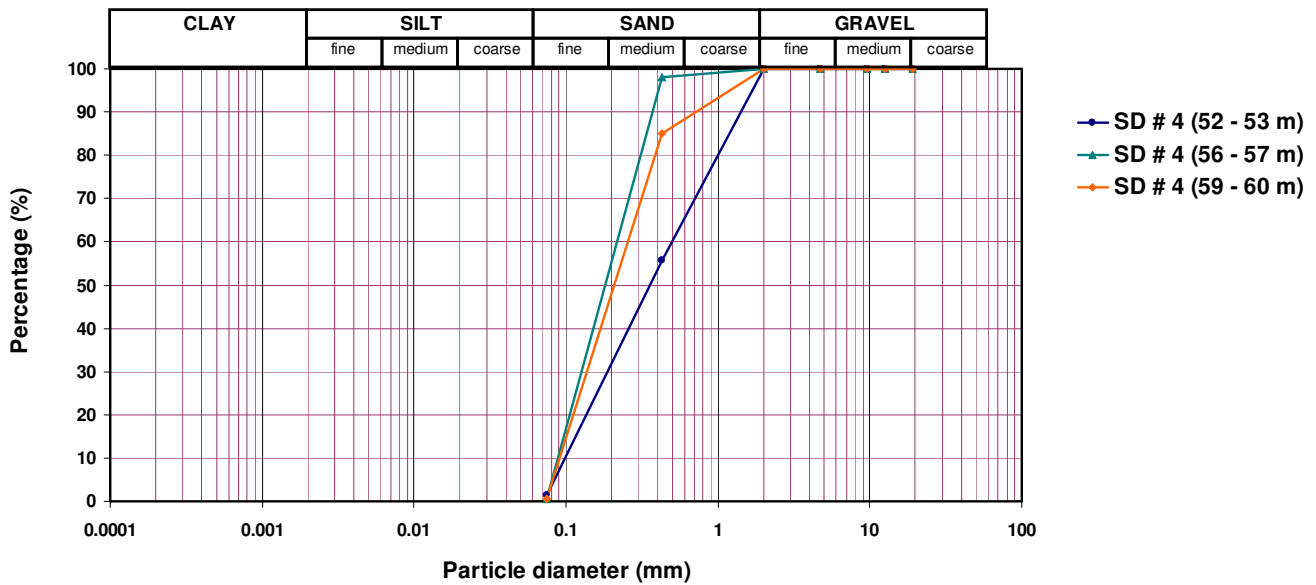
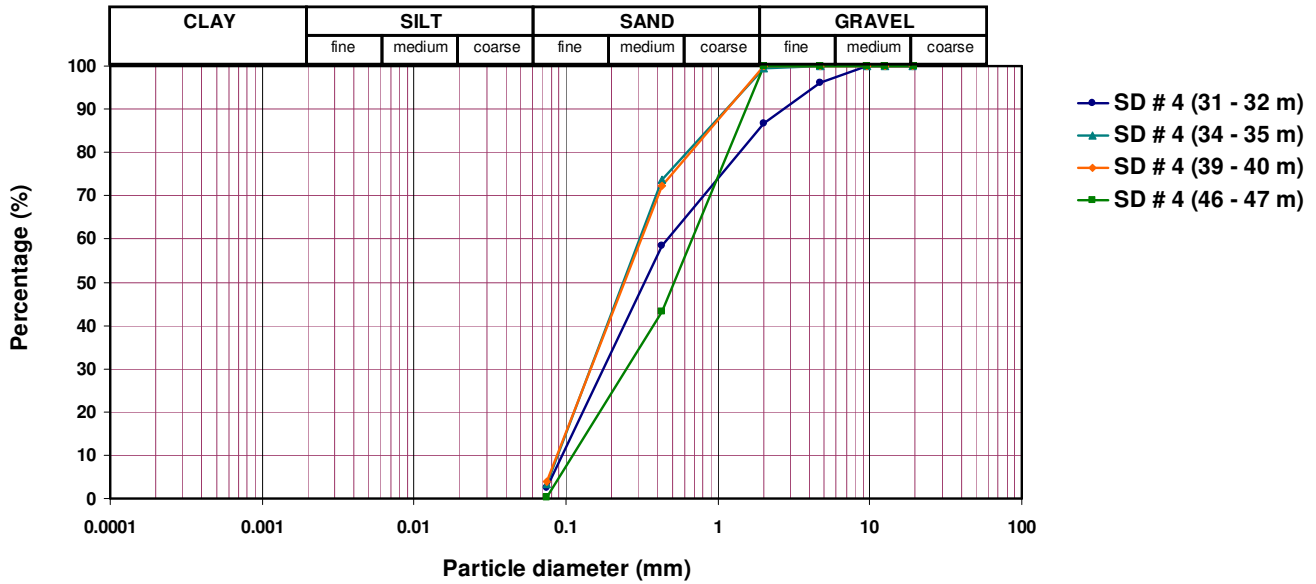
Appendix 1.2

Total sample dry weight: 275.80 g			Borehole no. : SD# 4 (59-60)m	
Sieve no.	Size (mm)	Cumulative Weight Retained (g)	Cumulative % Retained	Cumulative % Passing
3/4"	19.0		0.0	100.0
1/2"	12.5		0.0	100.0
3/8"	9.5		0.0	100.0
No. 4	4.75	0.0	0.0	100.0
No. 10	2.00	0.0	0.0	100.0
No. 40	0.425	41.4	15.01	84.99
No. 200	0.075	274.3	99.46	0.54



Appendices

Appendix 1.2



Appendices

Appendix 1.3

Summary of grain size distribution test results

Sample Depth (m)		Grain size distribution				Coefficient of Uniformity		
From	To	Gravel	Sand	Silt	Clay	D _{60%}	D _{10%}	Cu
		%	%	%	%	mm	mm	
Borehole # B1								
1.0	2.0	0.29	17.55	39.70	42.46			
5.0	6.0	0.00	5.91	94.09				
12.0	13.0	1.38	98.39	0.23		1.18	0.18	6.6
14.0	15.0	0.37	96.95	2.68		1.90	0.22	8.6
Borehole # B2								
2.0	2.5	0.48	13.14	41.20	45.18			
4.0	4.5	0.00	9.0	91.00				
5.0	6.0	0.00	9.6	90.41				
10.0	10.5	0.00	12.0	51.30	36.7			
14.0	14.5	1.70	48.06	50.24				
15.0	16.0	10.31	80.19	9.50		0.95	0.08	11.9
Borehole # B3								
2.0	3.0	0.00	7.12	49.98	42.90			
3.0	4.0	0.00	3.53	49.90	46.57			
9.0	10.0	0.60	57.03	42.37				
10.0	11.0	1.39	69.61	20.30	8.70			
13.0	14.0	3.98	93.03	2.99		0.39	0.12	3.3
Borehole # B4								
6.0	7.0	1.55	14.64	48.90	34.91			
14.0	14.5	0.00	88.71	11.29				
Borehole # B5								
5.0	5.5	2.81	13.32	83.87				
15.0	15.5	0.24	98.10	1.66		0.80	0.15	5.3
Borehole # B6								
3.2	3.5	5.48	68.97	25.55				
7.0	7.5	8.26	85.48	6.26		0.41	0.10	4.1
Borehole # B7								
2.0	2.5	0.00	33.12	66.88				
5.0	5.5	0.46	47.58	51.96				
8.0	8.5	4.75	89.99	5.26		0.41	0.11	3.7
Borehole # B8								
2.0	3.0	0.08	5.68	35.94	58.30			
4.0	4.5	0.00	4.25	95.75				
5.0	5.5	2.67	18.35	51.40	27.58			
6.5	7.5	0.28	26.29	73.43				
10.0	10.5	0.00	25.55	74.45				
13.0	13.5	4.25	61.39	34.36				

Appendices

Borehole # B9							
2.0	2.5	0.00	6.65	93.35			
3.0	4.0	0.00	8.36	46.80	44.84		
5.5	6.5	2.33	8.89	88.78			
7.5	8.0	0.00	18.92	81.08			
9.5	9.8	2.26	64.36	33.38			
Borehole # B10							
1.5	2.0	0.00	14.24	85.76			
3.0	4.0	0.00	14.23	45.97	39.80		
5.5	6.0	1.30	38.84	59.86			
11.5	12.0	0.15	85.61	14.24			
Borehole # B11							
1.5	1.8	0.00	51.30	48.70			
4.0	4.5	0.00	93.71	6.29	0.40	0.10	4.0
Borehole # SD1							
2.0	3.0	0.33	32.84	66.83			
4.0	4.5	23.39	44.32	32.29			
6.0	6.5	7.36	81.26	11.38			
8.0	9.0	1.92	90.96	7.12	0.40	0.08	5.0
10.0	10.5	17.07	73.88	9.05	0.50	0.10	5.3
11.0	12.0	8.41	87.70	3.89	0.40	0.12	3.3
14.0	14.5	12.16	83.54	4.30	0.40	0.11	3.6
16.5	17.0	13.11	77.99	8.90	0.50	0.09	5.5
20.0	20.5	29.93	64.21	5.86	1.10	0.11	10.0
26.0	27.0	16.33	80.69	2.98	1.70	0.15	11.3
30.0	31.0	19.55	77.30	3.15	2.10	0.16	13.1
35.0	36.0	0.88	82.61	16.51			
37.0	38.0	1.74	90.17	8.09	1.30	0.10	13.0
44.0	45.0	11.85	83.71	4.44	0.40	0.11	3.6
49.0	50.0	0.00	94.29	5.71	0.30	0.09	3.3
56.0	57.0	0.29	97.87	1.84	0.31	0.11	2.8
63.0	64.0	0.00	98.57	1.43	0.31	0.11	2.8
Borehole # SD2							
3.0	3.5	0.00	9.32	41.80	48.88		
5.0	5.5	0.00	22.15	77.85			
7.0	7.5	7.34	79.35	13.31			
12.0	12.5	1.20	92.57	6.23	0.31	0.09	3.4
14.0	15.0	0.69	96.63	2.68	0.40	0.12	3.3
17.0	18.0	0.12	95.91	3.97	0.39	0.10	3.9
19.0	20.0	0.00	98.10	1.90	0.38	0.12	3.2
22.0	23.0	0.00	68.09	31.91			
24.0	25.0	0.84	92.64	6.52	0.39	0.10	3.9
29.0	30.0	1.79	95.88	2.33	1.80	0.21	8.6
34.0	35.0	1.36	98.43	0.21	0.40	0.14	2.9
40.0	41.0	0.00	99.07	0.93			
45.0	46.0	0.00	99.18	0.82			
51.0	52.0	2.96	96.64	0.40			
55.0	56.0	0.00	99.61	0.39	0.39	0.13	3.0
60.0	61.0	0.00	99.76	0.24	0.39	0.13	3.0

Appendices

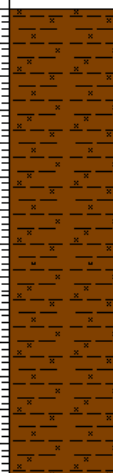
62.0	63.0	0.97	98.49	0.54	0.39	0.13	3.0
Borehole # SD3							
2.0	3.0	1.56	26.20	72.24			
4.0	4.5	0.00	4.82	95.18			
6.5	7.5	0.97	68.71	30.32			
9.0	9.5	12.23	77.82	9.95			
12.0	12.5	39.26	51.44	9.30			
15.0	15.5	7.13	62.44	30.43			
17.0	18.0	0.00	98.30	1.70	0.35	0.13	2.3
20.0	21.0	0.00	99.20	0.80	0.95	0.18	5.3
25.0	26.0	0.00	99.20	0.80	0.32	0.12	2.7
27.0	28.0	0.00	99.00	1.00	0.32	0.12	2.7
33.0	34.0	0.00	99.06	0.94	0.40	0.14	2.9
39.0	40.0	0.00	99.49	0.51	1.20	0.25	4.8
47.0	48.0	0.00	99.78	0.22	0.88	0.17	5.2
54.0	55.0	0.00	99.47	0.53	0.30	0.11	2.7
59.0	60.0	0.00	99.68	0.32	0.30	0.11	2.7
62.0	63.0	0.00	99.43	0.57	0.30	0.11	2.7
Borehole # SD4							
1.2	2.0	0.00	13.60	86.40			
3.0	4.0	0.50	16.97	82.53			
4.5	5.0	0.00	16.25	83.75			
6.0	7.0	0.00	6.21	93.79			
7.5	8.0	0.28	39.85	59.87			
12.0	12.5	3.17	82.25	14.58			
15.0	15.5	4.25	79.17	16.58			
20.0	20.5	0.06	94.49	5.45	0.80	0.11	7.3
23.0	23.5	8.12	73.06	18.82			
31.0	32.0	3.96	93.75	2.39	0.50	0.13	3.9
34.0	35.0	0.00	96.74	3.26	0.38	0.11	3.5
39.0	40.0	0.00	96.13	3.87	0.38	0.11	3.5
46.0	47.0	0.00	99.75	0.25	0.90	0.16	5.6
52.0	53.0	0.00	98.73	1.27	0.60	0.14	4.3
56.0	57.0	0.00	99.37	0.63	0.29	0.11	2.6
59.0	60.0	0.00	99.46	0.54	0.31	0.12	2.6

Appendix 1.4

Log of Borehole: B1

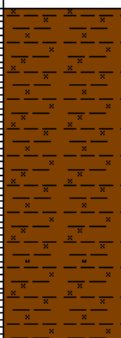
Depth(m)	Litholog. Symbol	Lithologic Description
0.0		Ground Surface
1.0		Silty Clay Brownish, slightly moist to moist, very stiff to hard slightly sandy and silty clay.
2.0		
3.0		
4.0		
5.0		
6.0		
7.0		
8.0		
9.0		
10.0		
11.0		Kurkar (sand and gravel) Yellowish, medium dense, fine to medium, uniform, dry sand with fine to medium gravels of sandstone.
12.0		
13.0		
14.0		
15.0		
16.0		End of Borehole
17.0		
18.0		
19.0		

Log of Borehole: B2

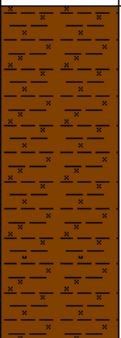
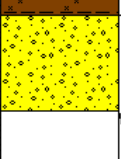
Depth(m)	Litholog. Symbol	Lithologic Description
0.0		Ground Surface
1.0		Silty Clay Brownish, slightly moist to moist, very stiff to hard slightly sandy and silty clay.
2.0		
3.0		
4.0		
5.0		
6.0		
7.0		
8.0		
9.0		
10.0		
11.0		
12.0		
13.0		
14.0		
15.0		Kurkar (sand and gravel) Yellowish, medium dense, fine to medium, uniform, dry sand with fine to medium gravels of sandstone.
16.0		
17.0		
18.0		
19.0		

Appendix 1.4

Log of Borehole: B3

Depth(m)	Litholog. Symbol	Lithologic Description
0.0		Ground Surface
1.0		<p><i>Silty Clay</i> Brownish, slightly moist to moist, very stiff to hard slightly sandy and silty clay.</p>
2.0		
3.0		
4.0		
5.0		
6.0		
7.0		
8.0		
9.0		
10.0		
11.0		<p><i>Kurkar (sand and gravel)</i> Yellowish, medium dense, fine to medium, uniform, dry sand with fine to medium gravels of sandstone.</p>
12.0		
13.0		
14.0		
15.0		End of Borehole
16.0		
17.0		
18.0		
19.0		

Log of Borehole: B4

Depth(m)	Litholog. Symbol	Lithologic Description
0.0		Ground Surface
1.0		<p><i>Silty Clay</i> Brownish, slightly moist to moist, very stiff to hard slightly sandy and silty clay.</p>
2.0		
3.0		
4.0		
5.0		
6.0		
7.0		
8.0		
9.0		
10.0		
11.0		<p><i>Kurkar (sand and gravel)</i> Yellowish, medium dense, fine to medium, uniform, dry sand with fine to medium gravels of sandstone.</p>
12.0		
13.0		
14.0		
15.0		End of Borehole
16.0		
17.0		
18.0		
19.0		

Appendix 1.4

Log of Borehole: B5

Depth(m)	Litholog-Symbol	Lithologic Description
0.0		Ground Surface
1.0		<p>Silty Clay Brownish, slightly moist to moist, very stiff to hard slightly sandy and silty clay.</p>
2.0		
3.0		
4.0		
5.0		
6.0		
7.0		
8.0		
9.0		
10.0		
11.0		
12.0		
13.0		
14.0		<p>Kurkar (sand and gravel) Yellowish, medium dense, fine to medium, uniform, dry sand with fine to medium gravels of sandstone.</p>
15.0		
16.0		
17.0		
18.0		End of Borehole
19.0		

Log of Borehole: B6

Depth(m)	Litholog-Symbol	Lithologic Description
0.0		Ground Surface
1.0		<p>Silty Clay Brownish, slightly moist to moist, very stiff to hard slightly sandy and silty clay.</p>
2.0		
3.0		
4.0		<p>Kurkar (sand and gravel) Yellowish, medium dense, fine to medium, uniform, dry sand with fine to medium gravels of sandstone.</p>
5.0		
6.0		
7.0		
8.0		End of Borehole
9.0		
10.0		
11.0		
12.0		
13.0		
14.0		
15.0		
16.0		
17.0		
18.0		
19.0		

Appendix 1.4

Log of Borehole: B7

Depth(m)	Litholog-Symbol	Lithologic Description
0.0		Ground Surface
1.0		Silty Clay Brownish, slightly moist to moist, very stiff to hard slightly sandy and silty clay.
2.0		
3.0		
4.0		
5.0		
6.0		Kurkar (Sand and gravel) Yellowish, medium dense, fine to medium, uniform, dry sand with fine to medium gravels of sandstone.
7.0		
8.0		
9.0		
10.0		
11.0		End of Borehole
12.0		
13.0		
14.0		
15.0		
16.0		
17.0		
18.0		
19.0		

Log of Borehole: B8

Depth(m)	Litholog-Symbol	Lithologic Description
0.0		Ground Surface
1.0		Silty Clay Brownish, slightly moist to moist, very stiff to hard slightly sandy and silty clay.
2.0		
3.0		
4.0		
5.0		
6.0		
7.0		
8.0		
9.0		
10.0		
11.0		
12.0		Kurkar (sand and gravel) Yellowish, medium dense, fine to medium, uniform, dry sand with fine to medium gravels of sandstone.
13.0		
14.0		
15.0		
16.0		
17.0		
18.0		End of Borehole
19.0		

Appendix 1.4

Log of Borehole: B9

Depth(m)	Litholog-Symbol	Lithologic Description
0.0		Ground Surface
1.0		Silty Clay Brownish, slightly moist to moist, very stiff to hard slightly sandy and silty clay.
2.0		
3.0		
4.0		
5.0		
6.0		
7.0		
8.0		
9.0		
10.0		Kurkar (sand and gravel) Yellowish, medium dense, fine to medium, uniform, dry sand with fine to medium gravels of sandstone.
11.0		
12.0		
13.0		
14.0		End of Borehole
15.0		
16.0		
17.0		
18.0		
19.0		

Log of Borehole: B10

Depth(m)	Litholog-Symbol	Lithologic Description
0.0		Ground Surface
1.0		Silty Clay Brownish, slightly moist to moist, very stiff slightly sandy and slitty clay.
2.0		
3.0		
4.0		
5.0		
6.0		
7.0		Kurkar (sand and gravel) Yellowish, medium dense, fine to medium, uniform, dry sand with fine to medium gravels of sandstone.
8.0		
9.0		
10.0		
11.0		End of Borehole
12.0		
13.0		
14.0		
15.0		
16.0		
17.0		
18.0		
19.0		

Appendix 1.4

Log of Borehole: B11

Depth(m)	Litholog. Symbol	Lithologic Description
0.0		Ground Surface
1.0		<i>silty clay</i> Brownish, slightly moist to moist, very stiff to hard sandy and silty clay.
2.0		
3.0		
4.0		
5.0		<i>Kurkar (sand and gravel)</i> Yellowish, medium dense, fine to medium, uniform, dry sand with fine to medium gravels of sandstone.
6.0		
7.0		
8.0		
9.0		End of Borehole
10.0		
11.0		
12.0		
13.0		
14.0		
15.0		
16.0		
17.0		
18.0		
19.0		

Log of Borehole: CD1

Depth(m)	Litholog. Symbol	Lithologic Description
0.0		Ground Surface
1.0		<i>Silty Clay</i> Brownish, slightly moist to moist, very stiff to hard slightly sandy and silty clay.
2.0		
3.0		
4.0		
5.0		<i>Kurkar (sand and gravel)</i> Yellowish, medium dense, fine to medium, uniform, dry sand with fine to medium gravels of sandstone.
6.0		
7.0		
8.0		
9.0		End of Borehole
10.0		
11.0		
12.0		
13.0		
14.0		
15.0		
16.0		
17.0		
18.0		
19.0		

Appendix 1.4

Log of Borehole: CD2

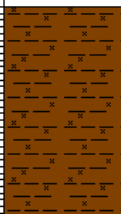
Depth(m)	Litholog-Symbol	Lithologic Description
0.0		Ground Surface
1.0		Silty Clay Brownish, slightly moist to moist, very stiff to hard slightly sandy and silty clay.
2.0		
3.0		
4.0		
5.0		
6.0		
7.0		
8.0		
9.0		
10.0		
11.0		
12.0		Kurkar (sand and gravel) Yellowish, medium dense, fine to medium, uniform, dry sand with fine to medium gravels of sandstone.
13.0		
14.0		
15.0		
16.0		
17.0		End of Borehole
18.0		
19.0		

Log of Borehole: CD3

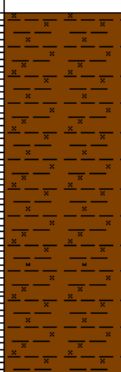
Depth(m)	Litholog-Symbol	Lithologic Description
0.0		Ground Surface
1.0		Silty clay Brownish, slightly moist to moist, very stiff to hard slightly sandy and silty clay.
2.0		
3.0		
4.0		
5.0		
6.0		
7.0		Kurkar (sand and gravel) Yellowish, medium dense, fine to medium, uniform, dry sand with fine to medium gravels of sandstone.
8.0		
9.0		
10.0		
11.0		End of Borehole
12.0		
13.0		
14.0		
15.0		
16.0		
17.0		
18.0		
19.0		

Appendix 1.4

Log of Borehole: CD4

Depth(m)	Litholog-Symbol	Lithologic Description
0.0		Ground Surface
1.0		Silty Clay Brownish, slightly moist to moist, very stiff to hard slightly sandy and silty clay.
2.0		
3.0		
4.0		
5.0		
6.0		
7.0		Kurkar (sand and gravel) Yellowish, medium dense, fine to medium, uniform, dry sand with fine to medium gravels of sandstone.
8.0		
9.0		End of Borehole
10.0		
11.0		
12.0		
13.0		
14.0		
15.0		
16.0		
17.0		
18.0		
19.0		

Log of Borehole: CD5

Depth(m)	Litholog-Symbol	Lithologic Description
0.0		Ground Surface
1.0		Silty Clay Brownish, slightly moist to moist, very stiff to hard slightly sandy and silty clay.
2.0		
3.0		
4.0		
5.0		
6.0		
7.0		
8.0		
9.0		
10.0		
11.0		Kurkar (sand and gravel) Yellowish, medium dense, fine to medium, uniform, dry sand with fine to medium gravels of sandstone.
12.0		
13.0		End of Borehole
14.0		
15.0		
16.0		
17.0		
18.0		
19.0		

Appendix 1.4

Log of Borehole: CD6

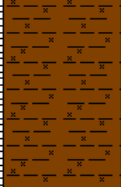
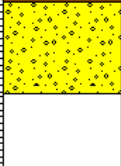
Depth(m)	Litholog. Symbol	Lithologic Description
0.0		Ground Surface
1.0		Silty Clay Brownish, slightly moist to moist, very stiff to hard slightly sandy and silty clay.
2.0		
3.0		
4.0		
5.0		Kurkar (sand and gravel) Yellowish, medium dense, fine to medium, uniform, dry sand with fine to medium gravels of sandstone.
6.0		
7.0		
8.0		
9.0		
10.0		End of Borehole
11.0		
12.0		
13.0		
14.0		
15.0		
16.0		
17.0		
18.0		
19.0		

Log of Borehole: CD7

Depth(m)	Litholog. Symbol	Lithologic Description
0.0		Ground Surface
1.0		Silty Clay Brownish, slightly moist to moist, very stiff to hard slightly sandy and silty clay.
2.0		
3.0		
4.0		
5.0		
6.0		
7.0		
8.0		
9.0		Kurkar (sand and gravel) Yellowish, medium dense, fine to medium, uniform, dry sand with fine to medium gravels of sandstone.
10.0		
11.0		
12.0		
13.0		
14.0		
15.0		
16.0		
17.0		
18.0		
19.0		

Appendix 1.4

Log of Borehole: CD8

Depth(m)	Litholog. Symbol	Lithologic Description
0.0		Ground Surface
1.0 2.0 3.0 4.0 5.0		Silty clay Brownish, slightly moist to moist, very stiff to hard slightly sandy and silty clay.
6.0 7.0 8.0 9.0		Kurkar (sand and gravel) Yellowish, medium dense, fine to medium, uniform, dry sand with fine to medium gravels of sandstone.
10.0 11.0 12.0 13.0 14.0 15.0 16.0 17.0 18.0 19.0		End of Borehole

Appendix 1.4

Log of Borehole: SB1

Depth(m)	Litholog Symbol	Lithologic Description
0		Ground Surface
0 - 5		Silty Clay Brownish, very stiff to hard, dry to moist silty clay.
5 - 20		Kurkar Yellowish, dense to very dense, fine to medium, uniform sand with fine to medium gravels of sandstone.
20 - 25		Silty Sand Brownish silty and slightly clayey fine sand with very low plasticity.
25 - 60		Kurkar Yellowish, dense to very dense, fine to medium, uniform sand with fine to medium gravels of sandstone.
60 - 70		Sand Yellowish, dense to very dense, fine to medium uniform sand
70 - 75		End of Borehole

Appendix 1.4

Log of Borehole: SD1

Depth(m)	Litholog Symbol	Lithologic Description
0		Ground Surface
0 - 5		Silty Clay Brownish, slightly moist to moist, very stiff slightly sandy and silty clay.
5 - 18		Kurkar (sand and gravel) Yellowish, dense to very dense, fine to medium, uniform sand with fine to medium gravels of sandstone.
18 - 20		Silty Sand Brownish, uniform silty fine sand
20 - 60		Kurkar
60 - 73		Sand Yellowish, dense to very dense, fine to medium, uniform sand
73 - 75		End of Borehole

Appendix 1.4

Log of Borehole: SD2

Depth(m)	Litholog Symbol	Lithologic Description
0		Ground Surface
0 - 5		Silty Clay Brownish, slightly moist to moist, very stiff to hard slightly sandy and silty clay.
5 - 23		Kurkar Yellowish, dense to very dense, fine to medium, uniform sand with fine to medium gravels of sandstone.
23 - 25		Silty Sand Brownish, uniform silty fine sand.
25 - 45		Kurkar Yellowish, dense to very dense, fine to medium, uniform sand with fine to medium gravels of sandstone.
45 - 67		Sand Yellowish, dense, fine to medium, uniform sand
67 - 70		Kurkar
70 - 75		End of Borehole

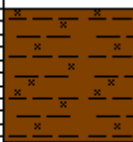
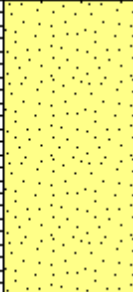
Appendix 1.4

Log of Borehole: SD3

Depth(m)	Litholog Symbol	Lithologic Description
0		Ground Surface
0 - 5		Silty Clay Brownish, slightly moist to moist, very stiff slightly sand and silty clay.
5 - 22		Kurkar Yellowish, medium dense to very dense, fine to medium, uniform sand with fine to medium gravels of sandstone.
22 - 25		Silty Sand Brownish uniform silty fine to medium sand.
25 - 50		Kurkar Yellowish, dense to very dense, fine to medium, uniform sand with fine to medium gravels of sandstone.
50 - 65		Sand Yellowish, medium dense to dense fine to medium, uniform sand.
65 - 75		End of Borehole

Appendix 1.4

Log of Borehole: SD4

Depth(m)	Litho log Symbol	Lithologic Description
0		Ground Surface
0 5 10		Silty Clay Brownish, slightly moist to moist, very stiff to hard slightly sandy and silty clay.
10 15 20 25 30 35 40		Kurkar Yellowish, dense to very dense, fine to medium, uniform sand with fine to medium gravels of sandstone.
45 50 55 60 65		Sand Yellowish, very dense, fine to medium sand
70 75		End of Borehole

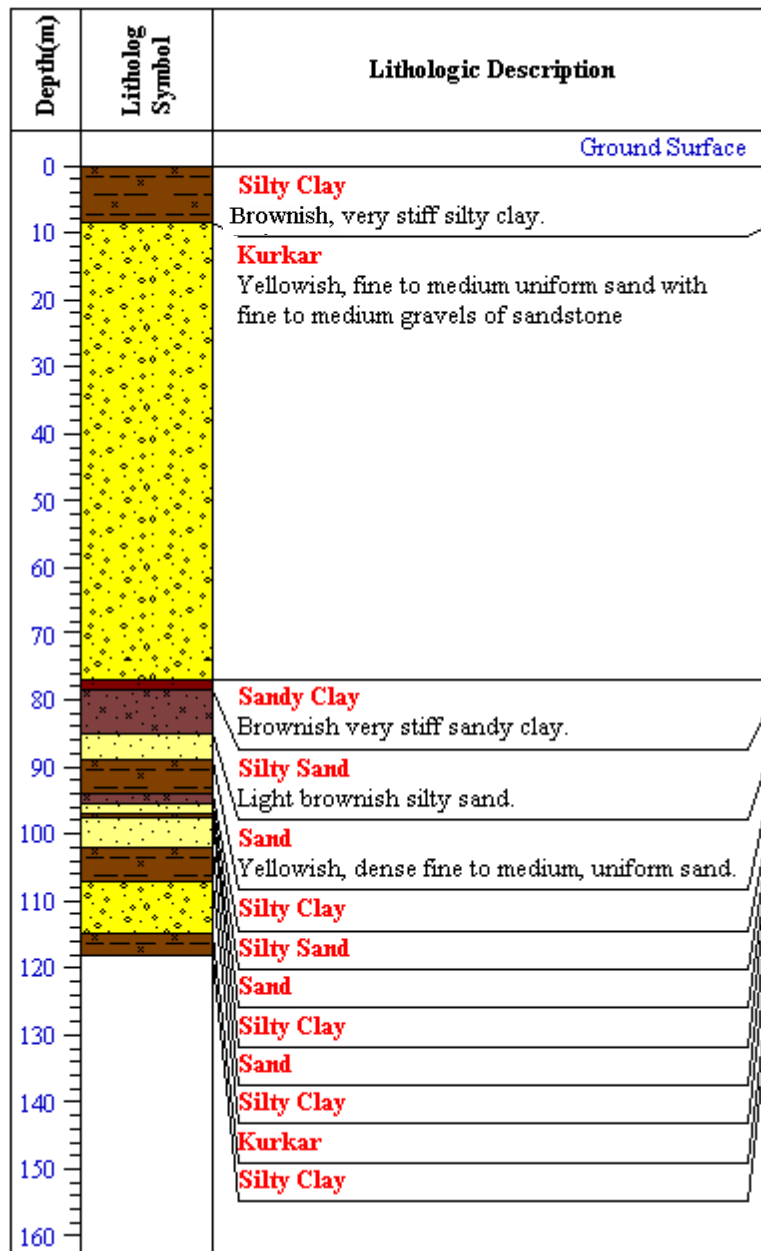
Appendix 1.4

Log of Borehole: DB1

Depth(m)	Litholog Symbol	Lithologic Description
0		Ground Surface
0 - 10		Silty Clay Brownish, very stiff silty clay
10 - 35		Kurkar Yellowish, very dense, fine to medium uniform sand with fine to medium gravels of sandstone
35 - 38		Silty Sand Brownish fine to medium very dense silty sand
38 - 42		Sandy Clay Brownish very stiff sandy clay
42 - 50		Kurkar
50 - 60		Sand Yellowish, fine to medium sand
60 - 100		Kurkar Yellowish, very dense sand with coarse gravel
100 - 120		

Appendix 1.4

Log of Borehole: DB2



Log of Borehole: DB3

Depth(m)	Litholog Symbol	Lithologic Description
0		Ground Surface
0 - 10		Silty Clay Brownish, very stiff silty clay
10 - 20		Kurkar Yellowish, fine to medium uniform sand with fine to medium gravels of sandstone
20 - 25		Silty Clay
25 - 60		Kurkar
60 - 70		Sand Yellowish, fine to medium sand
70 - 90		Kurkar
90 - 100		Sand Yellowish fine sand
100 - 105		Silty Clay
105 - 110		kurkar
110 - 120		Silty Clay

Appendix 1.4

Log of Borehole: DB4

Depth(m)	Litholog Symbol	Lithologic Description
0		Ground Surface
0 - 10		Silty Clay Brownish, very stiff silty clay
10 - 30		Kurkar Yellowish, fine to medium uniform sand with fine to medium gravels of sandstone
30 - 40		Sandy Clay Brownish, sandy clay
40 - 50		Kurkar
50 - 60		Sand Yellowish, fine to medium sand
60 - 90		Kurkar
90 - 100		Sand
100 - 110		Silty Clay
110 - 120		Kurkar
120 - 130		Kurkar
130 - 140		Silty Sand
140 - 150		Silty Clay
150 - 160		Shale
160 - 170		Marly Clay

Appendices

Appendix 1.5

Packer test data reduction

BH	Test range (m)	Test length L (m)	Borehole radius r (m)	Total head H_T (m)	Discharge Q (m ³ /min)	Hydraulic conductivity K (m/d)
B1	13.0 - 13.5	0.5	0.051	12.54	0.467	39.0
B2	11.0 - 12.0	1.0	0.051	21.33	0.0084	0.27
B3	6.2 - 7.2	1.0	0.051	19.67	0.0012	0.04
B3	11.8 - 12.3	0.5	0.051	20.90	0.1318	6.6
B5	8.5 - 9.5	1.0	0.051	15.68	0.01976	0.86
B5	14.5 - 15.0	0.5	0.051	21.38	0.194	9.5
B7	7.5 - 8.0	0.5	0.051	11.40	0.2292	21.0
B10	10.5 - 11.0	0.5	0.051	17.58	0.0234	1.4
SD1	13.5 - 14.0	0.5	0.051	19.95	0.0306	1.6
SD4	7.5 - 8.5	1.0	0.051	20.52	0.0009	0.03
SD4	13.0 - 13.5	0.5	0.051	20.43	0.0352	1.8

Appendices

Appendix 1.6

Infiltration Rate
(1m constant head)

Interval time (min)	PIT# 1	PIT# 2	PIT# 3	PIT# 4	PIT# 5
	H (mm)				
0	1000	1000	1000	1000	1000
5	900	935	950	900	930
10	800	875	825	820	870
15	710	840	710	760	810
20	620	800	630	700	760
25	542	755	560	650	705
30	472	710	465	595	650
35	396	675	410	540	600
40	333	630	350	490	530
45	270	590	290	440	470
50	208	550	230	400	420
55	155	510	190	355	380
60	100	470	120	315	330
65	50	431	70	270	300
70	End of test	402	23	235	260
75		375	End of test	215	230
80		334		185	205
85		302		153	175
90		270		130	140
95		239		End of test	95
100		208			45
105		174	10		
			End of test		End of test

Appendix 1.7

Pumping Well: DB4

Total depth: 156.0 m

Screen radius: 0.127 m

Screen Length: 37 m

Screen depth: 74 - 89 m and 113 – 135 m

Gravel pack radius: 0.178 m

Depth to static WL: 59.88 m

Time t (min)	Depth to WL m	Drawdown s (m)	t/r^2 min/m²	t' min	t/t'
0	59.88	0.00	0.00		
6	65.49	5.61	62.43		
8	65.68	5.80	83.25		
10	65.75	5.87	104.06		
15	65.81	5.93	156.09		
30	65.83	5.95	312.17		
240	65.86	5.98	2497.40		
360	65.98	6.10	3746.10		
480	65.98	6.10	4994.80		
720	66.20	6.32	7492.20		
1620	67.39	7.51	16857.44		
1830	67.40	7.52	19042.66		
1890	67.45	7.57	19667.01		
1950	67.48	7.60	20291.36		
1980	67.51	7.63	20603.54		
2160	67.55	7.67	22476.59		
2220	67.60	7.72	23100.94		
2490	67.65	7.77	25910.51		
2700	67.66	7.78	28095.73		
2805	67.67	7.79	29188.35		
3015	67.68	7.80	31373.57		
3360	67.69	7.81	34963.58		
4365	67.70	7.82	45421.44		
4380	67.70	7.82	45577.52		
4390	67.70	7.82	45681.58		
4700	65.85	5.97	48907.39	310	15.16
4760	65.25	5.37	49531.74	370	12.86
4820	64.75	4.87	50156.09	430	11.21
5710	62.15	2.27	59417.27	1320	4.33
8643	59.92	0.04	89937.57	4253	2.03

Appendix 1.7

Observation Well: DB1

Total depth: 100.0 m

Screen radius: 0.051 m

Screen Length: 25 m

Screen depth: 75 – 100 m

Gravel pack radius: 0.127 m

Depth to static WL: 55.75 m

Distance from pumping well: 127.44 m

Time t (min)	Depth to WL m	Drawdown s (m)	t/r^2 min/m²	t' min	t/t'
0	55.75	0.00	0.0000		
1440	55.87	0.12	0.0887		
1725	55.88	0.13	0.1062		
1825	55.90	0.15	0.1124		
2795	55.92	0.17	0.1721		
2910	55.94	0.19	0.1792		
3085	55.96	0.21	0.1900		
3350	55.98	0.23	0.2063		
4360	56.00	0.25	0.2685		
4390	56.00	0.25	0.2703		
5705	55.92	0.17	0.3513	1315	4.34
5885	55.89	0.14	0.3624	1495	3.94
7337	55.82	0.07	0.4518	2947	2.49
8643	55.79	0.04	0.5322	4253	2.03
9363	55.77	0.02	0.5765	4973	1.88

Appendix 1.7

Observation well: DB2

Total depth: 118.0 m

Screen radius: 0.051 m

Screen Length: 30 m

Screen depth: 85 – 115 m

Gravel pack radius: 0.127 m

Depth to static WL: 59.95 m

Distance from pumping well: 144.06 m

Time t (min)	Depth to WL m	Drawdown s (m)	t/r^2 min/m²	t' min	t/t'
0	59.95	0.00	0.0000		
355	59.96	0.01	0.0171		
480	59.97	0.02	0.0231		
540	59.98	0.03	0.0260		
1440	60.03	0.08	0.0694		
1825	60.04	0.09	0.0879		
1885	60.05	0.10	0.0908		
2910	60.08	0.13	0.1402		
3270	60.09	0.14	0.1576		
3330	60.10	0.15	0.1605		
4390	60.15	0.20	0.2115		
5860	60.08	0.13	0.2824	1470	3.99
6308	60.05	0.10	0.3040	1918	3.29
7317	60.03	0.08	0.3526	2927	2.50
8635	60.00	0.05	0.4161	4245	2.03
9354	59.98	0.03	0.4507	4964	1.88

Appendix 1.7

Observation Well: SD2

Total depth: 70.0 m

Screen radius: 0.051 m

Screen Length: 5 m

Screen depth: 65 – 70 m

Gravel pack radius: 0.076 m

Depth to static WL: 58.54 m

Distance from pumping well: 92.06 m

Time t (min)	Depth to WL m	Drawdown s (m)	t/r^2 min/m ²	t' min	t/t'
0	58.54	0.00	0.0000		
355	58.58	0.04	0.0419		
420	58.59	0.05	0.0496		
480	58.60	0.06	0.0566		
540	58.60	0.06	0.0637		
1440	58.70	0.16	0.1699		
1620	58.71	0.17	0.1911		
1735	58.72	0.18	0.2047		
1770	58.72	0.18	0.2088		
1830	58.73	0.19	0.2159		
1885	58.73	0.19	0.2224		
1945	58.74	0.20	0.2295		
2790	58.81	0.27	0.3292		
3090	58.82	0.28	0.3646		
3340	58.83	0.29	0.3941		
4390	58.83	0.29	0.5180		
5840	58.78	0.24	0.6891	1450	4.03
6308	58.75	0.21	0.7443	1918	3.29
7317	58.70	0.16	0.8634	2927	2.50
7740	58.66	0.12	0.9133	3350	2.31
8620	58.63	0.09	1.0171	4230	2.04

Appendix 1.7

Observation Well SD4

Total depth: 66.0 m
 Screen radius: 0.025 m
 Screen length: 5 m
 Screen depth: 61 – 66 m
 Gravel pack radius: 0.051 m
 Depth to static WL: 61.02 m
 Distance from pumping well: 106.69 m

Time t	Depth to WL m	Drawdown s (m)	t/r^2 min/m²	t' min	t/t'
0	61.02	0.00	0.0000		
240	61.03	0.01	0.0211		
360	61.04	0.02	0.0316		
420	61.05	0.03	0.0369		
480	61.06	0.04	0.0422		
540	61.07	0.05	0.0474		
1440	61.14	0.12	0.1265		
1950	61.15	0.13	0.1713		
2780	61.20	0.18	0.2442		
3270	61.21	0.19	0.2873		
3550	61.22	0.20	0.3119		
3610	61.23	0.21	0.3171		
3850	61.24	0.22	0.3382		
4390	61.25	0.23	0.3857		
4795	61.22	0.20	0.4213	405	11.84
4855	61.20	0.18	0.4265	465	10.44
4915	61.19	0.17	0.4318	525	9.36
4975	61.18	0.16	0.4371	585	8.50
5380	61.12	0.10	0.4726	990	5.43
7000	61.03	0.01	0.6150	2610	2.68

Appendix 1.7

Theis Recovery Test

When the pump is shut down after a pumping test, the water levels inside the pumping and observation wells will start to rise. This rise in water level is known as residual drawdown (s'). Recovery- test measurements allow the transmissivity of the aquifer to be calculated, thereby providing an independent check on the results of the pumping test.

Residual drawdown data can be more reliable than drawdown data because the recovery occurs at a constant rate whereas constant discharge pumping is often difficult to achieve in the field. Residual drawdown data can be collected from both the pumping and observation wells.

According to Thies (1935), the residual drawdown, after pumping has ceased, is

$$s' = \frac{Q}{4\pi T} [W(u) - W(u')]$$

where:

$$u = \frac{r^2 S}{4Tt} \qquad u' = \frac{r^2 S'}{4Tt'}$$

s' = residual drawdown (m)

r = distance from well to piezometer (m)

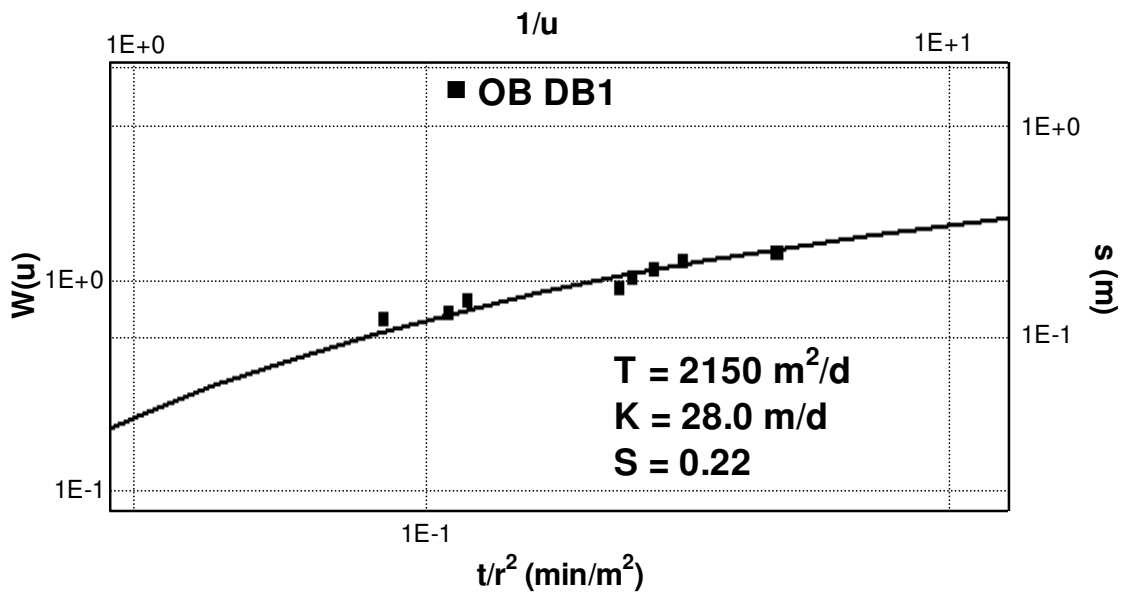
T = transmissivity of the aquifer (m^2/d)

S and S' = storativity values during pumping and recovery respectively.

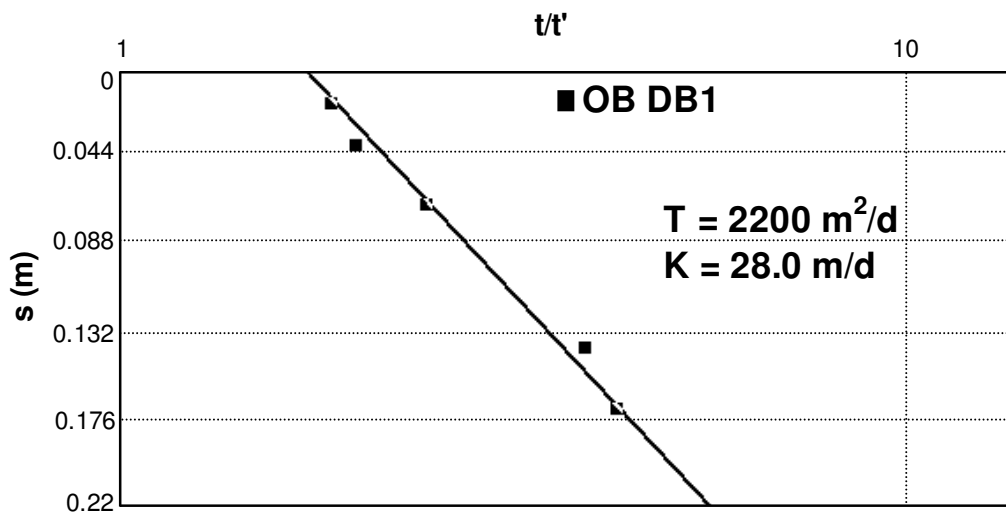
Appendices

T and t' = elapsed times (d) from the start and ending of pumping respectively.

To analyze the data, s' is plotted on logarithmic Y axis and time is plotted on the linear X axis as the ratio of t/t' total time since pumping began divided by the time since the pumping ceased.

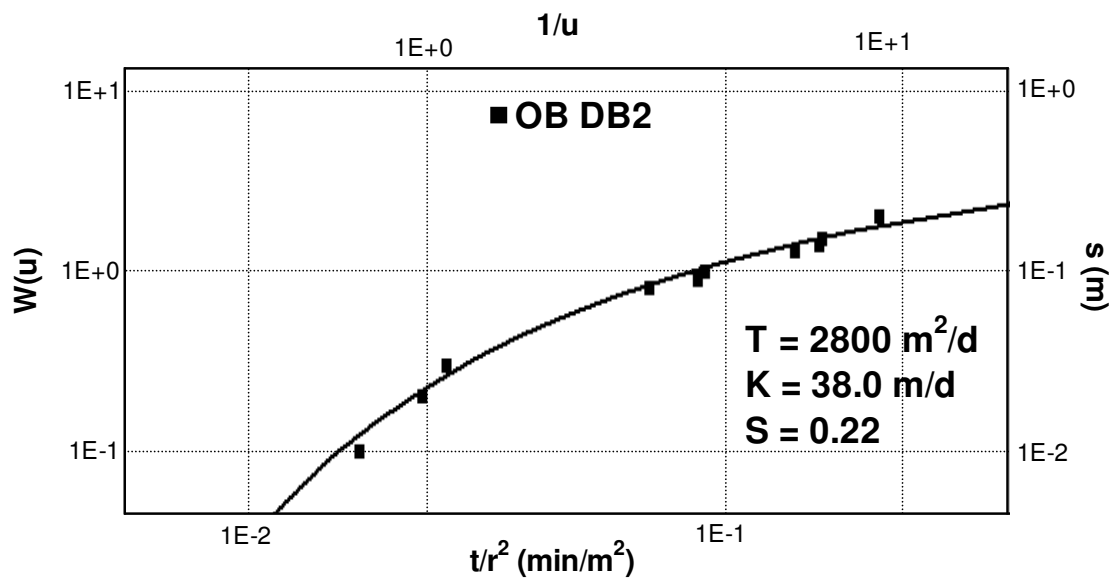


Results of the pumping test analysis by means of a Theis-curve fit

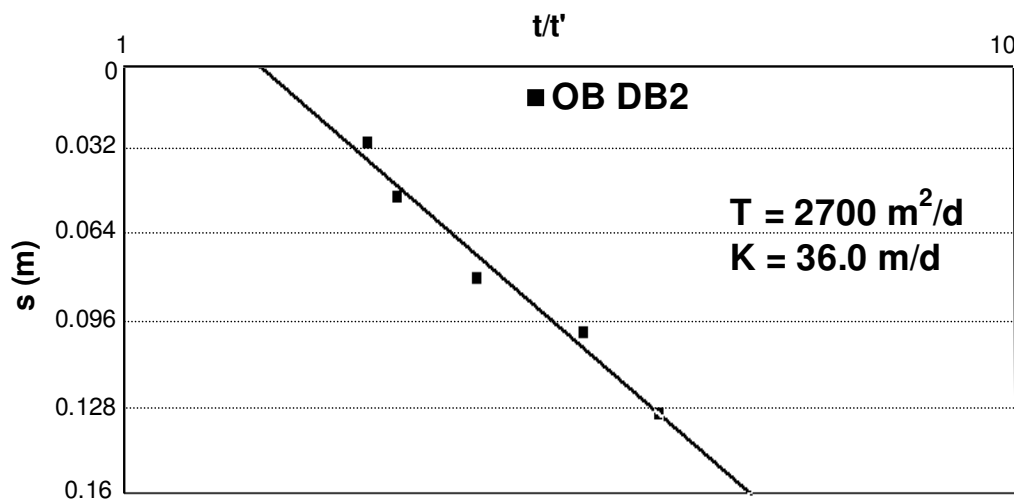


Results of the pumping test analysis by means of a Theis-recovery test

Appendix 1.7

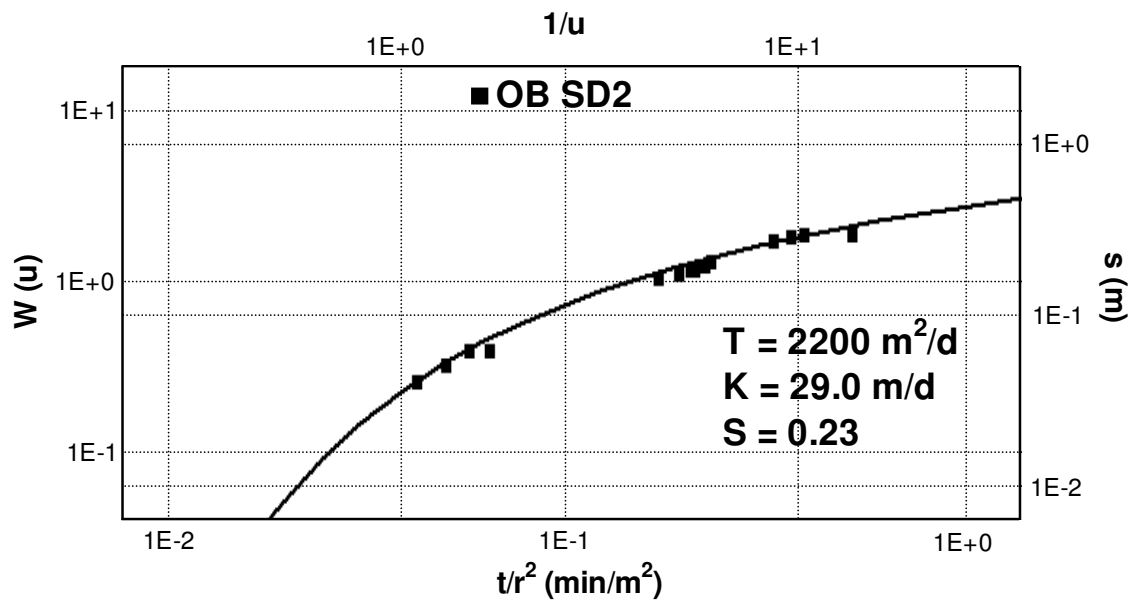


Results of the pumping test analysis by means of a Theis-curve fit

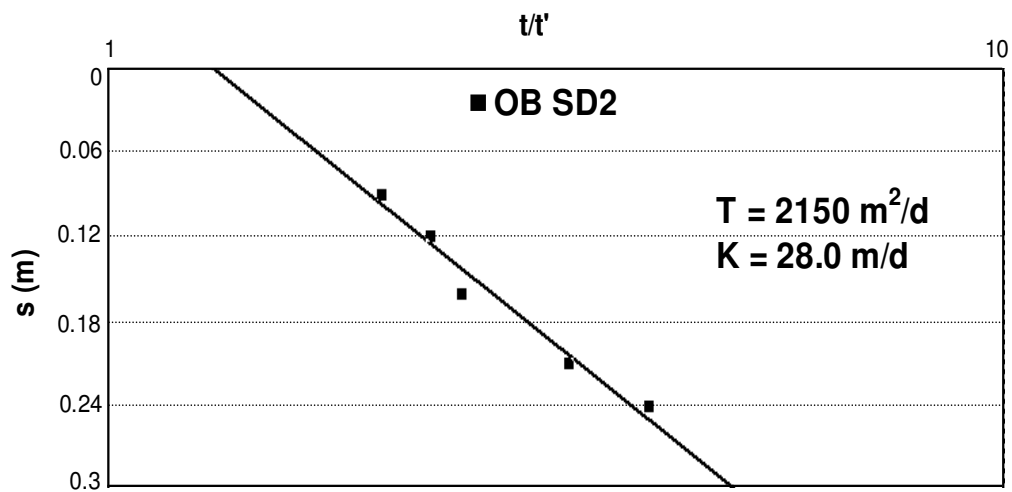


Results of the pumping test analysis by means of a Theis-recovery test

Appendix 1.7

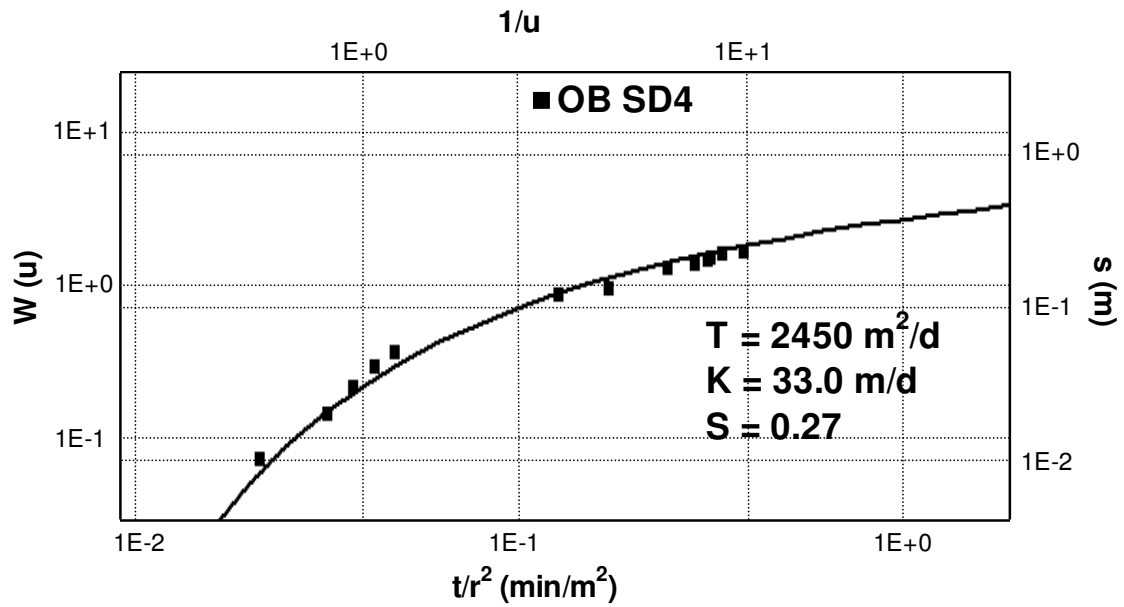


Results of the pumping test analysis by means of a Theis-curve fit

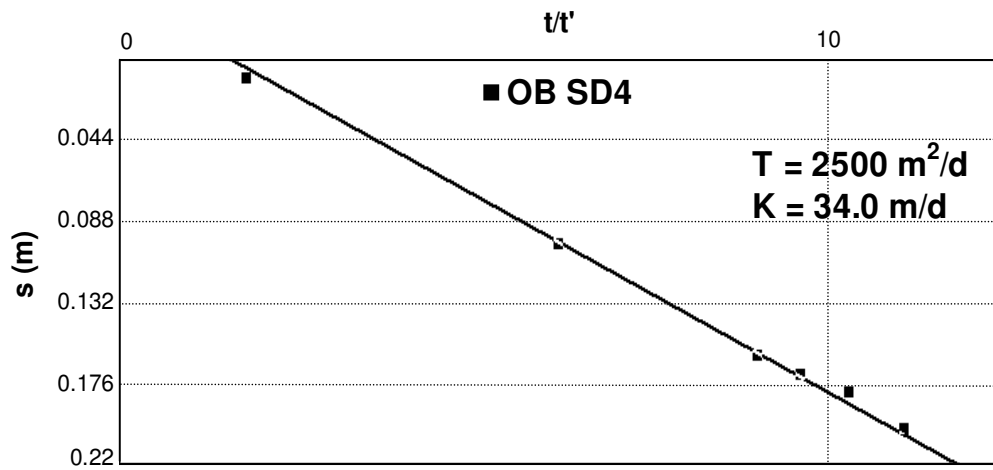


Results of the pumping test analysis by means of a Theis-recovery test

Appendix 1.7



Results of the pumping test analysis by means of a Theis-curve fit



Results of the pumping test analysis by means of a Theis-recovery test

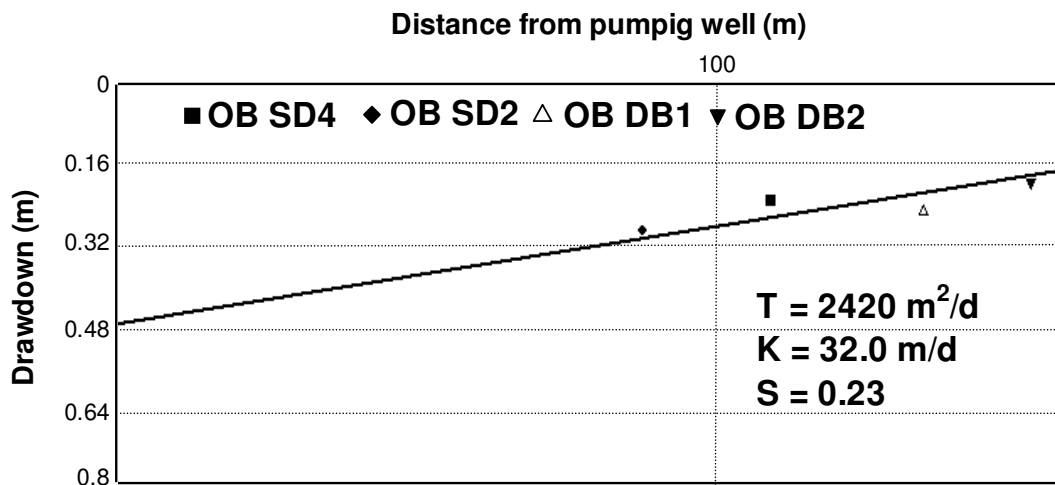
Appendix 1.7

COOPER and JACOB Distance-Drawdown

The COOPER and JACOP (1964) method is a simplification of the Theis method that is valid for greater time values and decreasing distance from the pumping well(smaller values of u) and simultaneous observations of drawdown in three or more observation wells. Transmissivity and storativity are calculated as follows:

$$T = \frac{2.3Q}{2\pi\Delta s} \qquad S = \frac{2.25Tt_o}{r_o^2}$$

where r_o is the distance (m) defined by the intercept of the zero-drawdown and the straight-line through the data points. The observation well distance is plotted along the logarithmic X axis, and drawdown is plotted along the linear Y axis.



Results of the pumping test analysis by means of Cooper and Jacob distance-drawdown

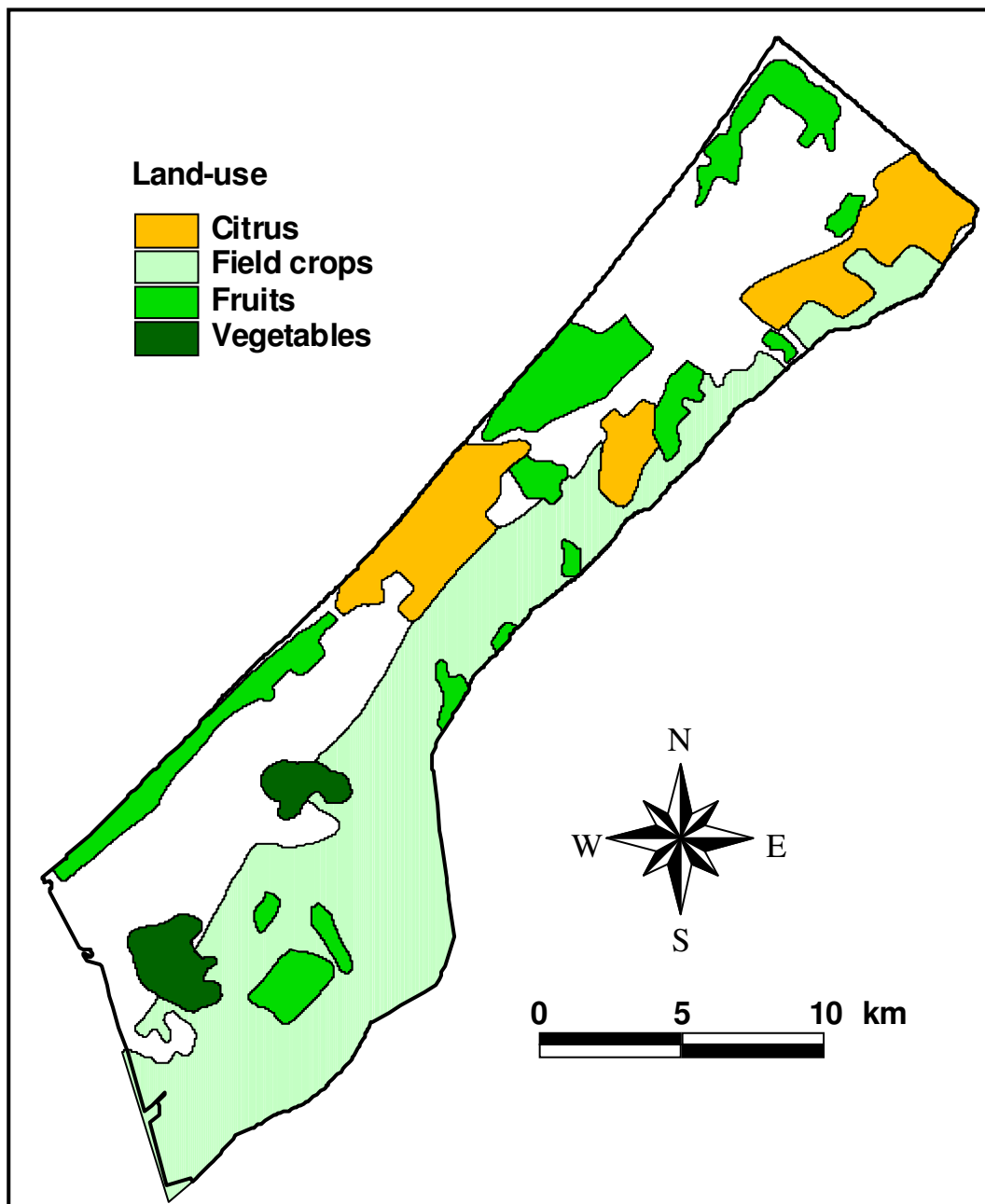
Appendix: 2

Appendices

Appendix 2.1

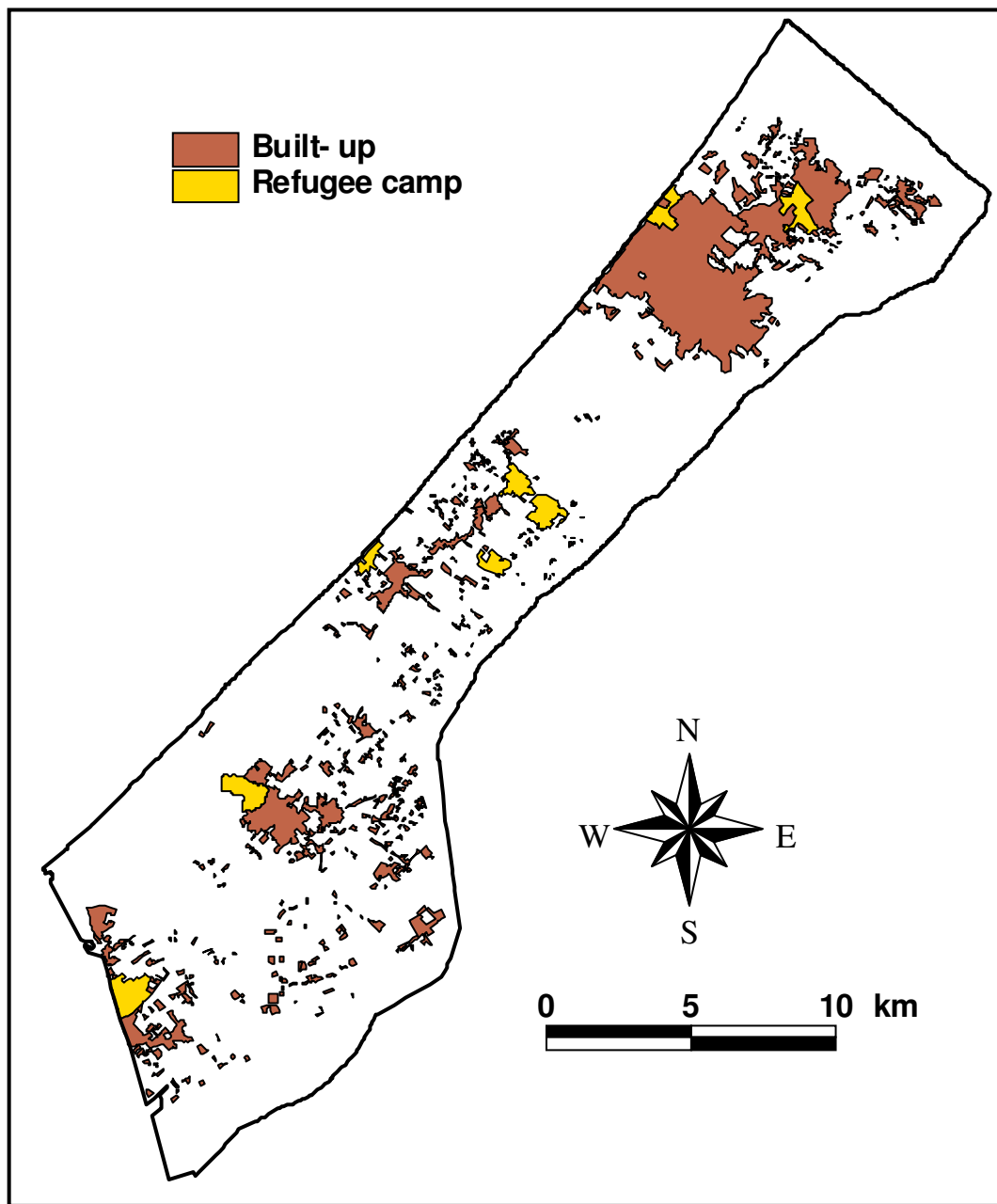
Linear interpolation in Hantush's table (S^* values)

α, β	S^*
0.01	0.002033
0.03	0.008753
0.05	0.019986
0.12	0.081581
0.28	0.275122
0.56	0.603940
1.10	0.919765
2.75	0.999949

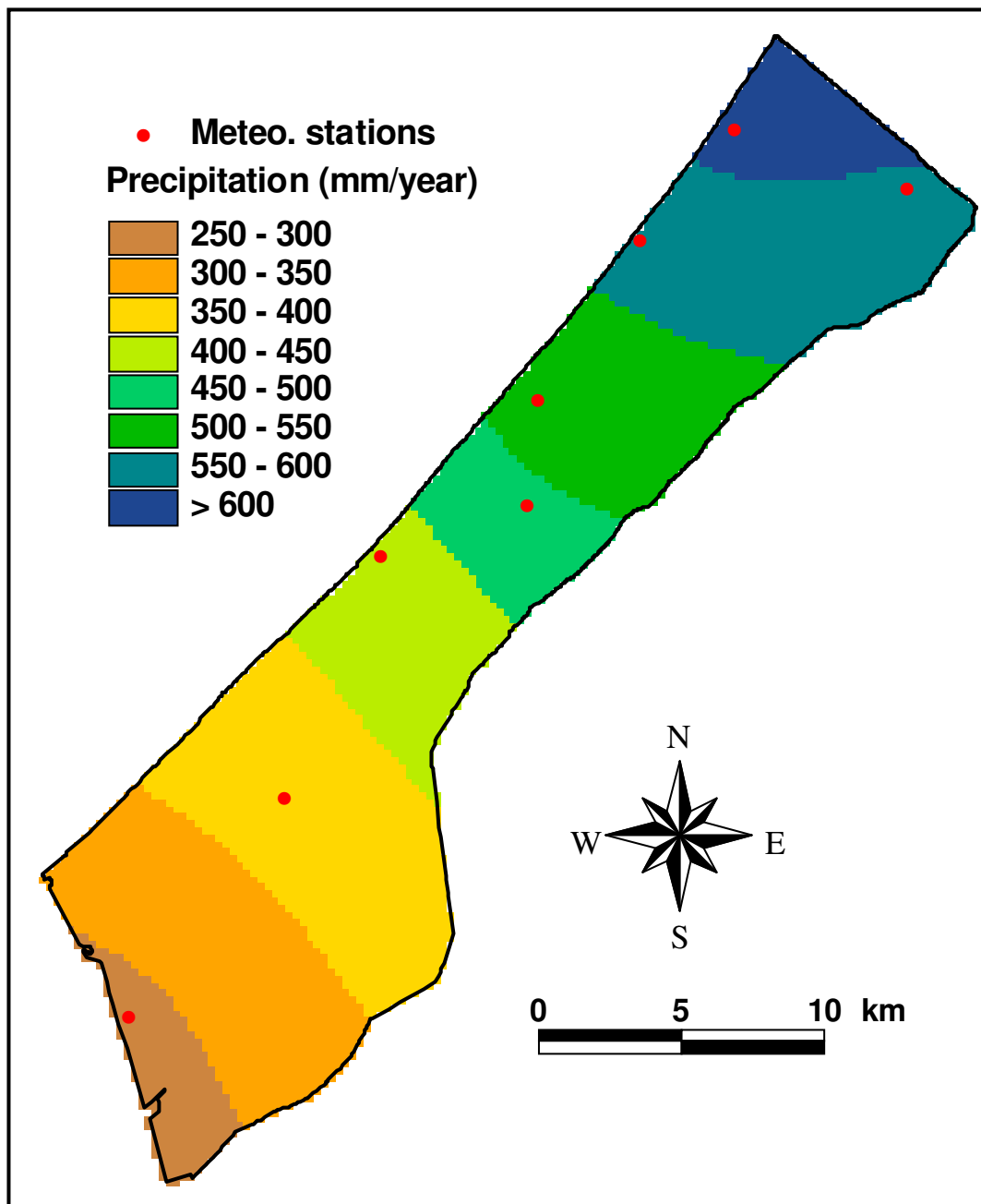


Map 1. Land-use in the Gaza Strip

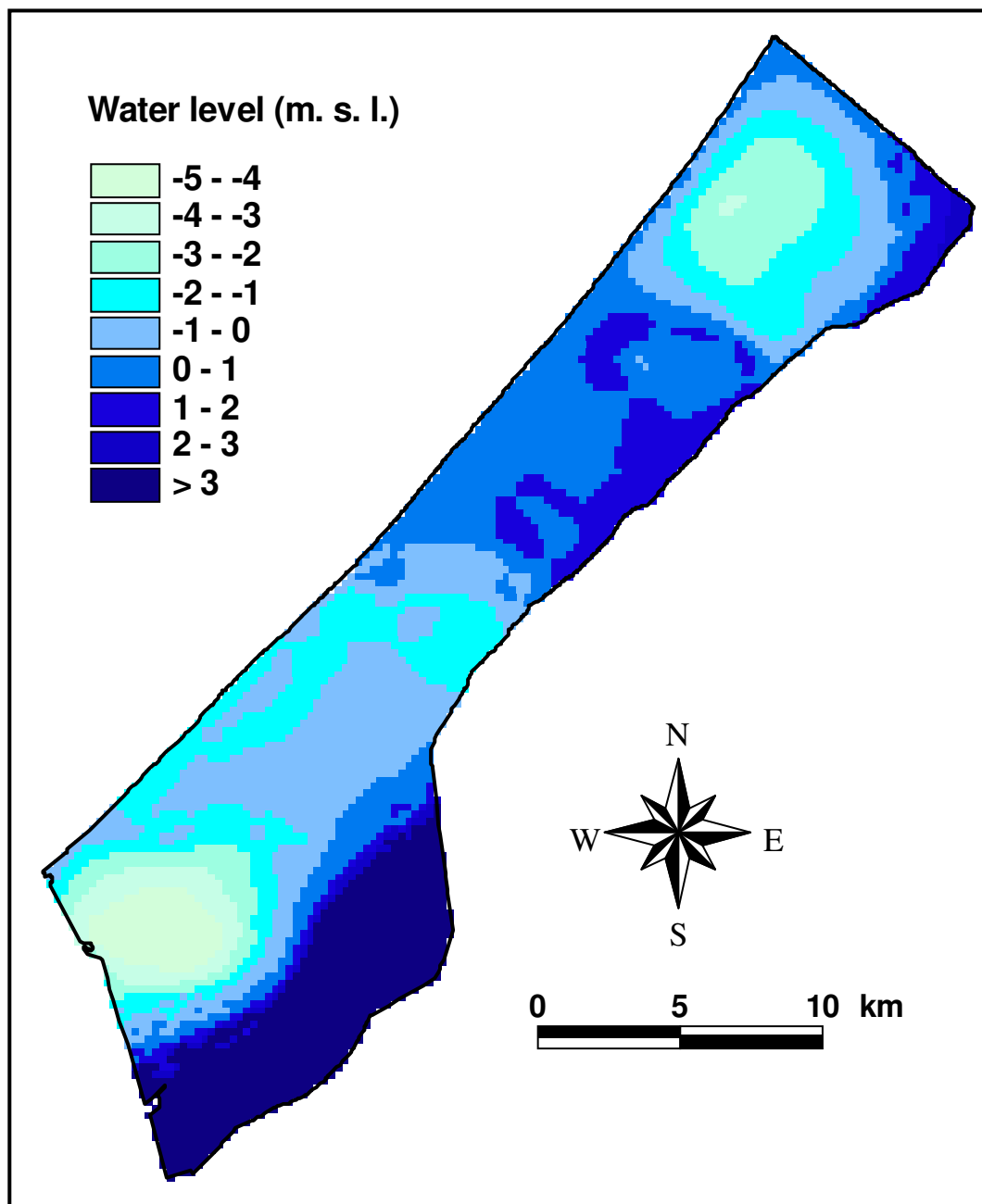
Appendix 2.2



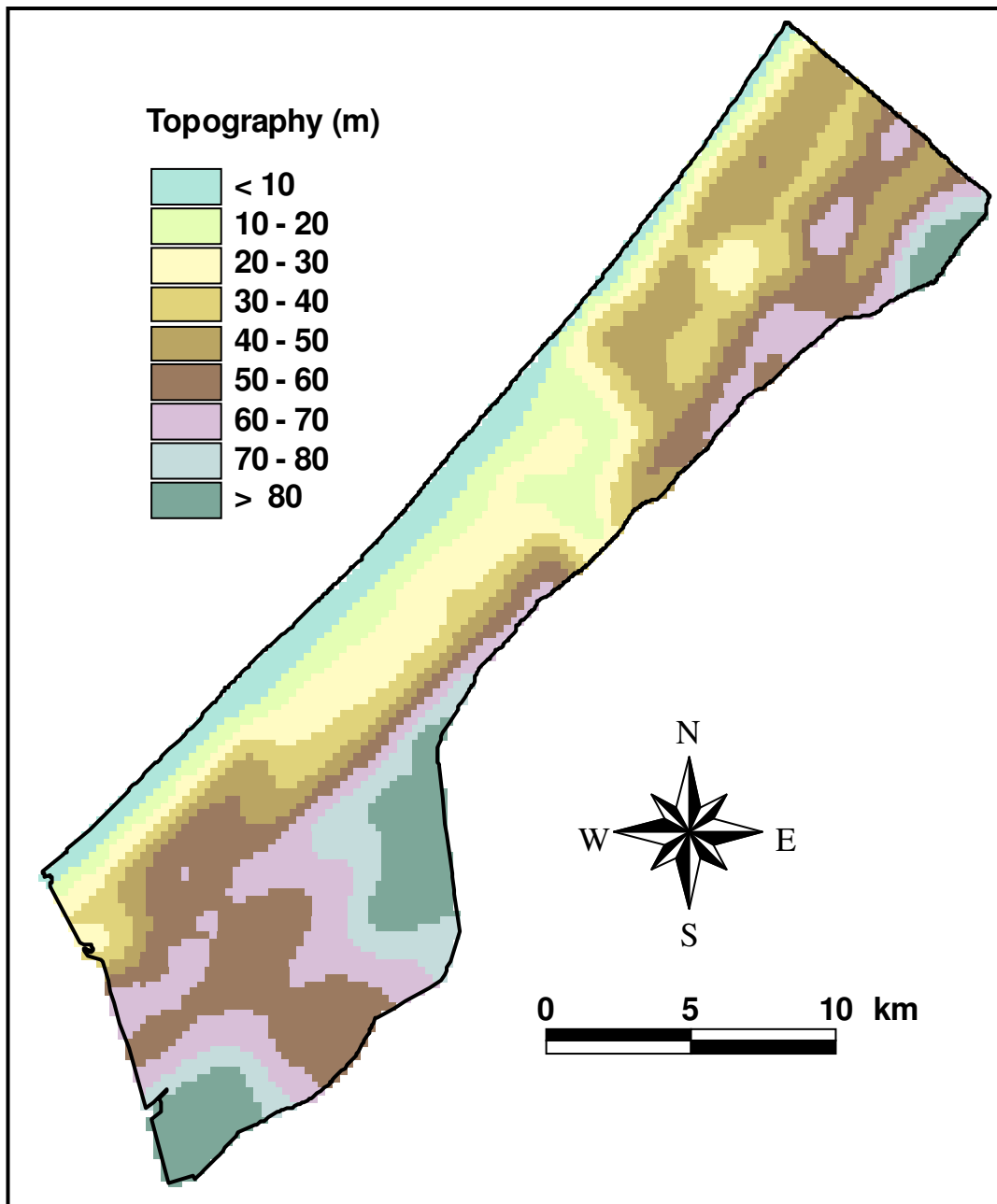
Map 2. Urban area in the Gaza Strip



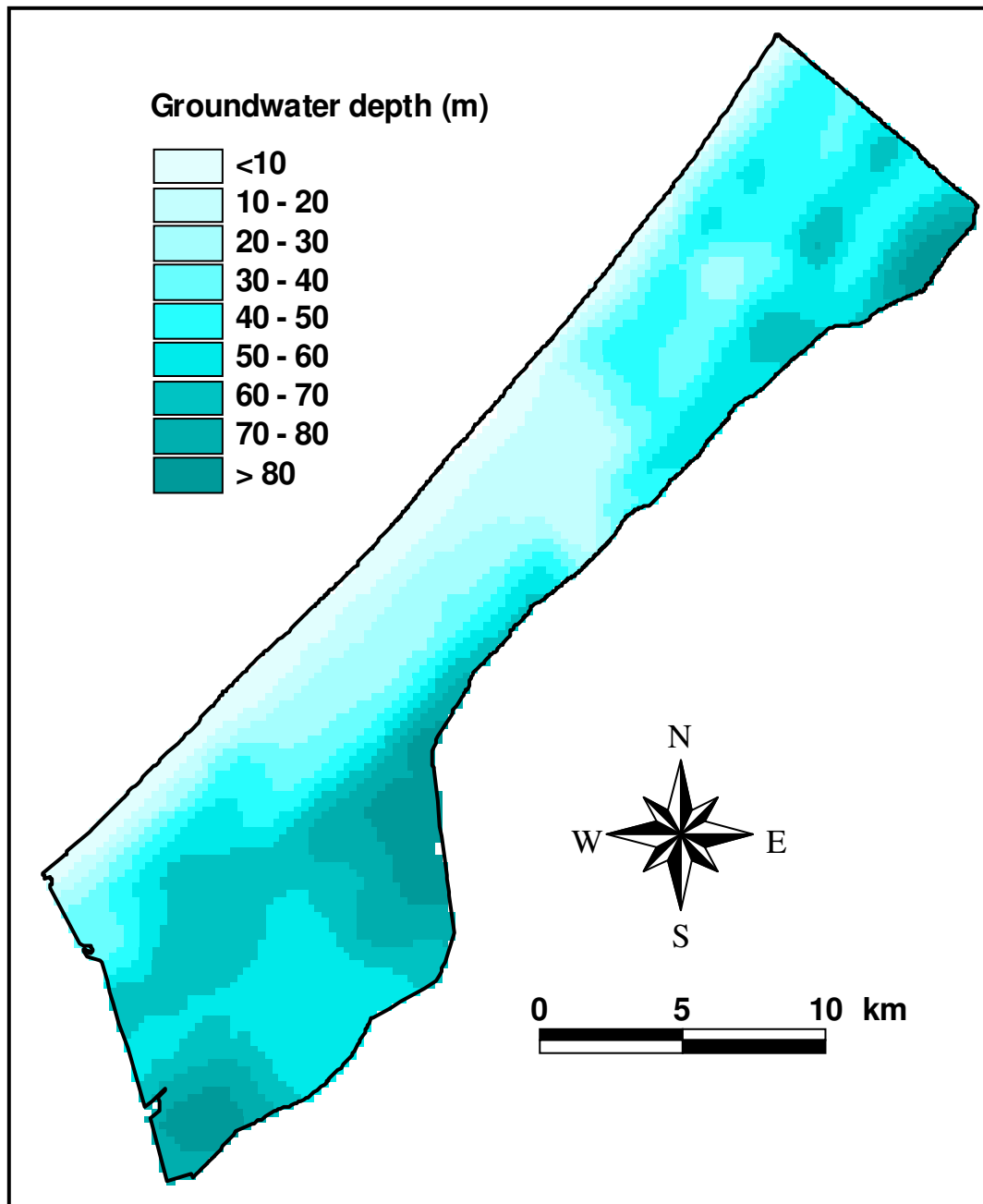
Map 3. Average annual precipitation in the Gaza Strip (year 2000)



Map 4. Groundwater level in the Gaza Strip (year 2000)



Map 5. Topography of the Gaza Strip



Map 6. Groundwater depth in the Gaza Strip (year 2000)